7.0 REVISED LOCAL PENETRATION POSTTEST MODEL ANALYSES

7.1 Overview of Pretest Local Models

The concrete and liner model for the pretest analysis E/H study is illustrated in Figure 7-1. The grid was developed by generating a concrete mesh based on the tendon layout and then joining the embedded edges of the T-anchor webs to the concrete mesh with the ABAQUS *SURFACE attachment command. The upper quadrant around the hatch was selected for modeling in order to have a local model completely encompassed by the 3DCM model. Five layers of concrete elements through the wall thickness were used, and the liner was modeled with shell elements so that liner bending and membrane behavior could be studied. The method of connecting the liner to the concrete (shown in Figure 7-2) was an important assumption, one that has been studied in the posttest analyses. In the pretest analysis, the liner had no bond or friction with the concrete, other than tying the T-anchor webs to the concrete. Rebar in the concrete wall was modeled with rebar subelements, and tendons were modeled explicitly with truss elements and friction truss-tie elements, as previously described.

The local E/H analyses results were reported as a function of pressure, and adjusted so the average hoop strains at the boundary matched the average hoop strains in the 3DCM model at the same location and pressure. Pretest E/H analysis revealed elevated liner strains 1) near hoop stiffeners that terminate near the 3:00 position of the edge of the insert plate, as indicated in Figure 7-3; 2) locally near the termination of vertical stiffeners; and 3) at the juncture to the wall embossment. Strains near the vertical stiffener exceed 16% at 3.2 Pd, which became the most probable failure pressure and failure location predicted for the PCCV model.

The A/L is the second-largest penetration in the PCCV model, located at the 62 degree azimuth at elevation 4.525 m. As with the E/H, there are liner connection and anchorage details near the A/L that cause large strain concentrations; this makes the region near the A/L another candidate for a liner tearing failure mode. It was modeled and analyzed in a similar fashion as the E/H.

The M/S is the third-largest penetration group, consisting of a group of four penetrations located at the 180 degree azimuth. (The F/W penetration group is similar to M/S penetration in geometry. However, since it is at a lower elevation at the same azimuth as the M/S, and was therefore assumed to see lower near-field strains, it was not explicitly modeled. The results of the M/S analysis should be applicable to the F/W penetration as well, however.) As with the E/H, there are liner connection and anchorage details near the M/S that cause strain concentrations, making the region near the M/S another candidate for liner tearing failure. The local M/S 3D model is illustrated in Figure 7-4. The modeling details for the local M/S model are similar to those developed for the E/H model. The liner-anchor interaction (shear force deflection behavior of the anchors) is modeled identically to the E/H, as is the method of attaching the liner/anchor mesh to the concrete mesh.

Unlike the E/H and A/L models, which were given symmetry boundary conditions on both vertical boundary planes, the M/S model was directly loaded with displacement versus pressure histories at every node along the boundaries of the model. These pressure histories (different at every node and in all three degrees of freedom) were obtained directly from the 3DCM model. The end result of the average hoop strain correlation approach used for the E/H and A/L is believed to be nearly the same as the direct application of displacements to nodes used in the M/S model. Some liner strain results for the pretest analysis of the M/S are shown in Figure 7-5. The "hot spots" for this region are near the vertical T-anchor terminations and the thickened insert plate surrounding the penetration group. Peak strains at 3.2 Pd are only about 3%, and these were generally lower than those predicted for the E/H.

7.2 E/H Model Posttest Analysis

As reported in the test-to-analysis comparisons of Chapter 4, liner strains in the vicinity of the E/H penetration collar were much lower than predicted by analysis. Since these predicted high-strain locations were fundamental to the failure predictions, significant effort was conducted toward reevaluating and reanalyzing the E/H model after the test.

Since the highest measured strains in the E/H region were observed on the side away from the buttress, the E/H model was converted to a 3D concrete and liner model for the upper quadrant around the E/H opening between azimuth 18 degrees and 324 degrees for posttest evaluation. This model was developed and modified from a similar E/H local model with buttress that was used in the pretest analysis. Figure 7-6 illustrates the finite element model and boundary conditions used in the posttest analyses. Unlike the pretest analysis, the radial displacement at the bottom boundary of the model (elev. 15.34 feet) was not specified according to results from axisymmetric analysis and only vertical displacement was applied (fixed) at the boundary. Figures 7-7 and 7-8 plot the rebar, tendon and liner details around the E/H opening.

In the search to understand the sources of differences between the local E/H predictions and the test observations, a number of changes were introduced into the posttest analysis:

1. The buttress was removed and the model shifted to the other side of the hatch;

2. Rebars were regenerated (this was necessary to extend the model to 18 degrees, but a few refinements were also made);

3. The liner was made continuous at azimuth 18 degrees, removing a discontinuity that had been present at the edge of the pretest model;

4. A circular cross section (CIRC) for tendon beams was used instead of the pipe cross section previously used;

5. A pressure (stress) boundary condition was applied at the top boundary. This was incorrectly applied in the pretest analysis:

6. The orientation of friction truss-ties were adjusted for hoop tendons that are straight in elevation view (i.e. the tendons that are not wrapped around the E/H opening). This change was based on the observation that tendon friction behavior at high pressure did not necessarily follow the friction orientation set at the beginning of the analysis (i.e., the friction orientation assumed in design); the friction was essentially set to zero for these portions of tendons; and

7. The tendons were all pulled at the 18 degree azimuth edge of the model because of difficulties encountered at the 324 degree boundary. Tendon strains at the 324 degree symmetry plane were unrealistic until this change was made.

The posttest model with these changes was referred to as Model A.

With this set of changes (and the calibration provided from the LST) the posttest E/H model's hoop expansion behavior correlates well with global displacement behavior. The adjustment to the pressure function required in the pretest analysis to match average hoop strains between the E/H and 3DCM is no longer needed, and the overall confidence in the predictive aspects of the model has been significantly improved.

7.3   E/H Posttest Results and Comparisons

Results of the basic E/H posttest model (Model A) are plotted in Figures 7-9 through 7-16. Comparing these plots to those of the pretest analysis report [1] shows a uniform displaced shape and deformation pattern that agrees better with the test. In other words, adjustments to the pressure scale for matching hoop displacements were no longer needed. At pressure beyond 3.5 Pd, liner and tendon strains grew larger and tendons reached strains approaching rupture in the zone between 0 degrees and 6 degrees azimuth. This was caused by a discontinuity in wall reinforcement. (The percentage of hoop reinforcement decreases in this region between the free-field percentage and the extra added around the E/H.) A high strain zone also exists just above the E/H. The liner strains near the E/H collar, though significantly lower than in the pretest analysis, were still elevated and show similarities to the pretest analysis, which, based on the LST strain measurements, is a generally incorrect prediction. The strains near the edge of the embossment are also generally lower than what was measured in the test. The authors have proposed a hypothesis for each of these observations, which were tested by the following variations of posttest analysis shown in Table 7-1.

Table 7-1. Variations of Posttest Analysis

Model	Liner/Concrete Friction Bond	Precrack at Edge of Embossment
A	No	No
B	Yes	No
C	No	Yes

Hypothesis 1: In the PCCV tests, the liner in the E/H area had a high degree of bond-friction with concrete, preventing slippage of the liner relative to the concrete; relative slippage is required for elevated strains to develop near local discontinuities like T-anchors and stiffeners.

Hypothesis 2: Formation of a major crack near the edge of the E/H embossment further concentrated the liner strains at the edge of the embossment. (Posttest inspection revealed the presence of a large void in the concrete behind the liner at this location and a significant crack was also observed on the outside surface of the concrete at this location.)

The hypotheses are examined in Cases B and C. Case B uses the contact surface sticking/friction capability in ABAQUS. Contact with friction bonding properties were assigned to the liner-concrete interaction surface for Case B. The results of Case B are plotted in Figures 7-17 through 7-22. They show that by preventing relative slip between liner and concrete, the overall behavior of the system (concrete strains, tendon strains, liner strains away from the hatch) remains the same, but the elevated strains close to the collar are completely eliminated.

The results of Case C are plotted in Figures 7-23 through 7-29. The ANACAP-U pre-cracking algorithm was used to introduce pre-cracking along the edge of the embossment. According to the liner strain results, however, the pre-cracking has only a minor effect on liner strain localization. Based on this result, investigating this phenomena may require a discrete crack approach, where a double row of concrete nodes along the embossment are introduced and allowed to open.

Thus, Hypothesis 1 has been clearly demonstrated to be true. Smeared crack analysis, however, has been unable to demonstrate Hypothesis 2.

The liner areas near the E/H that have hoop stiffener splices (rat-holes), some of which exhibited tears, are shown in Figures 7-30 and 7-31. To further investigate Hypothesis 2, and to develop a model that even more closely simulates what occurred in the test, two more analyses were performed, as shown in Table 7-2.

Table 7-2. Additional Analyses for Hypothesis 2

Cases	Liner/Concrete Friction Bond	Precrack at Edge of Embossment
D	Yes	Yes
E	Yes	Yes-Discrete Crack

The first (Case D) is an extension of the previous analysis series; namely, the liner/concrete friction bond was applied to the pre-cracked case (directed crack at element integration points). The liner strain results of this case are summarized in Figure 7-32, 7-33, and 7-34. The results are similar to Case C, except that now the liner strain concentrations near the Hatch collar insert plate are (for the most part) eliminated, as they were in Case B.

In the final case (Case E), the integration point directed crack is reduced to one row of elements and a discrete crack is formed by adding double rows of nodes along an assumed crack line, as shown in Figure 7-35. The double row of nodes could not be extended all the way through the wall section because it would interrupt the modeling of the reinforcement (modeled with subelements within the concrete elements). However, just "unzipping" the first element layer (which has no reinforcement) to simulate a discrete crack partway through the wall thickness was found to create a liner elevated strain phenomenon.

The results of Case E are illustrated in Figures 7-36 through 7-39, at pressures of 2.8, 3.0, 3.2, 3.5, and 3.6 Pd. At this point, a mild strain concentration emerged at the edge of the wall embossment. The peak strain predictions of this wall embossment edge are listed in Table 7-3.

Table 7-3. Peak Strains Calculated at Edge of Wall Embossment, E/H

Pressure	Peak Strain at Wall Embossment	Rat-Hole Strain Concentration		e_{peak} Pristine	e_{peak} w/Grinding
		Pristine	With Grinding		
2.8 Pd	0.0036	45	59	0.16	0.21
3.0 Pd	0.0047	"	"	0.21	0.28
3.2 Pd	0.0053	"	"	0.24	0.31

Note from Figures 7-30 and 7-31 that the mild strain concentration simulated in E/H Model Case E coincides with rat-hole weld seam details. Numerous tears occurred at these details (see Figure 1-5). Based on the results of the detailed liner rat-hole (weld-seam) analysis (Chapter 8), the additional strain concentration associated with these local details is approximately 45 for a pristine rat-hole detail and about 59 for locations with severe (~40% reduction in thickness) local liner thinning by grinding from the weld repairs. (These strain concentrations would be applied to free-field liner strains away from all discontinuities). As reported in [8], there was extensive liner thinning at most of these tear locations. The tears at the edge of the embossment can be explained by magnifying the strains calculated in the E/H analysis by the strain concentration factors from Chapter 8. This calculation is shown in Table 7-3. It shows that with discrete crack modeling and local rat-hole modeling, a liner tear would be predicted to occur as early as 2.8 Pd. Based on the evidence provided by liner strain gages and acoustic monitoring, one of the tears along this embossment edge may have even occurred as early as 2.5 Pd.

The posttest E/H study thus presents a modeling strategy with results that correlate well with the LST measurements and observations. A somewhat higher strain prediction might be possible if a discrete crack (separate rows of nodes) were propagated all the way through the concrete wall, but this would require a complete change in rebar modeling strategy to (a discrete element representation of rebar) - one that is probably not practical even for very detailed analytical evaluations of containments.

7.4   M/S Model Posttest Analysis

The M/S penetration consists of a group of four penetrations located at the 180 degree azimuth. As with the other penetrations, there are liner connection and anchorage details near the M/S that cause strain concentrations, making the region near the M/S another candidate for liner tearing failure. The local M/S 3D model is illustrated in Figure 7-4. The liner-anchor interaction (shear force deflection behavior of the anchors) is modeled identically to the E/H, as is the method of attaching the liner/anchor mesh to the concrete mesh. Unlike the E/H and A/L models, however, the M/S model was loaded directly with displacement versus pressure histories at every node along the boundaries of the model, plus internal pressure. These pressure histories (different at every node and in all three degrees of freedom) were obtained directly from the 3DCM model. Some liner strain results for the pretest analysis of the M/S were shown in Figure 7-5. The hot spots for this region are near the vertical T-anchor terminations and the thickened insert plate surrounding the penetration group.

The posttest analysis effort for the M/S penetration began with detailed checking of model geometry, but no changes to the M/S model were found to be necessary, other than updating the applied displacement versus pressure histories. These displacement histories were obtained from 3DCM posttest Model 9, the final 3DCM analysis which gave radial displacement history at the 180 degree azimuth, agreeing well with the test results.

Posttest analysis strain contour results are shown in Figures 7-40 through 7-44. The figures show a little larger strains than in the pretest analysis but still not large enough for a liner tearing prediction. At 3.3 Pd (the end of the LST), the strains around the edge of the liner insert collar are between 2% and 3%. As shown in Section 7.5, this agrees fairly well with liner strain measurements taken during the LST.

After studying the F/W geometry in the posttest phase of the project, it was determined that a F/W penetration model would essentially consist of a scaled-down version of the M/S model, with the same displacement histories applied. Because of the similarities between the M/S penetration model and an F/W model, the posttest studies did not analyze the F/W model. Instead, the results of the posttest M/S model analysis were assumed to represent the F/W penetrations, as well. Comparisons to test measurements at both the M/S and F/W locations are made in Section 7.5.

7.5   M/S and F/W Results and Comparisons with the Test

Figure 7-45 shows the M/S penetration geometry and the strain concentration locations predicted in the pretest work. Similar conditions exist at the F/W penetrations, as shown in Figure 7-46. An additional concentration location not specifically called out in Figure 7-45 is the liner-to-collar transition at the 3:00 and 9:00 positions of the penetration group (using a clock-face analogy). All of these strain concentration locations were well-instrumented for the LST, as shown in Figure 7-47. The figure also shows where tears were observed, and highlights gages at strain concentration locations that are compared to analysis. Strain versus pressure histories for all of the M/S and F/W liner strain gages are plotted in Figures 7-48 and 7-49. It is interesting to note the wide variation in peak strain measurements, even at locations that are theoretically identical; for example, locations 4 and 14 at the 9:00 and 3:00 positions of the M/S. Gage 14 measures twice as much as 4, even though nominal geometric conditions are the same. Of course, there are many contributing factors to these differences, most significantly, variations in as-built conditions–slight variations in liner thickness (due to manufacturing and weld repair grinding) from one side to the other, gage placement relative to the collar/weld, material properties (including welding heat effects), etc. Also note that many of the highest liner strains recorded anywhere on the model during the LST are near the M/S (e.g., 4.6% for gage 19) and the F/W (e.g., 6.4% for Gage 33).

Finally, it is worth noting that the highest strain measurements can, but do not always, correspond to tear locations. Examples supporting this are:

Gages 40 and 41, which are close to the long tear (tear 3) at the F/W, have relatively low strains. Gage 40, in particular, shows evidence of rising strain prior to tear occurrence; then, starting at about 2.9 Pd, declining strain from stress relief caused by the tear.

Gage 33, on the other hand, may have been located near the tip of the crack of tear 3. Gage 33 shows quite low strain up to 3.1 Pd and then a sudden jump. This supports a hypothesis that tear 3 initiated at a pressure of 2.9 Pd at the 7:30 o'clock position (midpoint of the tear) and then between 2.9 Pd and 3.1 Pd, the tear ran along a band of equally high strain (as evidenced by analysis) around the perimeter of the thickened collar and up to nearly the 9 o'clock position. When it reached that position, Gage 33 shot up due to localized crack tip effects.

Figure 7-50 shows the locations extracted from the local penetration analysis to compare liner strains with the M/S and F/W measurements. The locations are labeled A, B, C, and D. Figures 7-51 through 7-54 compare the M/S and F/W liner strain gages that correspond to these locations. These figures show that the posttest analysis of the M/S penetrations captures the strains measured in the LST quite well for both the M/S and F/W penetrations. Note that the free-field hoop strains near the F/W are 10% - 15% lower than at the M/S (based on measured radial displacement), explaining why measured strains near the M/S were initially larger than near the F/W. It is likely, however, that the occurrence of tears at the F/W versus non-tears at the M/S is due to the more extensive weld repair in the F/W area.

7.6   Conclusions on Local Penetrations Analysis

Liner strains measured in the vicinity of the E/H penetration collar were much lower than predicted by pretest analysis. Since the predicted high strain locations were fundamental to the failure predictions, significant effort was made to reanalyze the E/H model after the test. With a set of changes that included conversion of the model to the other side of the hatch (away from the buttress) and a correction to the vertical stress boundary condition, posttest E/H model's hoop expansion behavior correlated much better with measured global displacement behavior. The hoop deformation correlation-to-pressure function introduced in the pretest work was no longer needed.

Two hypotheses were developed and subsequently proven by the posttest analyses.

Hypothesis 1: The liner in the E/H area had a high degree of bond-friction with concrete, preventing slippage of the liner relative to the concrete; relative slippage is required for elevated strains to develop near local discontinuities like T-anchors and stiffeners.

Hypothesis 2: Formation of a major crack near the edge of the E/H embossment further concentrated the liner strains at the edge of the embossment.

The hypotheses were examined by several analysis cases. They showed that by preventing relative slip between liner and concrete, the overall behavior of the system (concrete strains, tendon strains, liner strains away from the hatch) remained the same, but the elevated strains close to the collar were eliminated. In the final case, integration point directed cracks were introduced to one row of elements and a discrete crack was formed by adding double rows of nodes along an assumed crack line. The double row of nodes was not extended all the way through the wall section due to difficulties with modeling reinforcement. However, just unzipping the first element layer to simulate a discrete crack partway through the wall thickness created a liner elevated strain phenomenon. The mild strain concentration that was simulated in Case E coincides, in location, with rat-hole weld seam details, and in the LST, numerous tears occurred at these details. Based on results of detailed liner rat-hole (weld-seam) analysis (Chapter 8), the additional strain concentration associated with these details is enough to make a tear prediction at the edge of the embossment. This shows that with discrete crack modeling and local rat-hole modeling, a liner tear could have been predicted to occur as early as 2.8 Pd. Based on the evidence provided by liner strain gages and acoustic monitoring, one of the tears along this embossment edge may have even occurred as early as 2.5 Pd. The posttest E/H study thus presents a modeling strategy with results that correlate well with the LST measurements and observations. A somewhat higher strain prediction might be possible if a discrete crack (separate rows of nodes) were propagated all the way through the concrete wall, but this would require a change in rebar modeling strategy–one that is probably not practical even for very detailed analytical evaluations of containments.

The M/S and F/W penetration hot spots (both analysis and LST observations) occurred near the vertical T-anchor terminations and the thickened insert plate surrounding the penetration group, e.g. at the 3:00 and 9:00 positions. For the posttest analysis effort, no changes to the M/S model were necessary, other than updating the applied displacement versus pressure histories that were obtained from 3DCM posttest Model 9, the final 3DCM analysis, which gave radial displacement history at the 180 degree azimuth, agreeing well with the test results. After studying the F/W geometry in the posttest phase of the project, it was determined that the F/W penetration model was so similar to the M/S penetration model that it was not necessary to pursue analysis of the F/W model; the posttest M/S model analysis was assumed to represent the F/W penetrations, as well.

Several noteworthy observations could be made from the well-instrumented M/S and F/W locations that are relevant to penetration response prediction and evaluation.

1. Many of the highest strains recorded during the LST are near the M/S (e.g., 4.6% for Gage 19) and the F/W (e.g., 6.4% for Gage 33).

2. There is a wide variation in peak strain measurements, even at locations that are theoretically identical. Of course, there are many contributing factors to these differences: slight variations in liner thickness (due to manufacturing and weld repair grinding), gage position relative to the collar/weld, material properties (including welding heat effects), etc.

3. The highest strain measurements can, but do not always, correspond to tear locations. Examples supporting this are:

   A. Gage 40, near the long tear (tear 3) at the F/W, shows evidence of rising strain prior to tear occurrence; then, starting at 2.9 Pd, declining strain due to the stress relief caused by the tear.

B. Gage 33, on the other hand, located near the crack tip, shows quite low strain up to 3.1 Pd and then a sudden jump. This supports a hypothesis that tear 3 initiated at a pressure of 2.9 Pd at about the 7:30 position (midpoint of the tear) and then between 2.9 Pd and 3.1 Pd, the tear ran along a band of equally high strain (as evidenced by analysis) around the perimeter of the thickened collar and up to the 9:00 position, at which time Gage 33 shot up due to localized crack tip effects.

Plots comparing the analysis to the M/S and F/W liner strain gages show that the posttest analysis of the M/S penetrations captures the strains measured in the LST quite well for both the M/S and F/W penetrations.
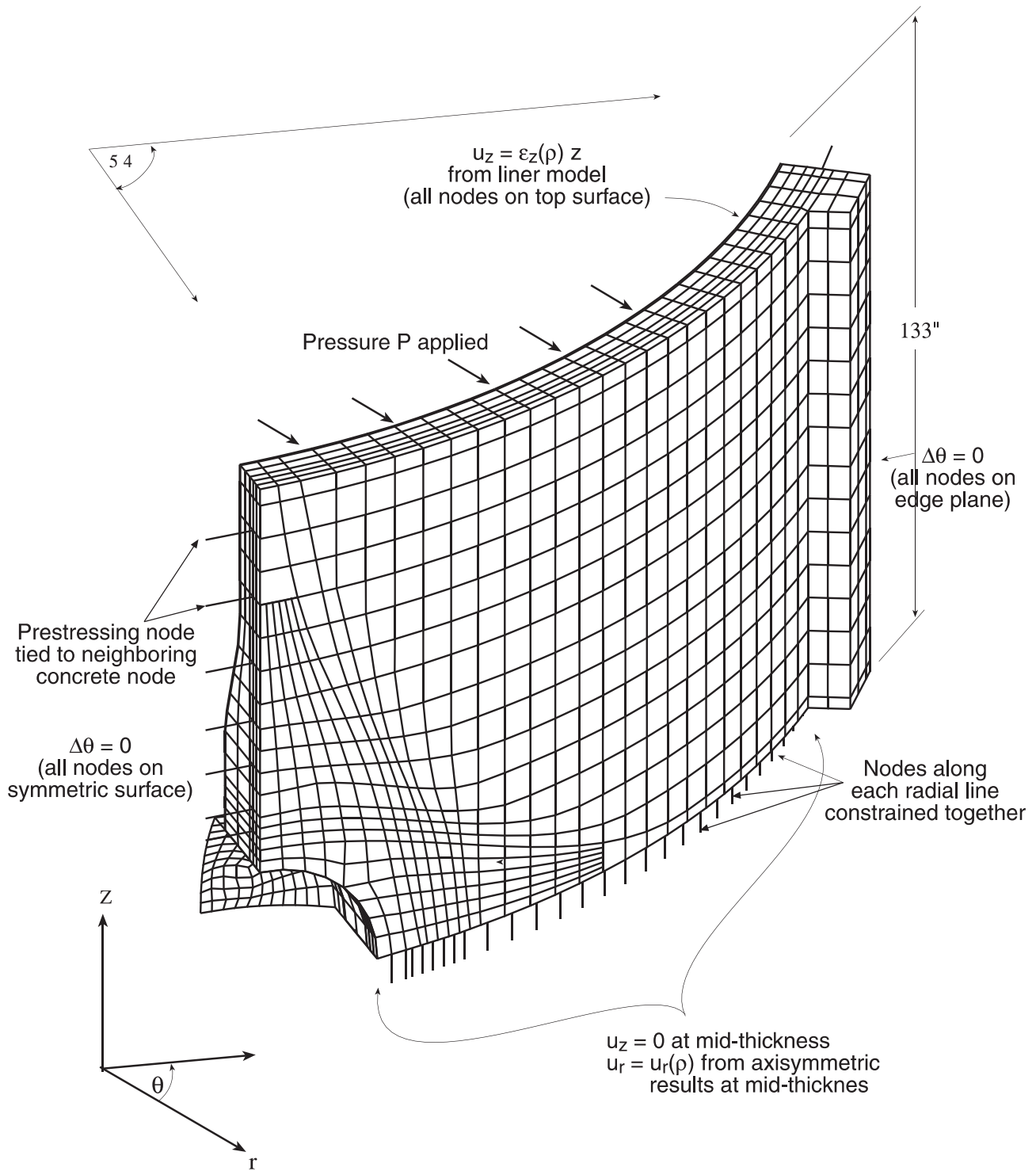
Figure 7-1. Boundary Conditions and Geometry for 3D E/H Model Used in Pretest Analysis [1]
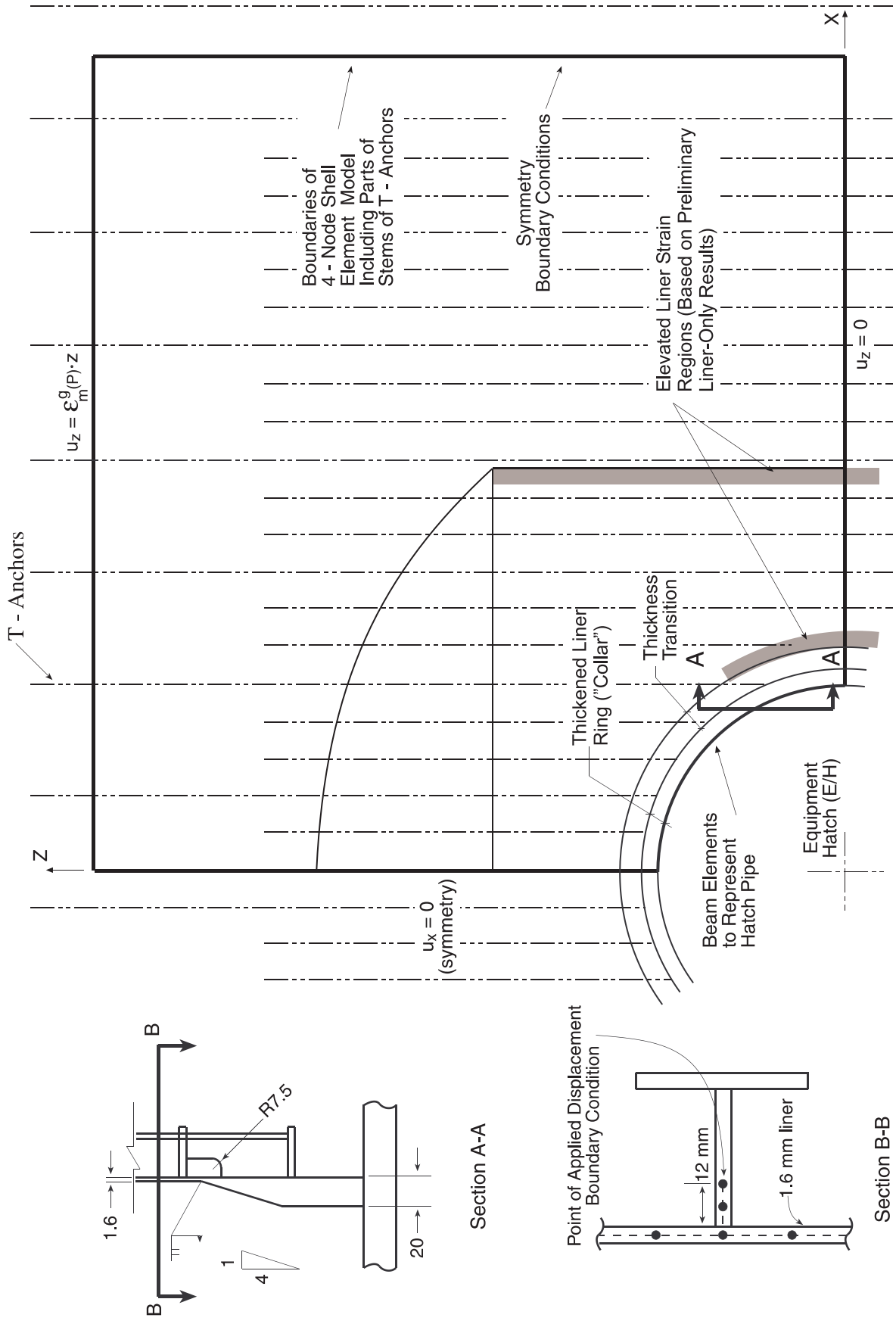
Figure 7-2. Additional Details of Pretest E/H Model (View from Inside PCCV Looking Out Radially)

Liner Strain Concentration Types

Type #1

Hoop Strain

SECTION POINT 1

E11	VALUE
	-4.79E-03
	+8.78E-03
	+2.24E-02
	+3.59E-02
	+4.95E-02
	+6.31E-02
	+7.67E-02
	+9.03E-02
	+1.04E-01
	+1.17E-01
	+1.31E-01
	+1.45E-01
	+1.58E-01
	+1.72E-01

Type #2

Type #3

—— Stiffeners
—— T-anchors

Vertical Strain

SECTION POINT 1

E22	VALUE
	-1.65E-02
	-1.41E-02
	-1.16E-02
	-9.22E-03
	-6.80E-03
	-4.37E-03
	-1.95E-03
	+4.72E-04
	+2.89E-03
	+5.32E-03
	+7.74E-03
	+1.02E-02
	+1.26E-02
	+1.50E-02

Type #3
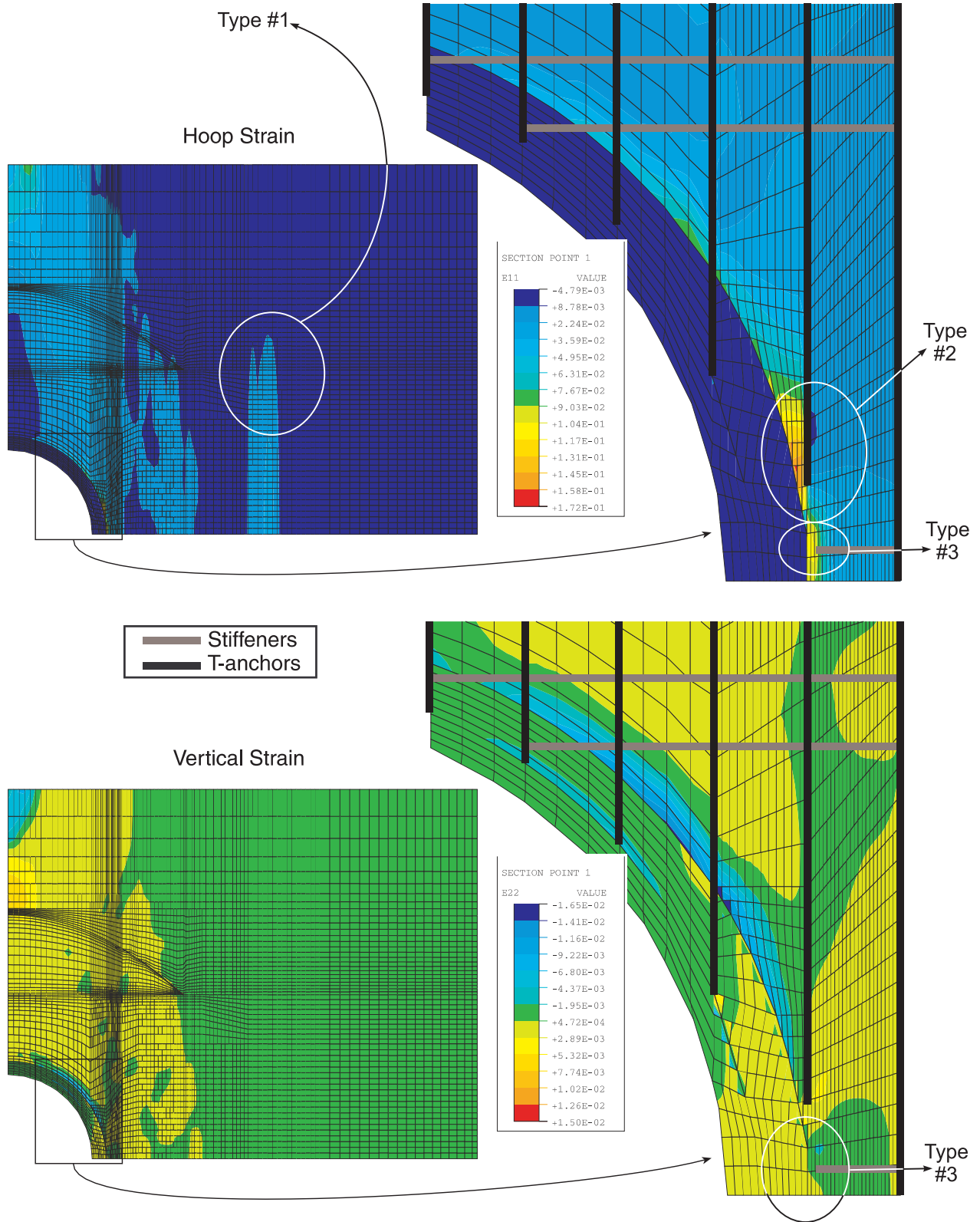
Figure 7-3. Liner Contour Strain Plots at P = 3.2 Pd for E/H from Pretest Analysis [1]

224

Anchors

Liner

Collar plate

Graduated thickness

four-node shells used
for liner and anchors

Eight-node continuum
elements

Pressure applied to concrete
to prohibit liner elements
from "passing through"
concrete elements

Anchor nodes linearly
constrained to inner
concrete wall nodes

Liner nodes only
connected to anchors
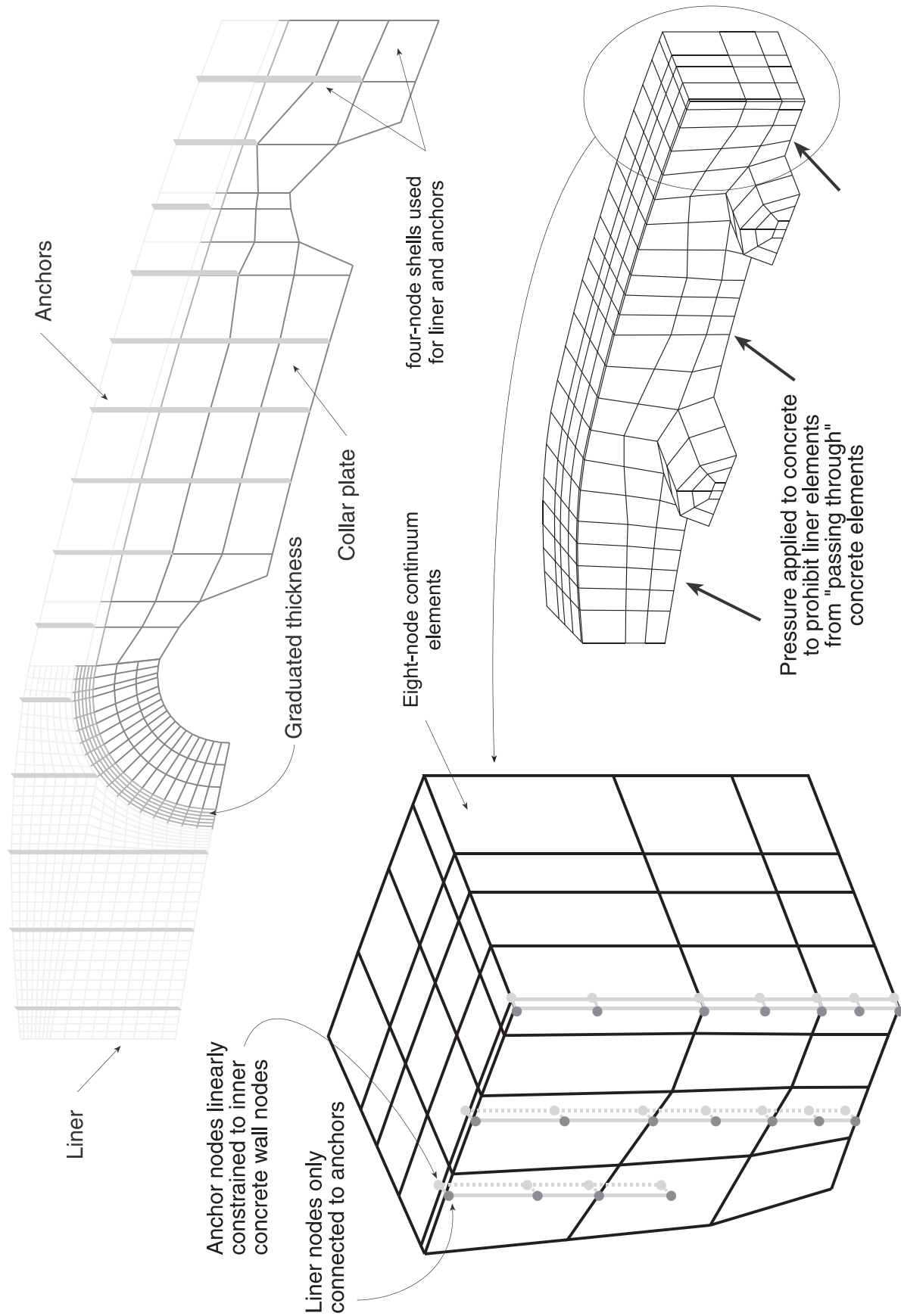
Figure 7-4. M/S Local Model Liner Details from Pretest Analysis
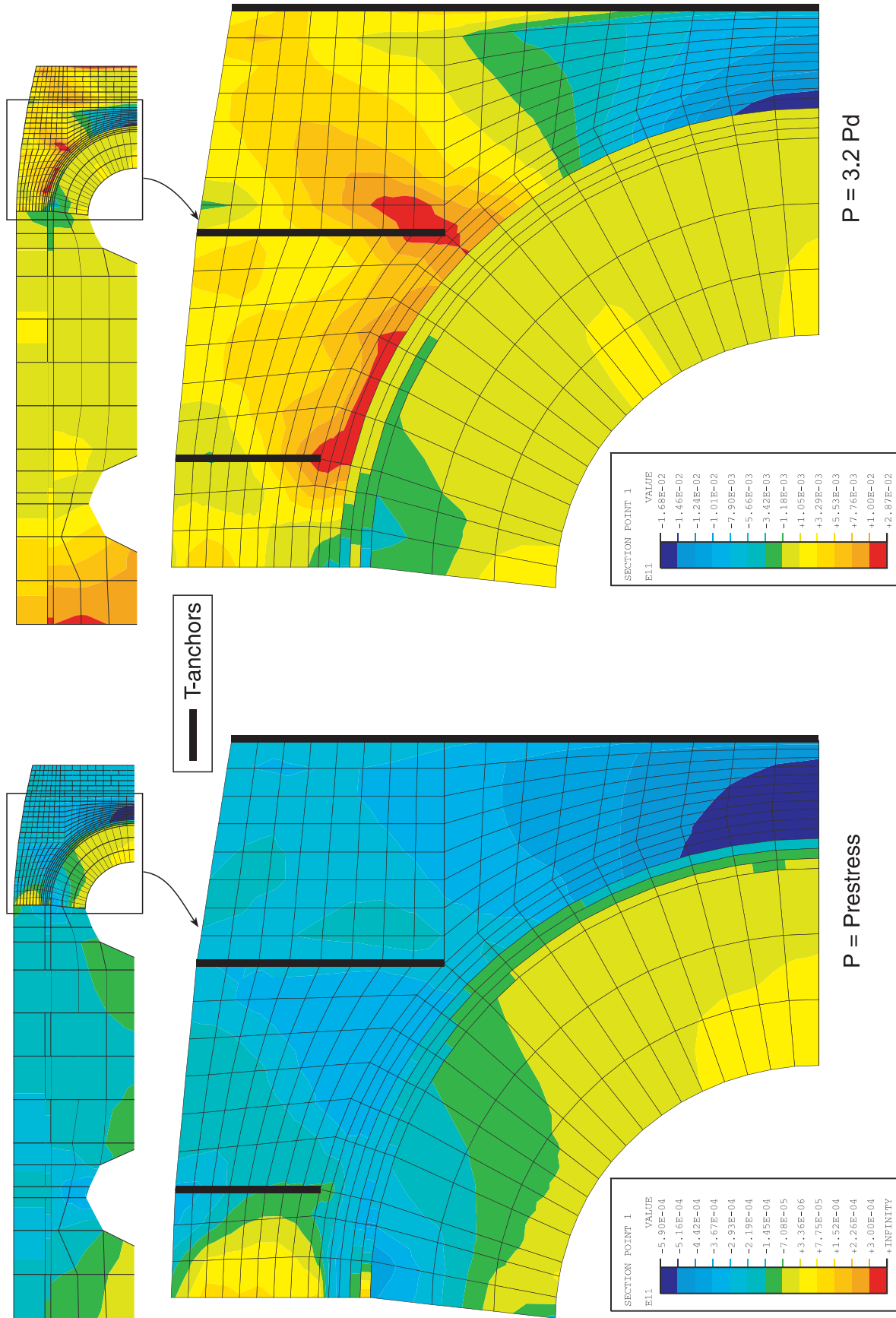
Figure 7-5. Liner Contour Hoop Strain Plots from Pretest M/S Model Analysis
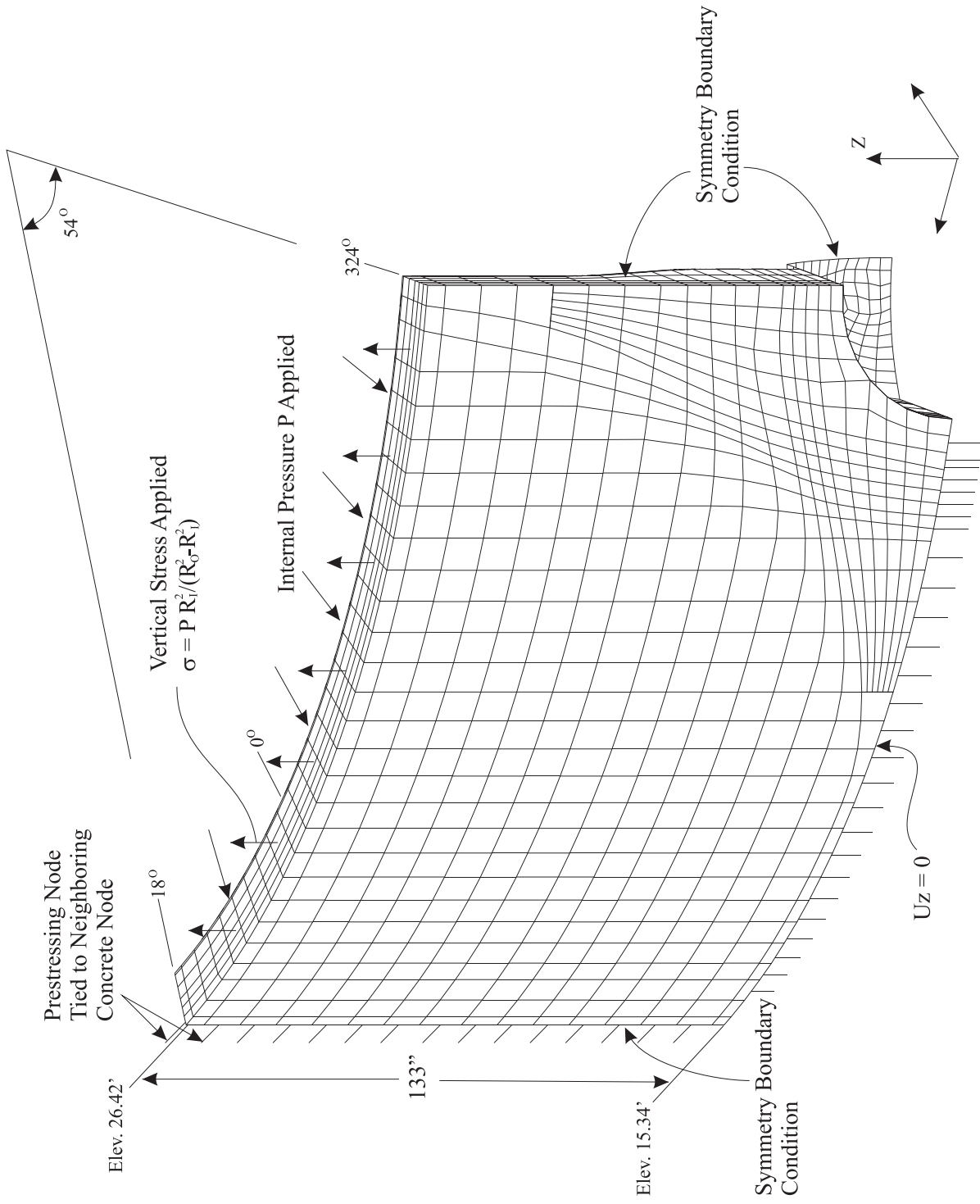
Figure 7-6. Finite Element Mesh and Boundary Conditions for 3D E/H Model

The figure includes the following labels:

- 54°
- 324°
- Symmetry Boundary Condition
- z
- Internal Pressure P Applied
- Vertical Stress Applied $\sigma = P\,R_i^2/(R_o^2 - R_i^2)$
- Prestressing Node Tied to Neighboring Concrete Node
- 0°
- 18°
- Elev. 26.42'
- 133"
- Symmetry Boundary Condition
- Elev. 15.34'
- Uz = 0

Inside Hoop Rebars

D19
D16
D13

Outside Hoop Rebars

D19
D16
D13

358°

0.2°

Inside Vertical Rebars

D19
D16
D16*0.5
D13
D13*0.5
D10

Outside Vertical Rebars

D16*0.5
D16
D13
D13*0.5
D10

Figure 7-7. Schematic of Hoop and Vertical Rebars in E/H Region

228
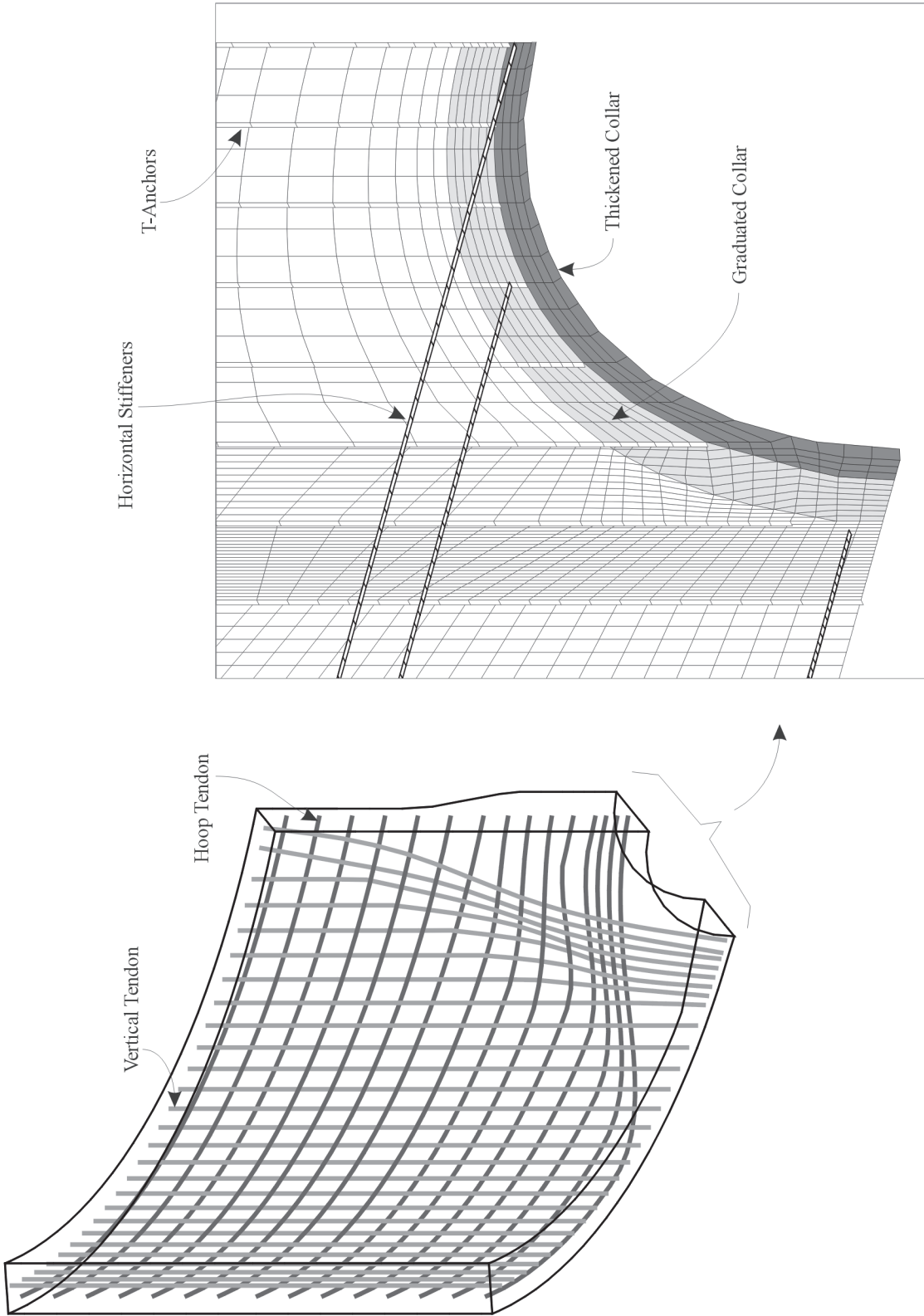
Figure 7-8. E/H Finite Element Model Including Tendons, Liner, Anchors, and Stiffeners

T-Anchors

Thickened Collar

Graduated Collar

Horizontal Stiffeners

Hoop Tendon

Vertical Tendon

P=3.6 Pd

P=3.55 Pd
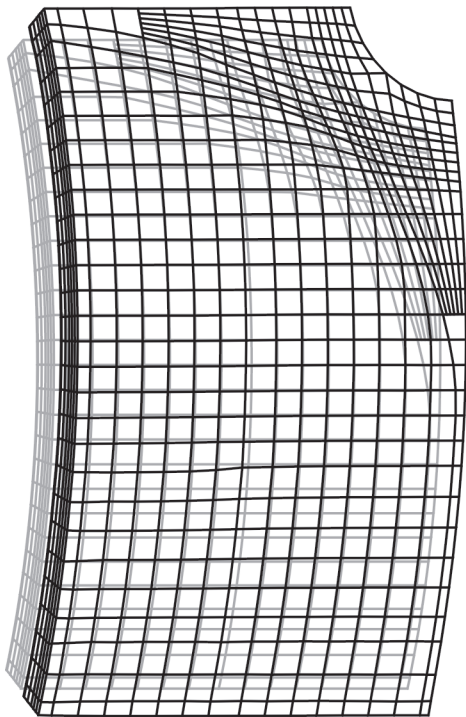
Undeformed
Deformed
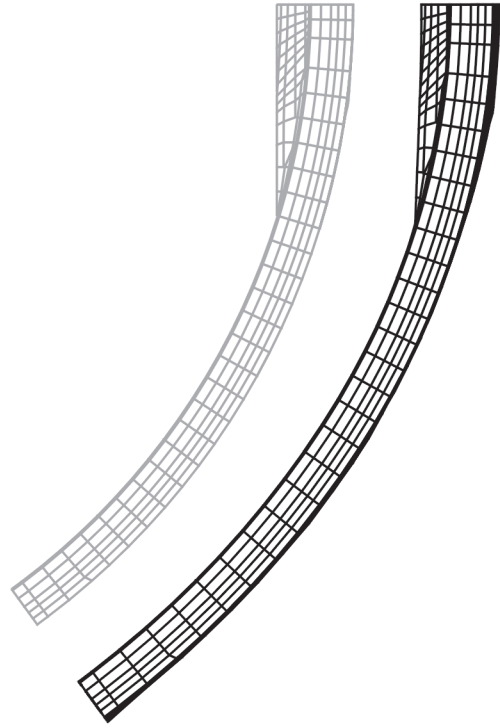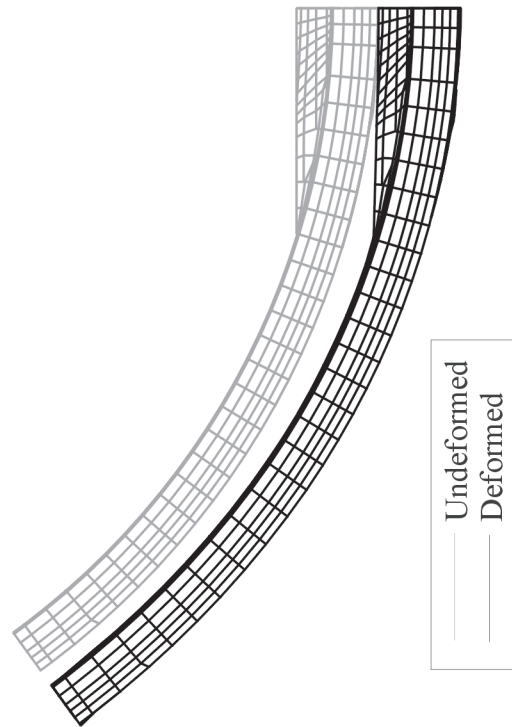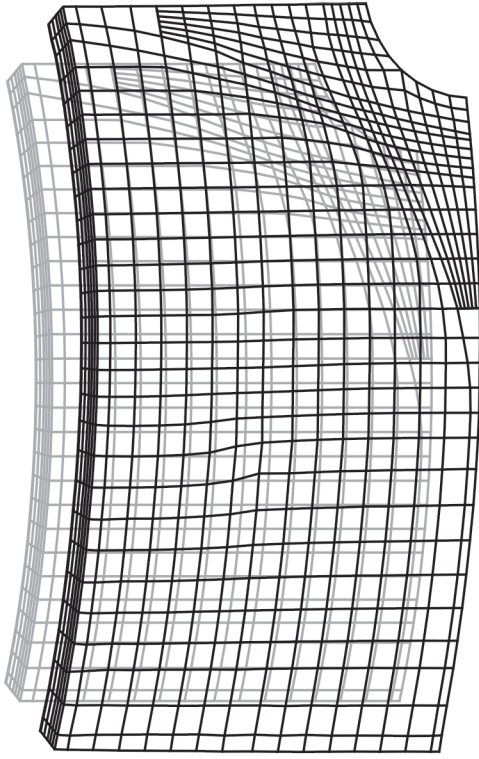
Figure 7-9. Deformed Shape of E/H Mode, Case A (Magnification Factor = 10)

230
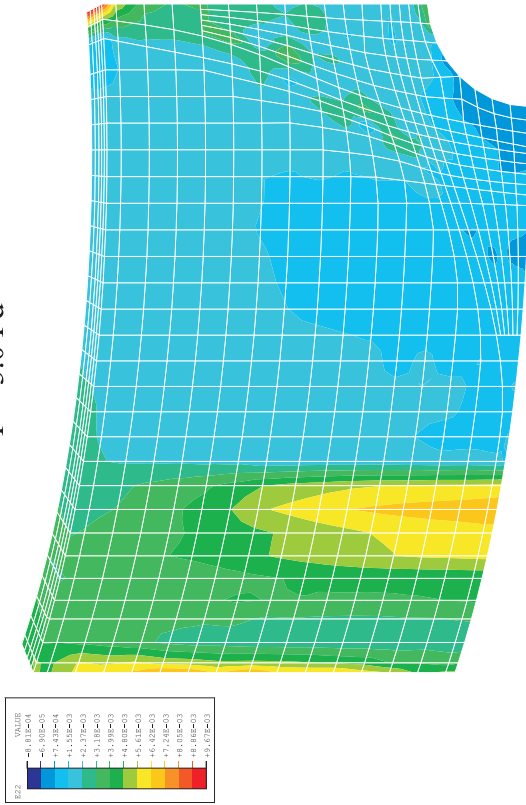
P = 3.0 Pd

P = 3.5 Pd
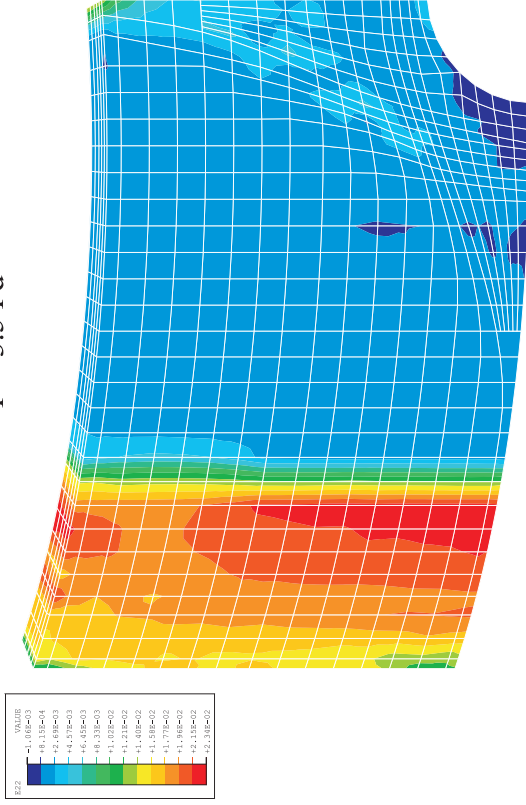
P = 3.55 Pd
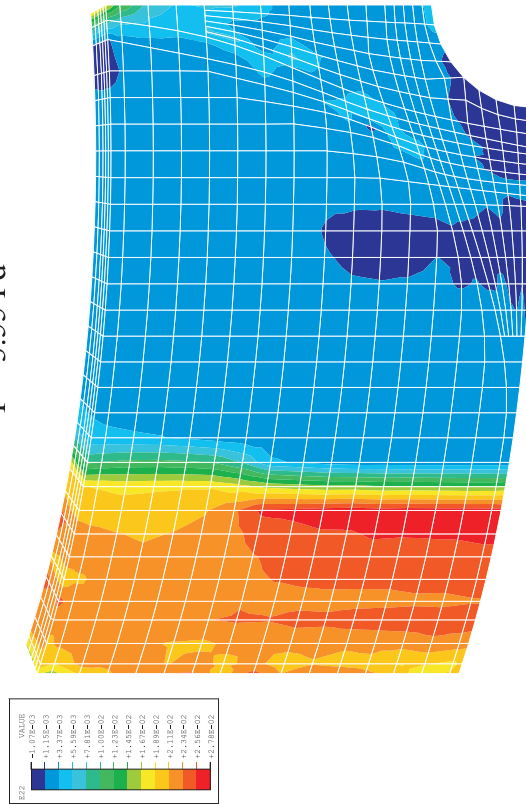
P = 3.6 Pd
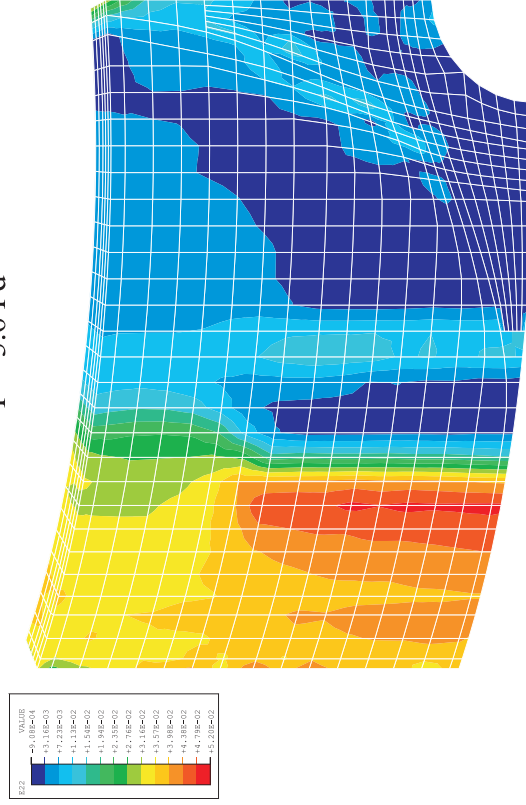
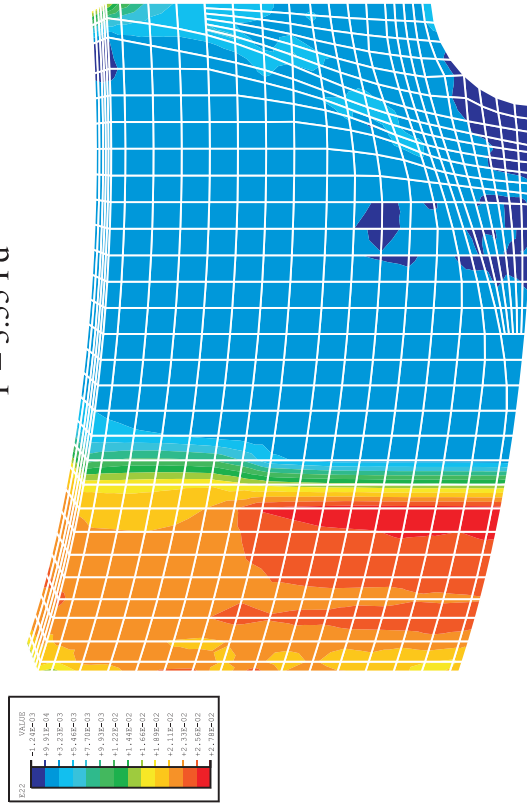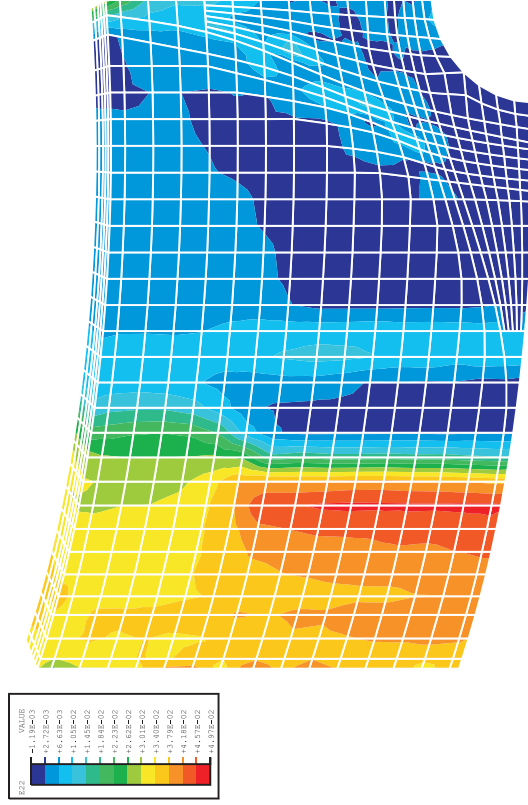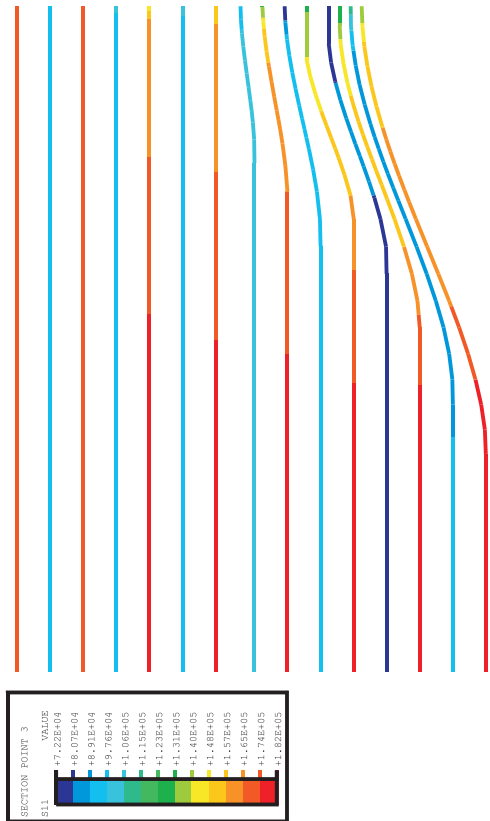Figure 7-10. Concrete Hoop Strain Contours, Posttest Analysis Case A

231
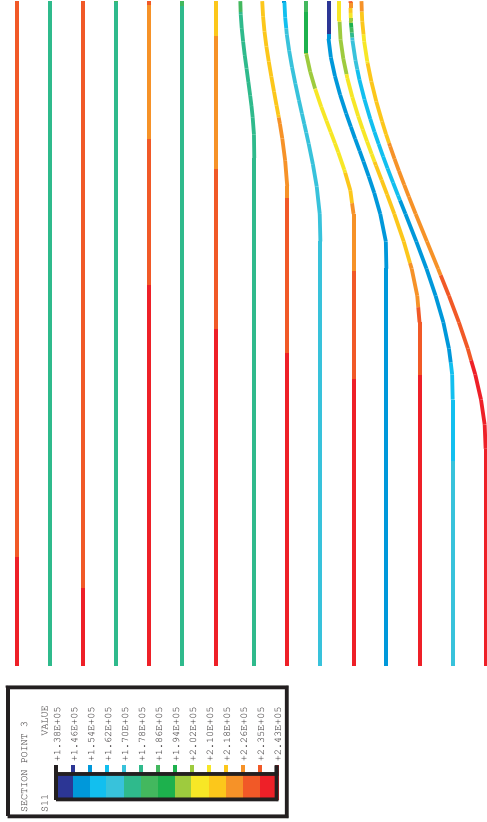
Stress, P = 3.0 Pd

Stress, Prestress

Strain, P = 3.0 Pd
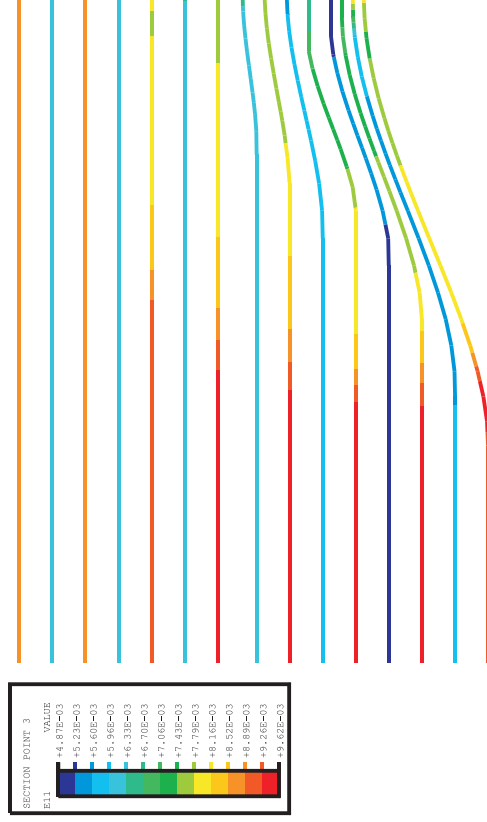
Strain, Prestress

Figure 7-11. Hoop Tendon Stresses and Strains, Posttest Analysis Case A, at Prestress and at 3.0 Pd
(Stresses in psi; multiply by 0.00690 for MPa)
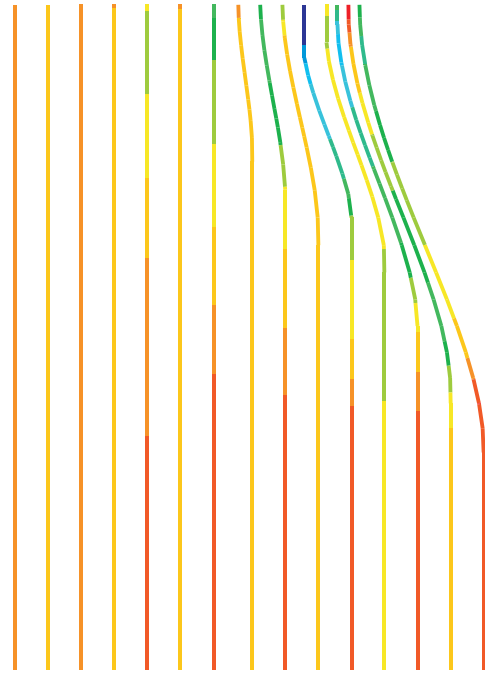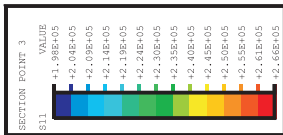
Stress, P = 3.6 Pd
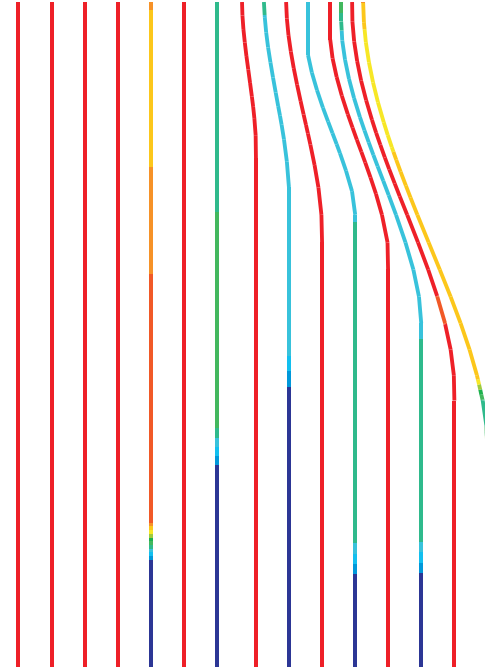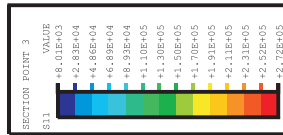
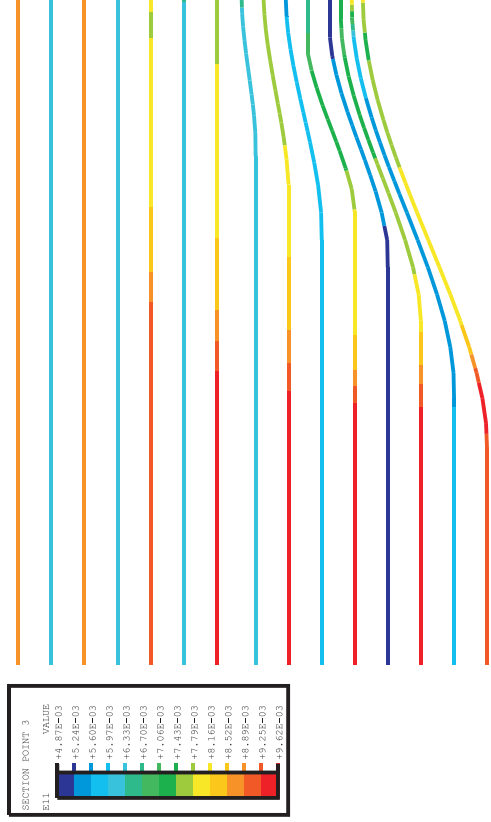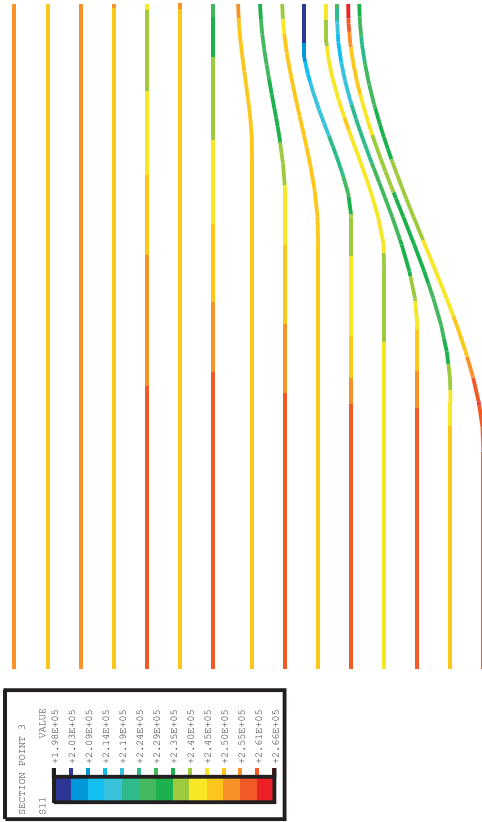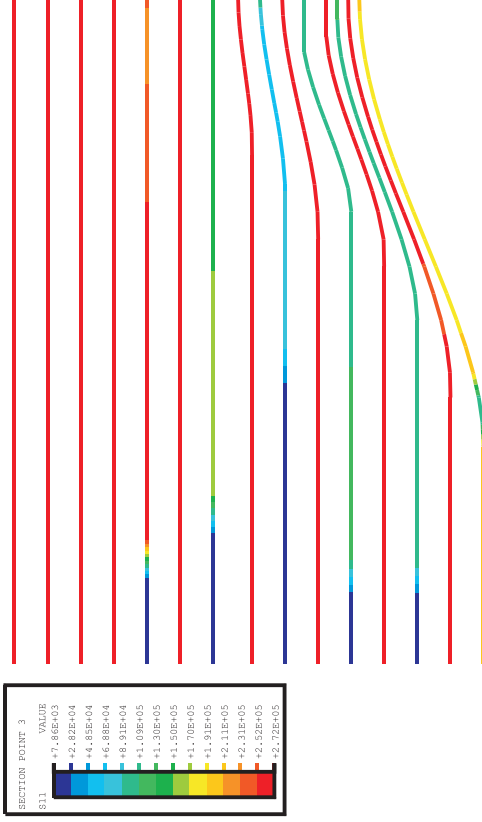Strain, P = 3.6 Pd
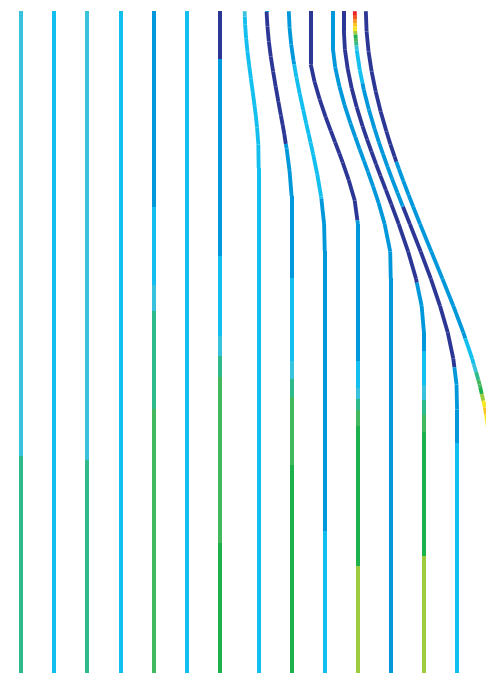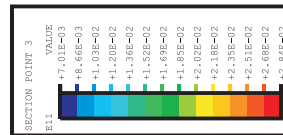
Stress, P = 3.5 Pd
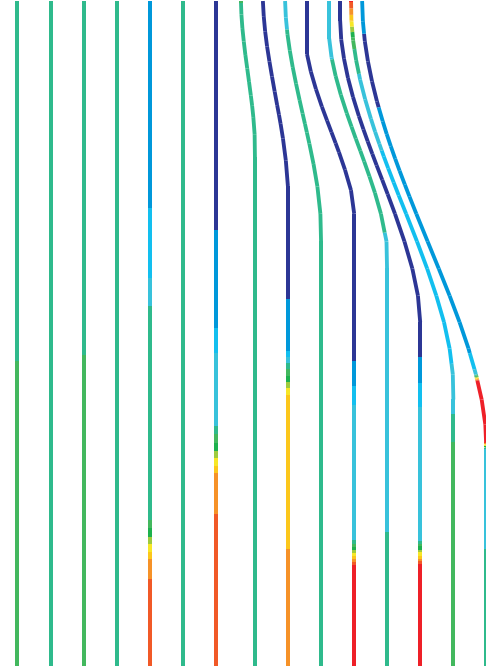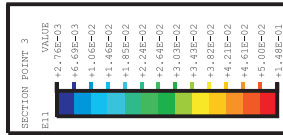
Strain, P = 3.5 Pd

Figure 7-12. Hoop Tendon Stresses and Strains, Posttest Analysis Case A, at 3.5 Pd and 3.6 Pd
(Stresses in psi; multiply by 0.00690 for MPa)
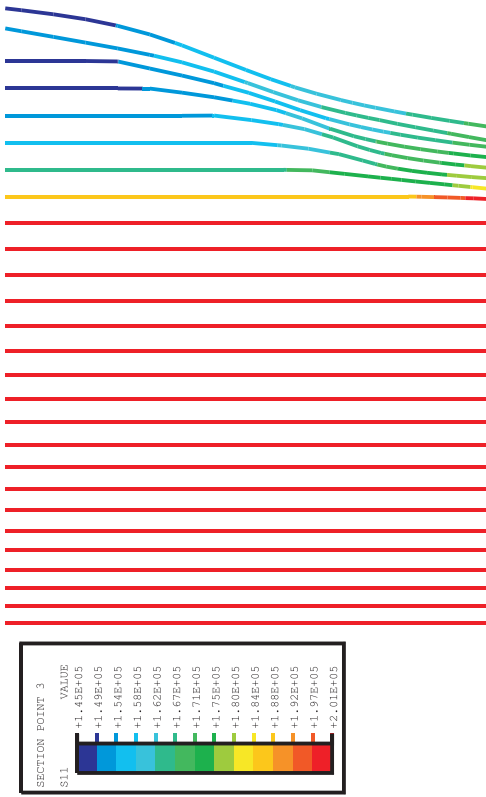
Stress, P = 3.6 Pd
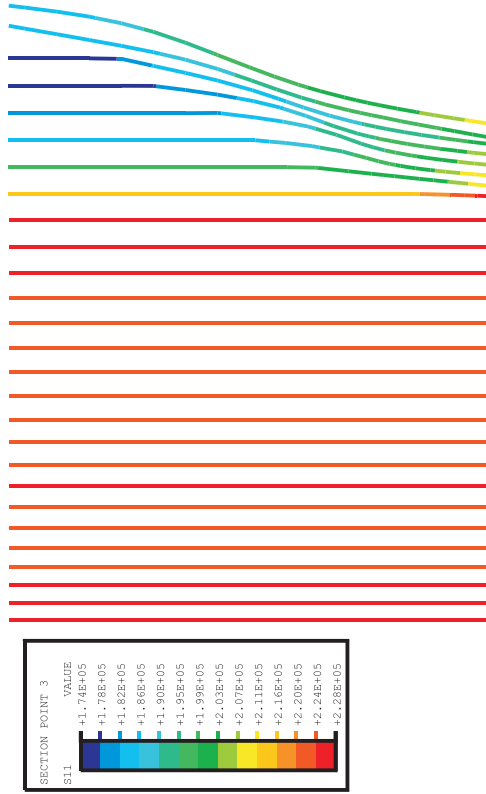
Strain, P = 3.6 Pd

Stress, Prestress
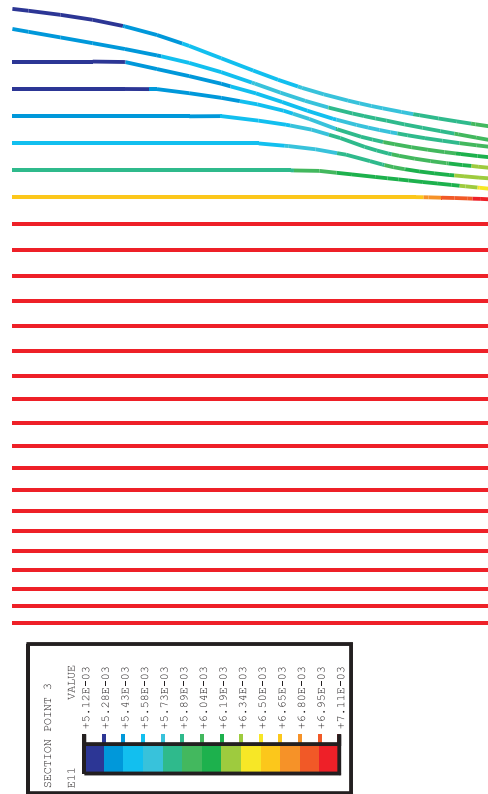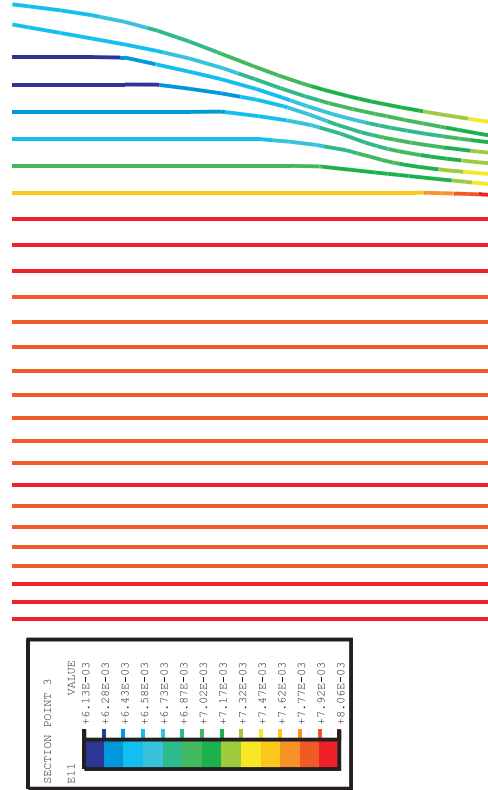
Strain, Prestress

Figure 7-13. Vertical Tendon Stresses and Strains, Posttest Analysis Case A, at Prestress and 3.6 Pd
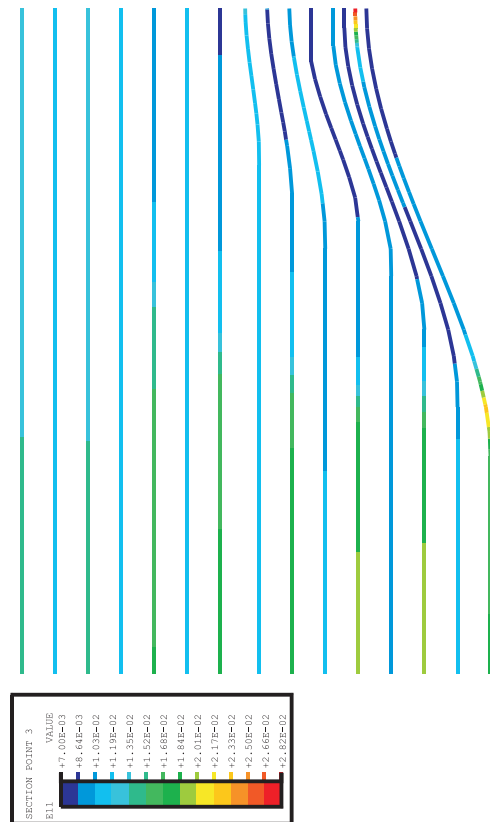(Stresses in psi; Multiply by 0.00690 for MPa)

234

SECTION POINT 2

E11   VALUE
    -8.80E-06
    +8.55E-04
    +1.72E-03
    +2.58E-03
    +3.45E-03
    +4.31E-03
    +5.17E-03
    +6.04E-03
    +6.90E-03
    +7.76E-03
    +8.63E-03
    +9.49E-03
    +1.04E-02
    +1.12E-02
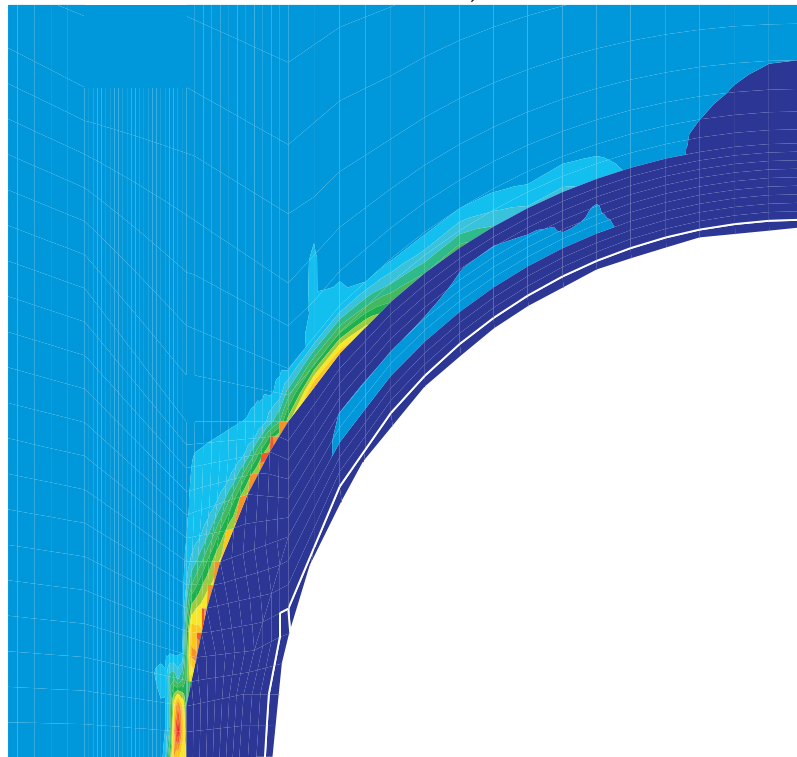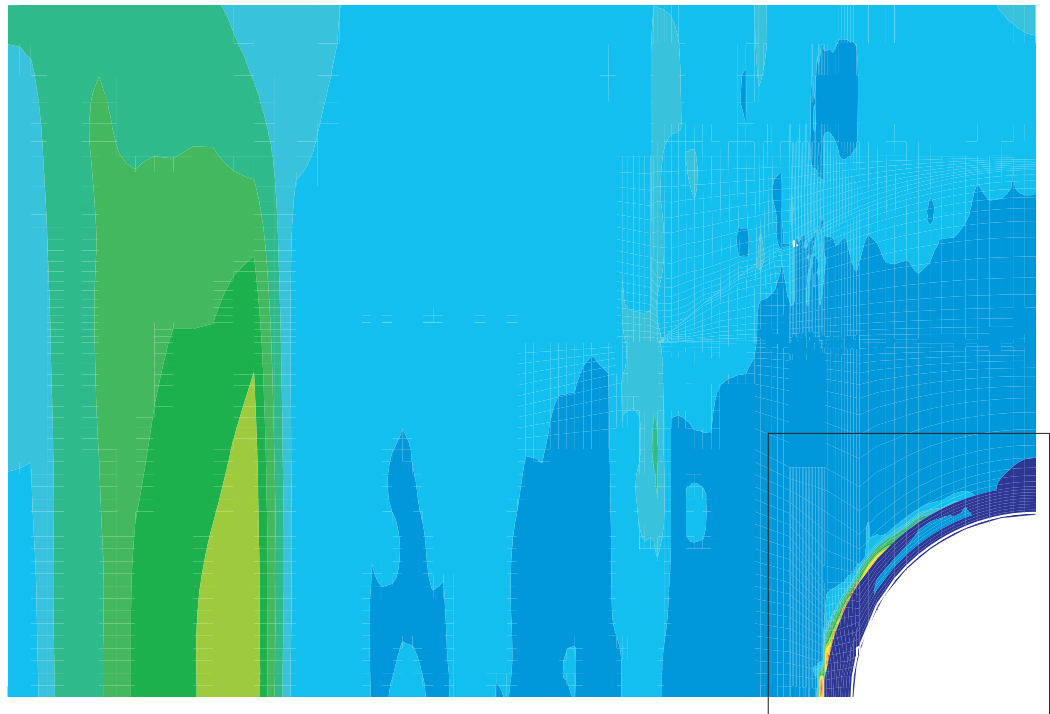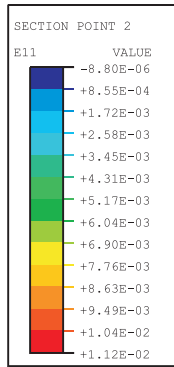
Figure 7-14. Liner Hoop Strains, Posttest Analysis Case A, at 3.0 Pd

235

SECTION POINT 2

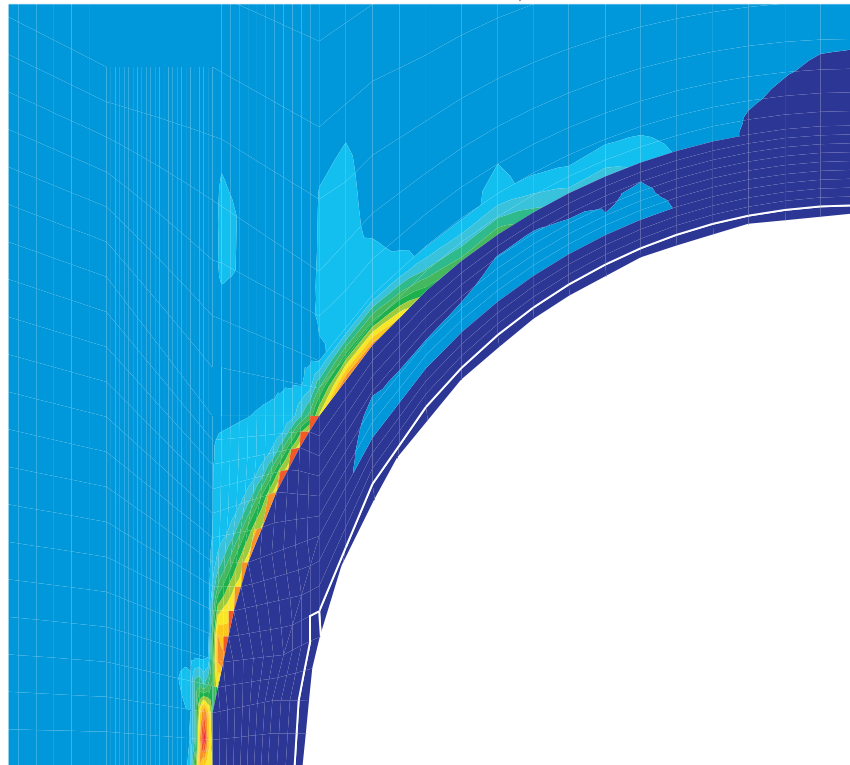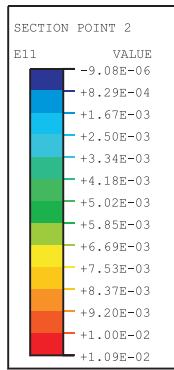| E11	VALUE
	-1.11E-05
	+1.18E-03
	+2.38E-03
	+3.57E-03
	+4.77E-03
	+5.96E-03
	+7.16E-03
	+8.36E-03
	+9.55E-03
	+1.07E-02
	+1.19E-02
	+1.31E-02
	+1.43E-02
	+1.55E-02
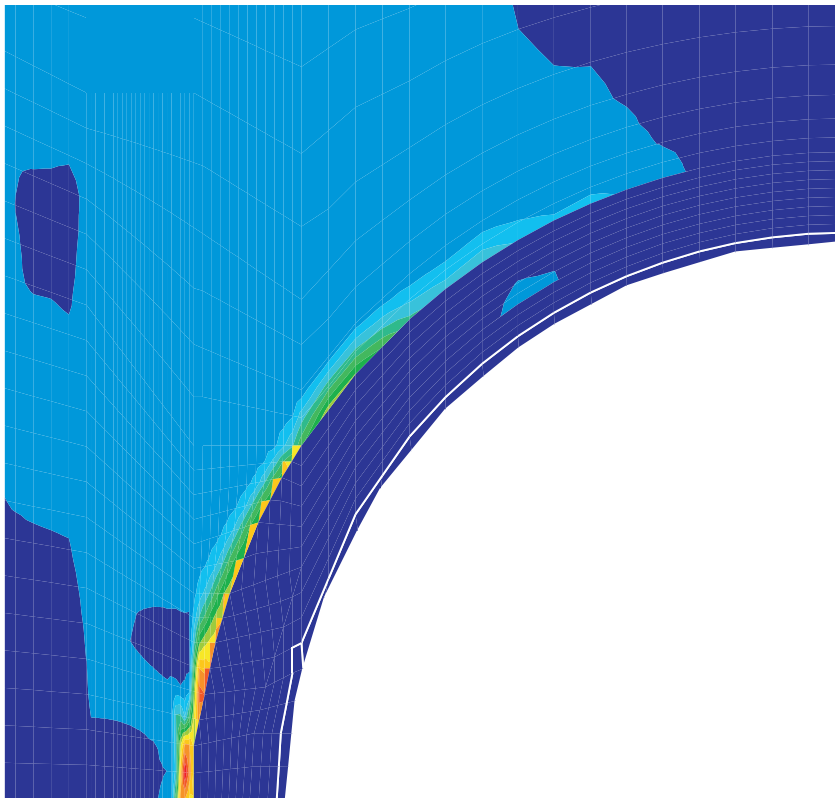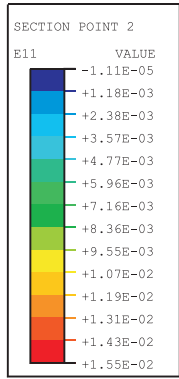
Figure 7-15. Liner Hoop Strains, Posttest Analysis Case A, at 3.2 Pd

P = 3.5 Pd

SECTION POINT 2

E11   VALUE
    -1.55E-05
    +1.77E-03
    +3.56E-03
    +5.35E-03
    +7.13E-03
    +8.92E-03
    +1.07E-02
    +1.25E-02
    +1.43E-02
    +1.61E-02
    +1.79E-02
    +1.96E-02
    +2.14E-02
    +2.32E-02
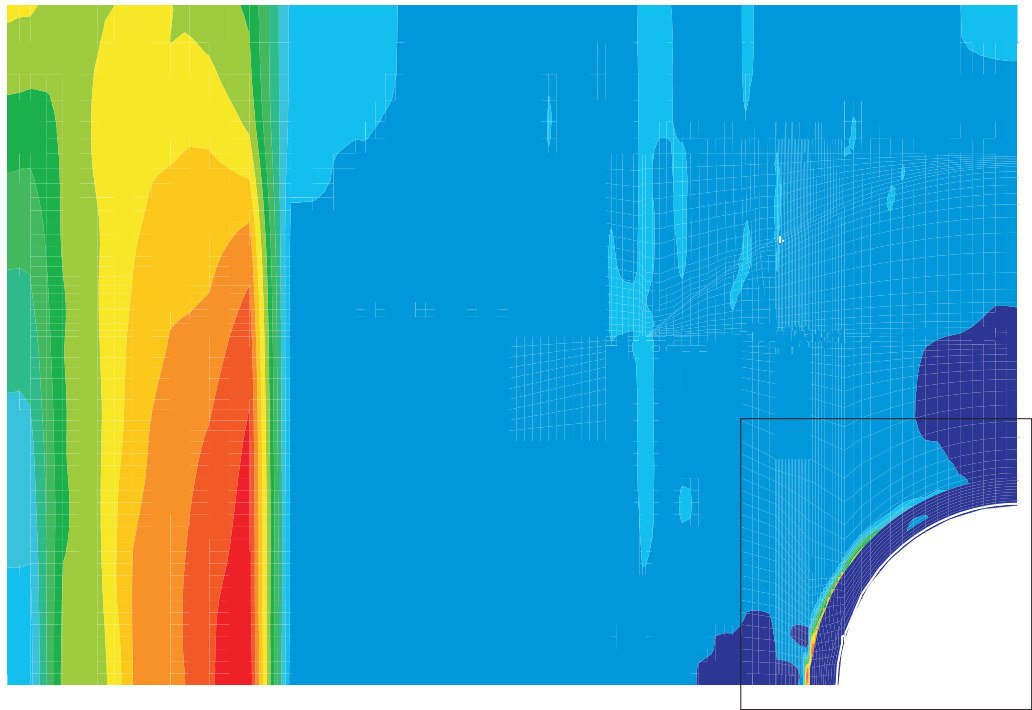
P = 3.6 Pd

SECTION POINT 2

E11   VALUE
    -2.79E-05
    +3.63E-03
    +7.29E-03
    +1.10E-02
    +1.46E-02
    +1.83E-02
    +2.19E-02
    +2.56E-02
    +2.93E-02
    +3.29E-02
    +3.66E-02
    +4.02E-02
    +4.39E-02
    +4.76E-02
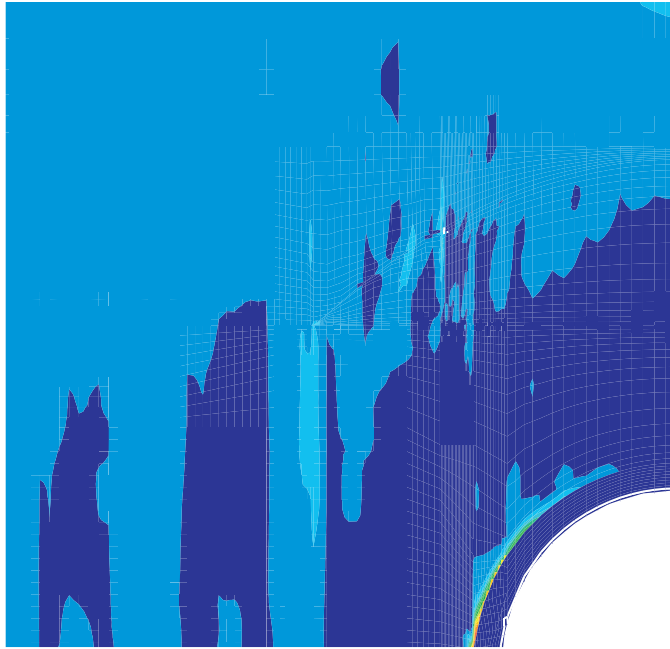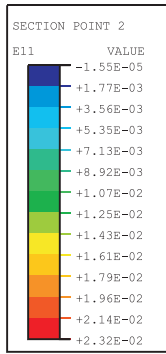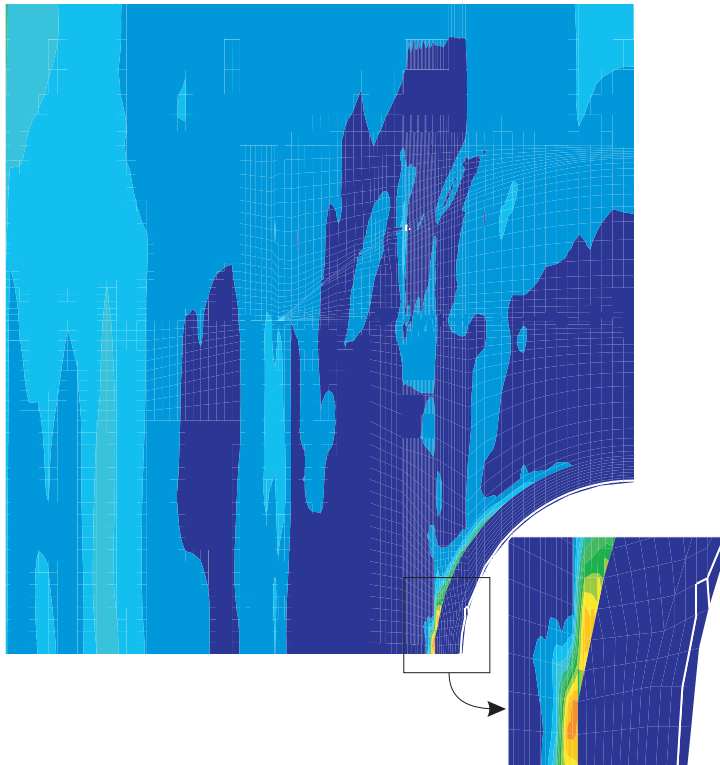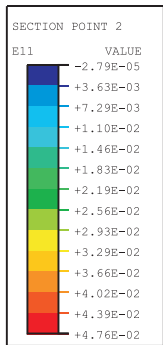
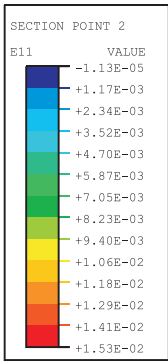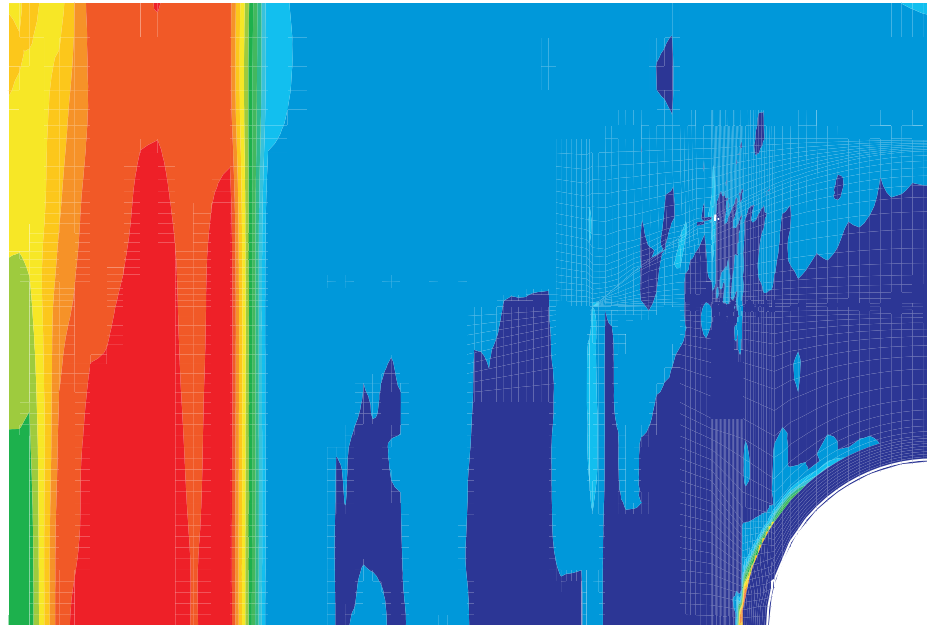Figure 7-16. Liner Hoop Strains, Posttest Analysis Case A, at 3.5 Pd and 3.6 Pd

P = 3.5 Pd

P = 3.6 Pd

P = 3.0 Pd

P = 3.55 Pd
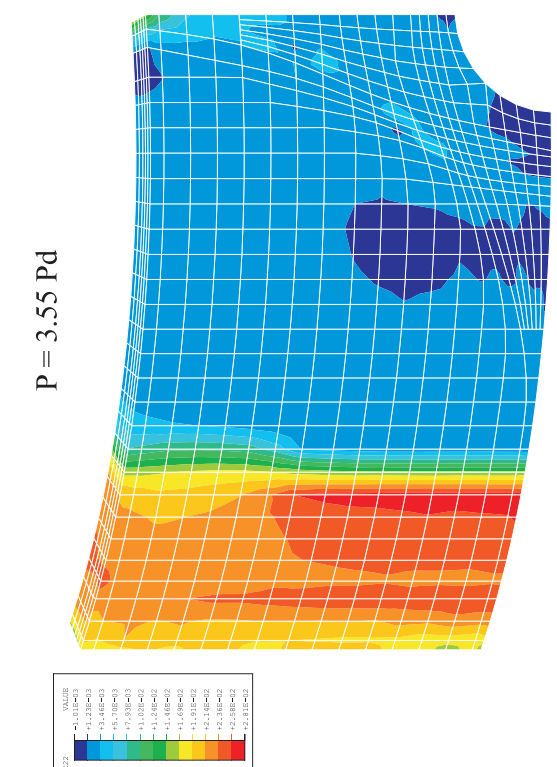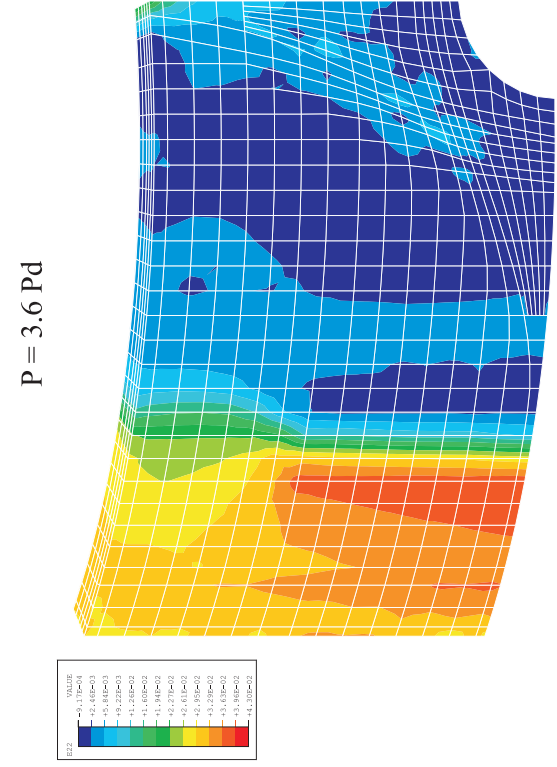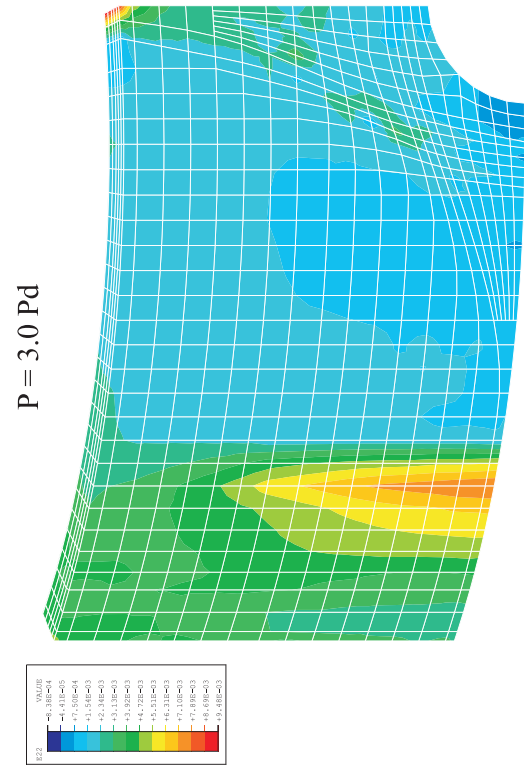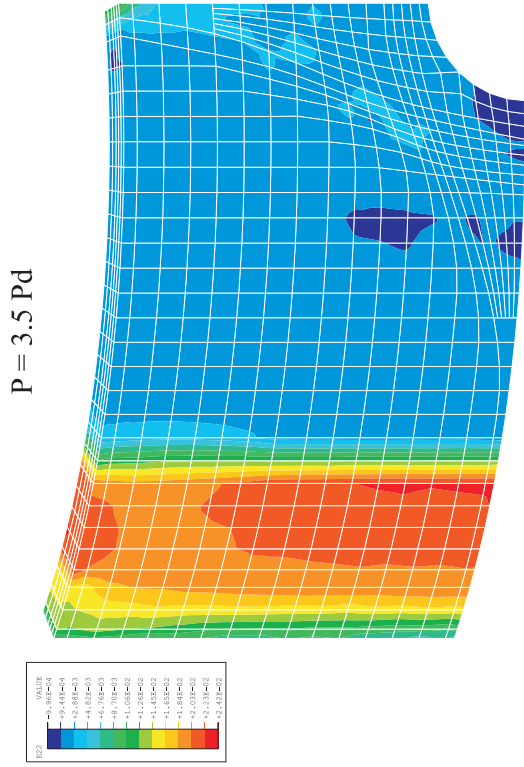
Figure 7-17. Concrete Hoop Strain Contours, Posttest Analysis Case B

Stress, P = 3.0 Pd

SECTION POINT 3
S11 VALUE
+1.39E+05
+1.47E+05
+1.55E+05
+1.63E+05
+1.71E+05
+1.79E+05
+1.87E+05
+1.95E+05
+2.03E+05
+2.11E+05
+2.19E+05
+2.27E+05
+2.35E+05
+2.43E+05

Strain, P = 3.0 Pd

SECTION POINT 3
E11 VALUE
+4.93E-03
+5.29E-03
+5.65E-03
+6.01E-03
+6.38E-03
+6.74E-03
+7.10E-03
+7.46E-03
+7.82E-03
+8.19E-03
+8.55E-03
+8.91E-03
+9.27E-03
+9.63E-03

Stress, Prestress

SECTION POINT 3
S11 VALUE
+7.22E+04
+8.07E+04
+8.92E+04
+9.77E+04
+1.06E+05
+1.15E+05
+1.23E+05
+1.32E+05
+1.40E+05
+1.49E+05
+1.57E+05
+1.65E+05
+1.74E+05
+1.82E+05

Strain, Prestress

SECTION POINT 3
E11 VALUE
+2.55E-03
+2.85E-03
+3.15E-03
+3.45E-03
+3.75E-03
+4.05E-03
+4.35E-03
+4.65E-03
+4.95E-03
+5.25E-03
+5.55E-03
+5.85E-03
+6.15E-03
+6.45E-03

Figure 7-18. Hoop Tendon Stresses and Strains, Posttest Analysis Case B, at Prestress and 3.0 Pd
(Stresses in psi; Multiply by 0.00690 for MPa)

239
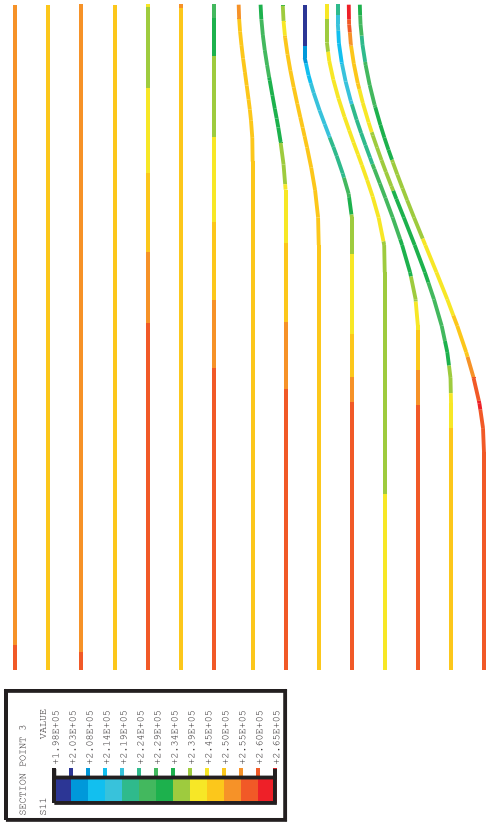
Stress, P = 3.6 Pd
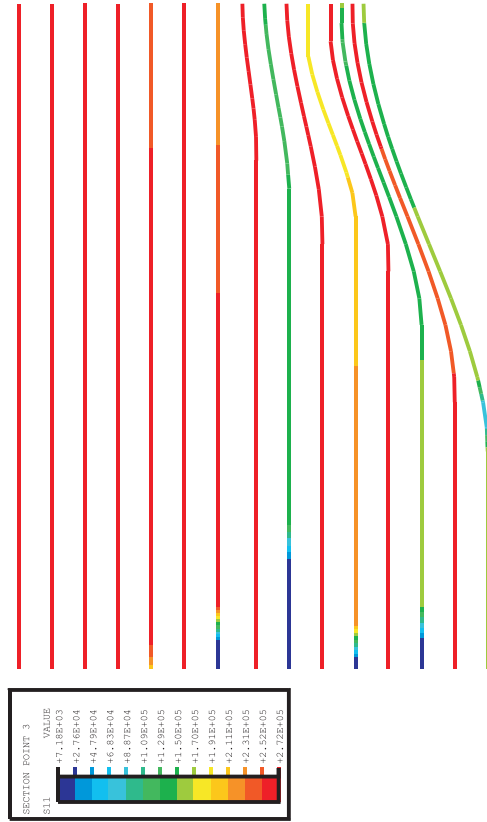
Stress, P = 3.5 Pd
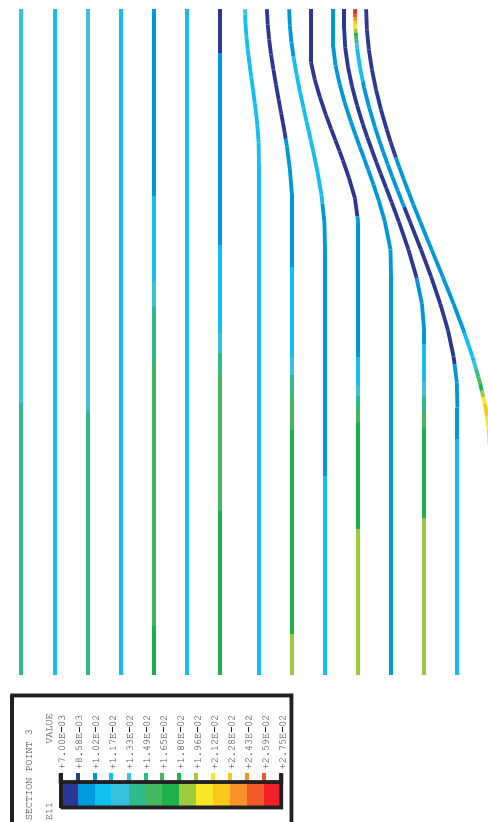
Strain, P = 3.6 Pd

Strain, P = 3.5 Pd
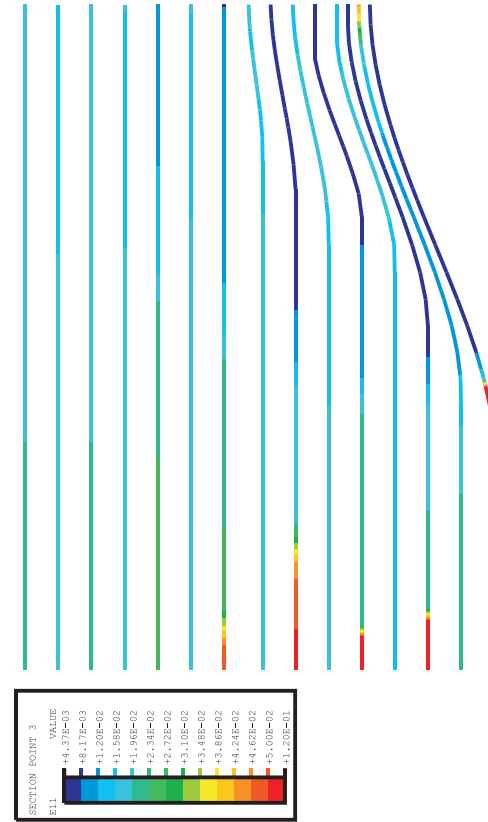
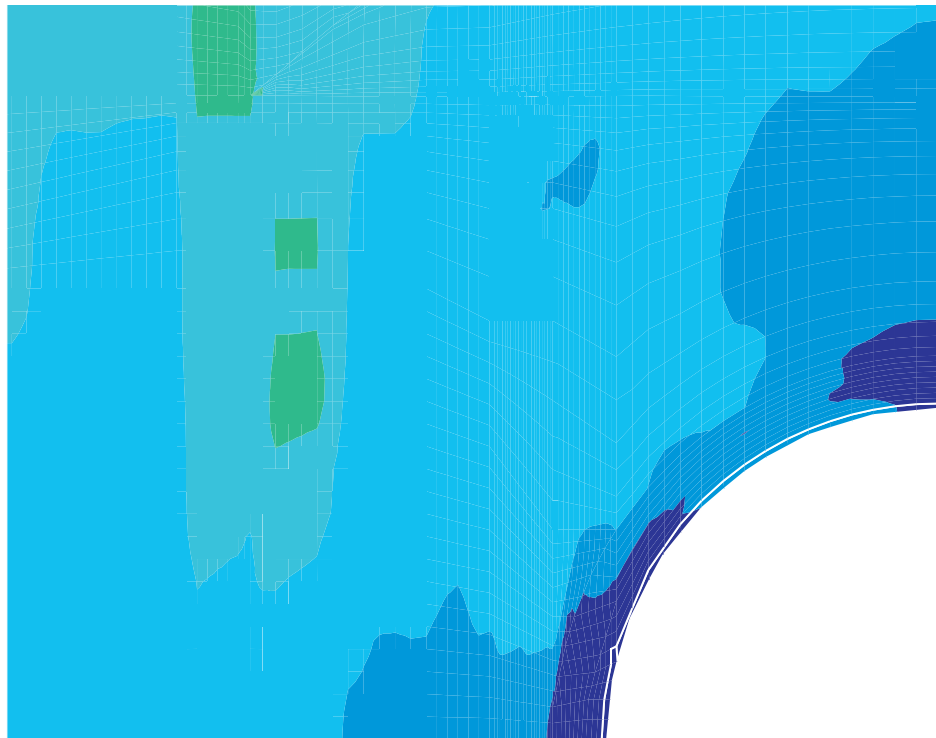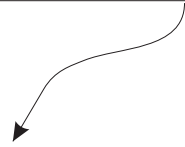Figure 7-19. Hoop Tendon Stresses and Strains, Posttest Analysis Case B, at 3.5 Pd and 3.6 Pd
(Stresses in psi; Multiply by 0.00690 for MPa)

240

SECTION POINT 2

E11   VALUE
-2.47E-05
+5.64E-04
+1.15E-03
+1.74E-03
+2.33E-03
+2.92E-03
+3.51E-03
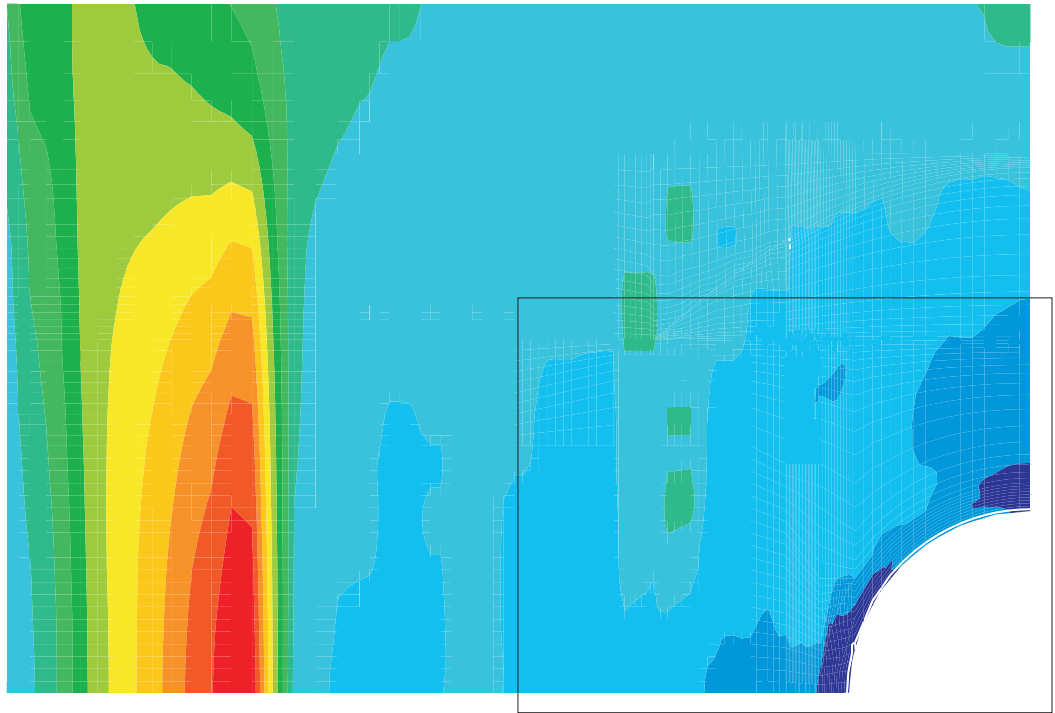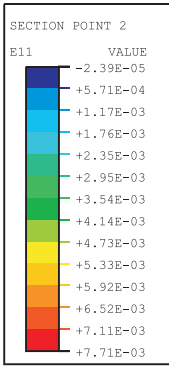+4.10E-03
+4.69E-03
+5.28E-03
+5.87E-03
+6.45E-03
+7.04E-03
+7.63E-03
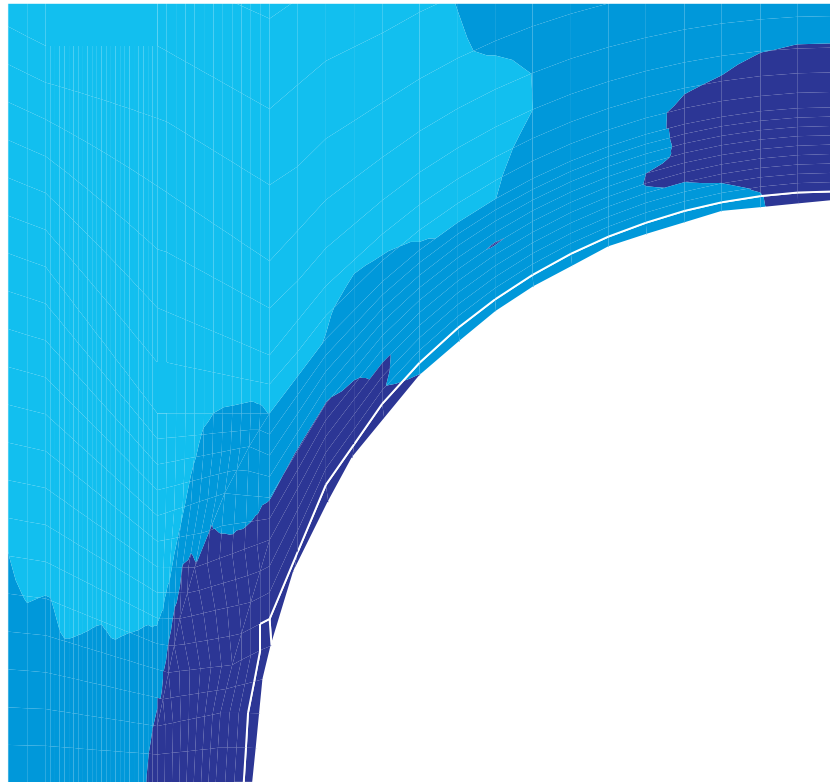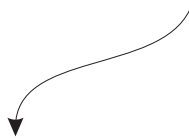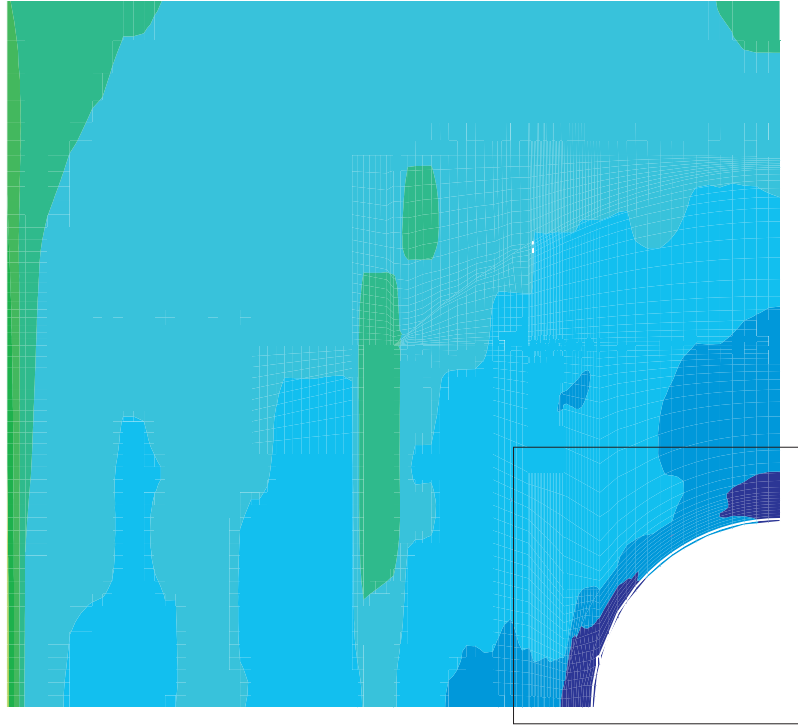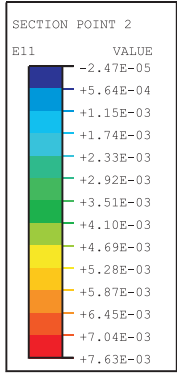
Figure 7-20. Liner Hoop Strains, Posttest Analysis Case B, at 3.0 Pd

SECTION POINT 2

E11   VALUE
    -2.20E-05
    +1.23E-03
    +2.47E-03
    +3.72E-03
    +4.97E-03
    +6.21E-03
    +7.46E-03
    +8.71E-03
    +9.96E-03
    +1.12E-02
    +1.25E-02
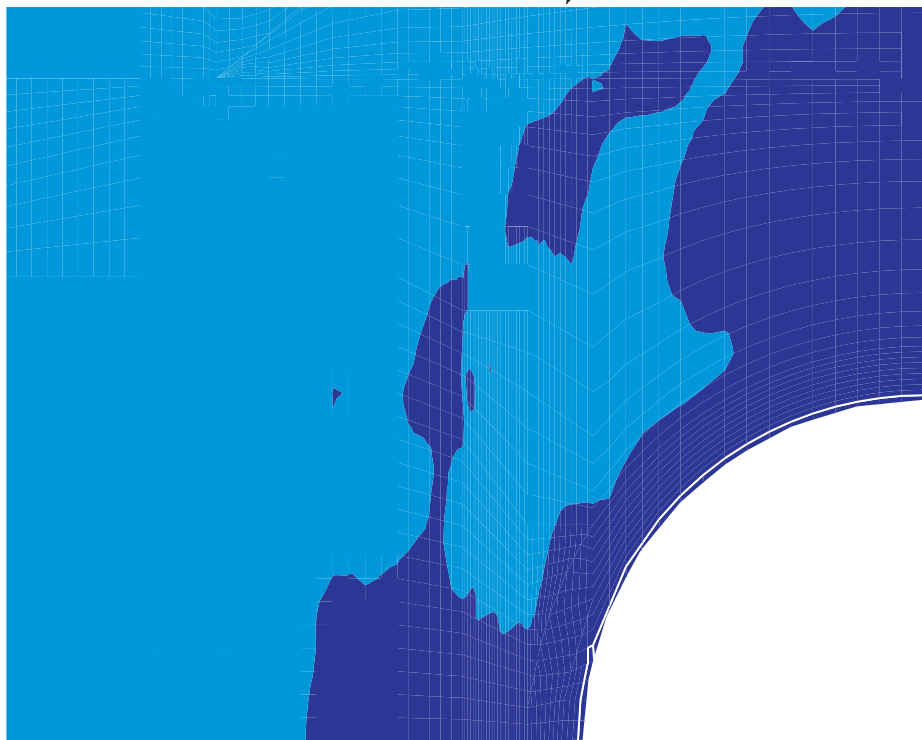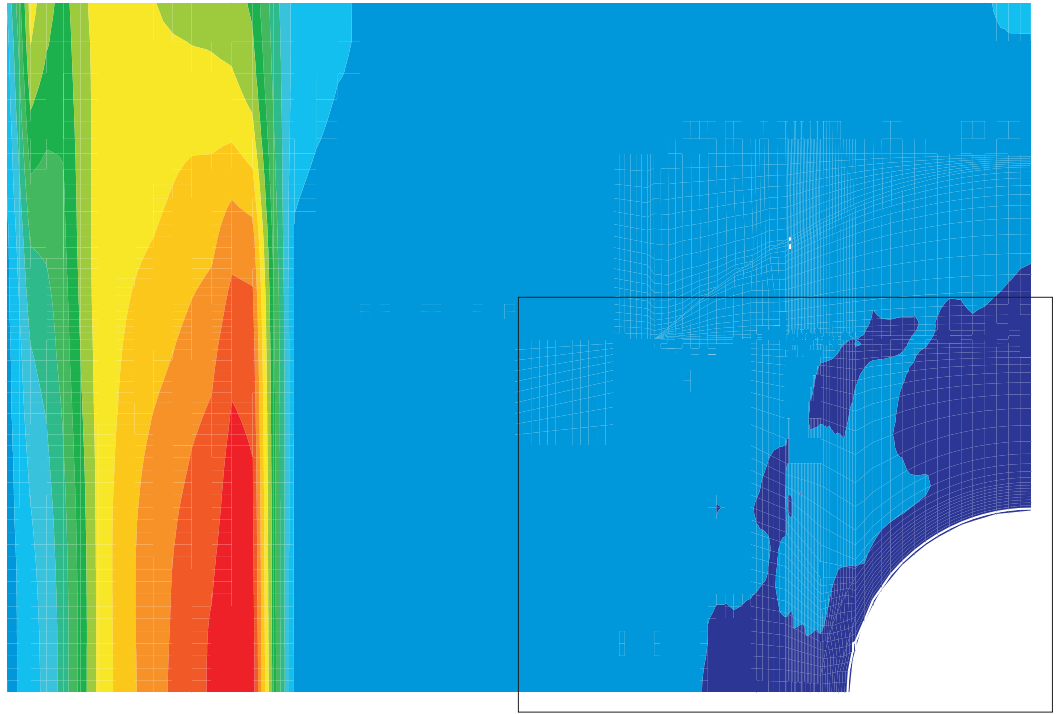   +1.37E-02
    +1.49E-02
    +1.62E-02
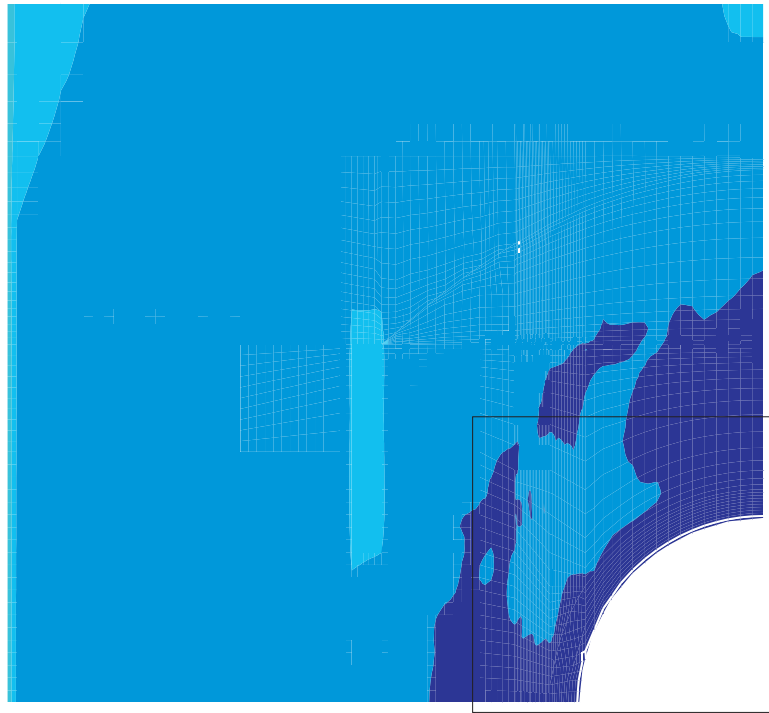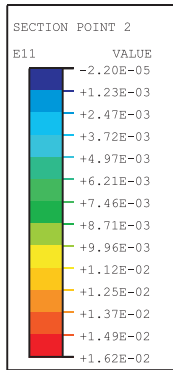
Figure 7-21. Liner Hoop Strains, Posttest Analysis Case B, at 3.2 Pd

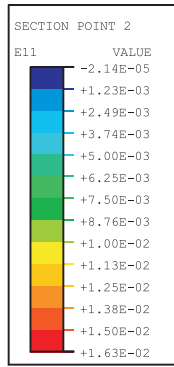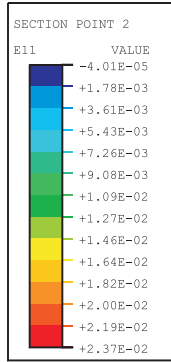P = 3.5 Pd

SECTION POINT 2

E11   VALUE
    -4.12E-05
    +1.83E-03
    +3.71E-03
    +5.58E-03
    +7.46E-03
    +9.33E-03
    +1.12E-02
    +1.31E-02
    +1.50E-02
    +1.68E-02
    +1.87E-02
    +2.06E-02
    +2.24E-02
    +2.43E-02

P = 3.6 Pd

SECTION POINT 2

E11   VALUE
    -7.33E-05
    +3.09E-03
    +6.26E-03
    +9.42E-03
    +1.26E-02
    +1.58E-02
    +1.89E-02
    +2.21E-02
    +2.53E-02
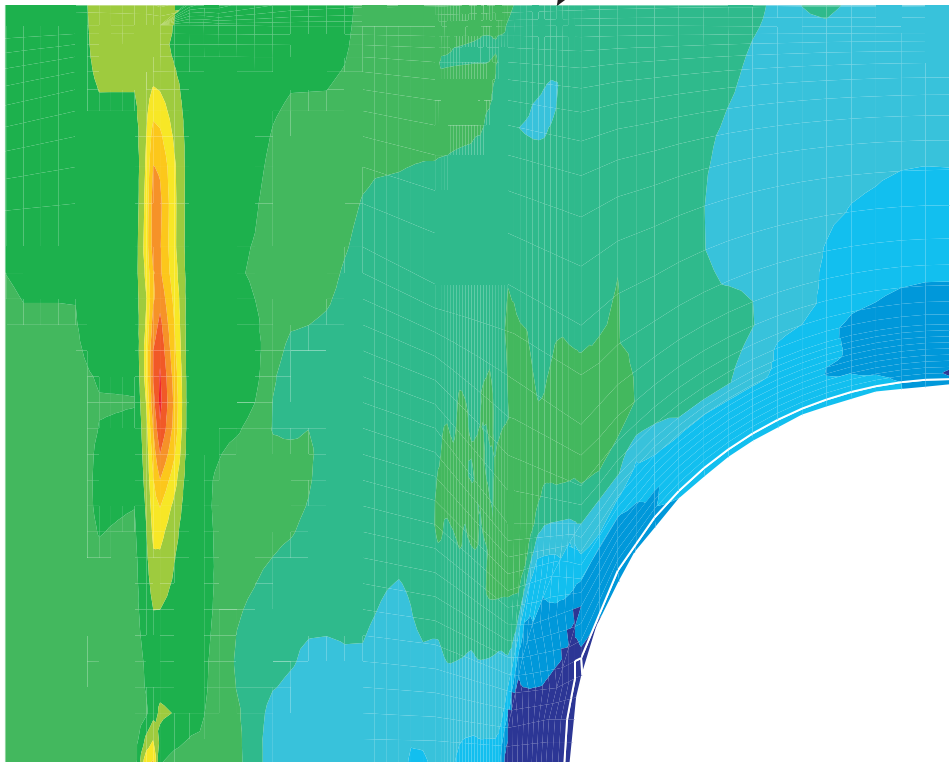   +2.84E-02
    +3.16E-02
    +3.47E-02
    +3.79E-02
    +4.11E-02
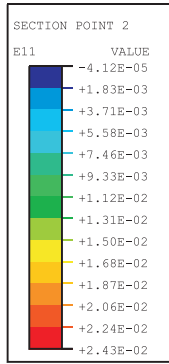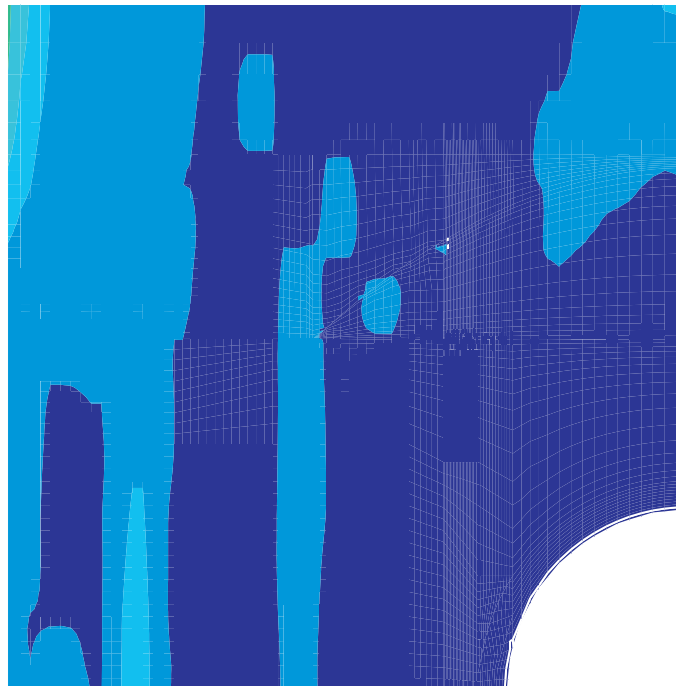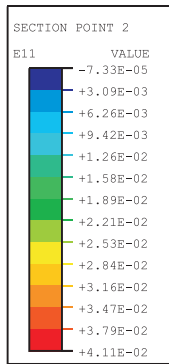
Figure 7-22. Liner Hoop Strains, Posttest Analysis Case B, at 3.5 Pd and 3.6 Pd

243

Top View
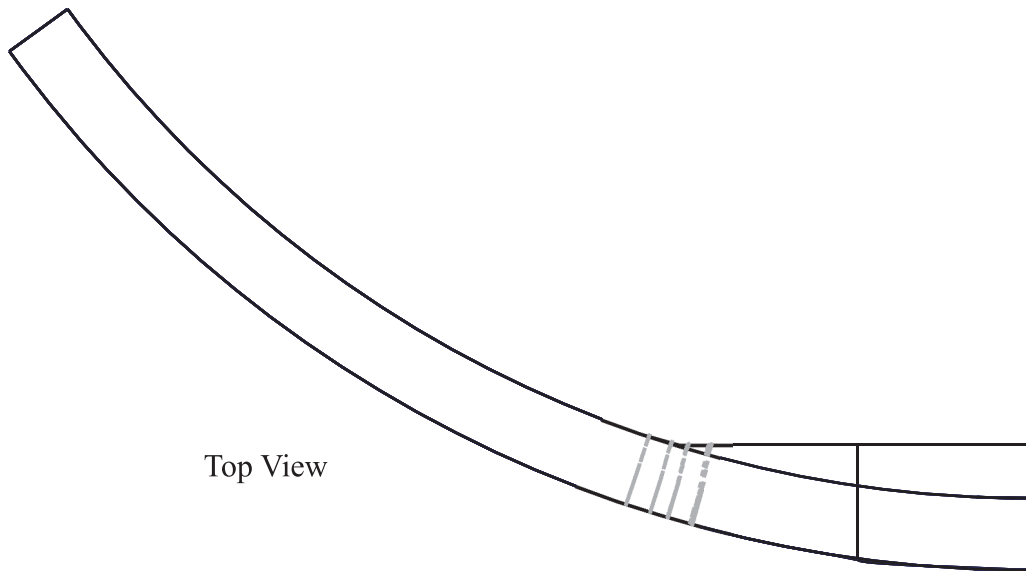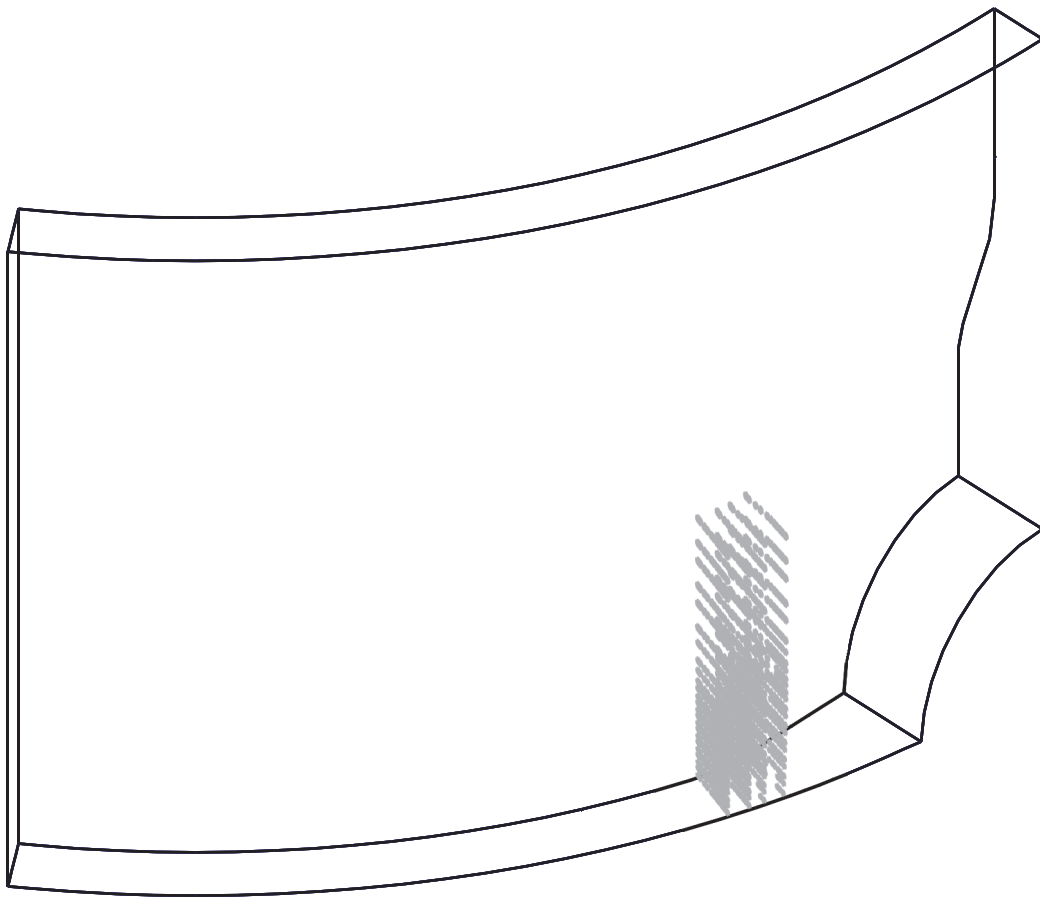
Figure 7-23. Pre-Cracking along Edge of E/H Embossment

P = 3.5 Pd
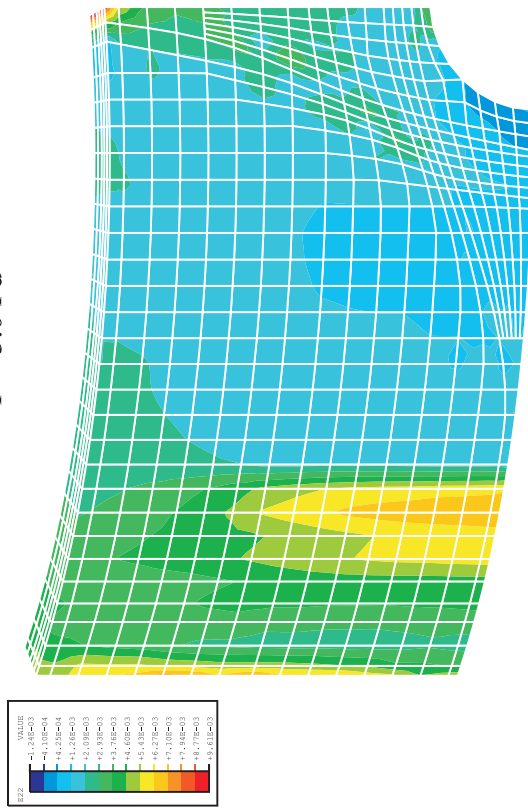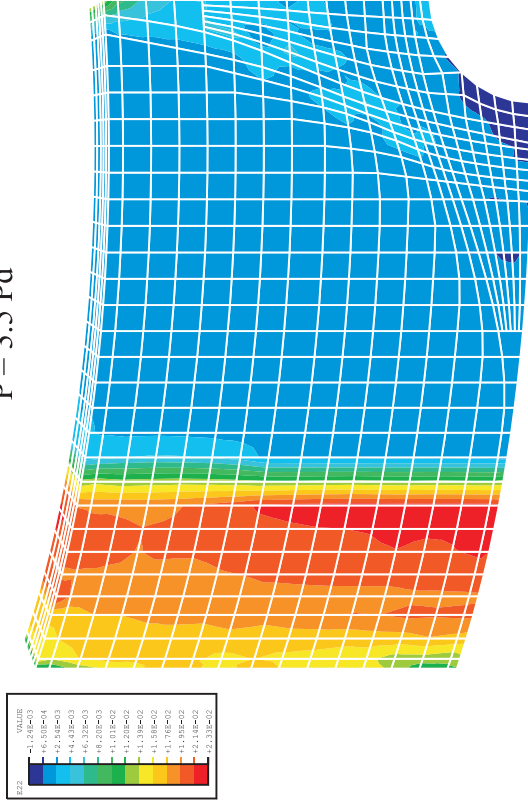
P = 3.6 Pd

P = 3.0 Pd

P = 3.55 Pd

Figure 7-24. Concrete Hoop Strain Contours, Posttest Analysis Case C

245

Stress, P = 3.0 Pd
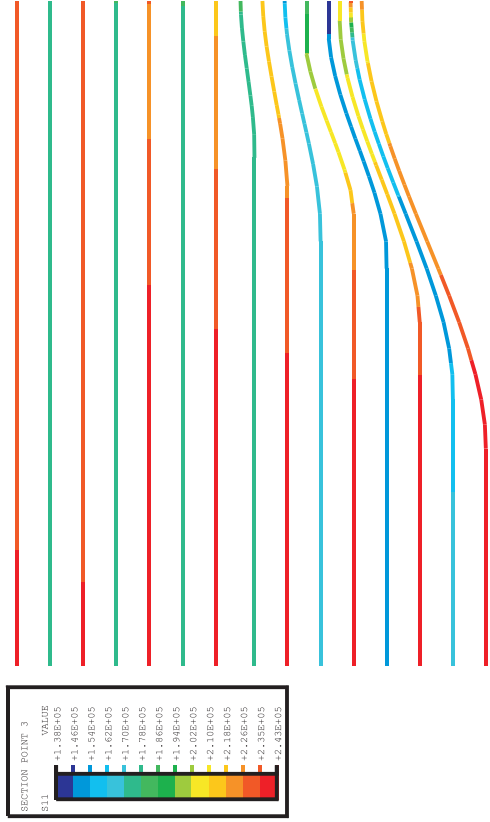
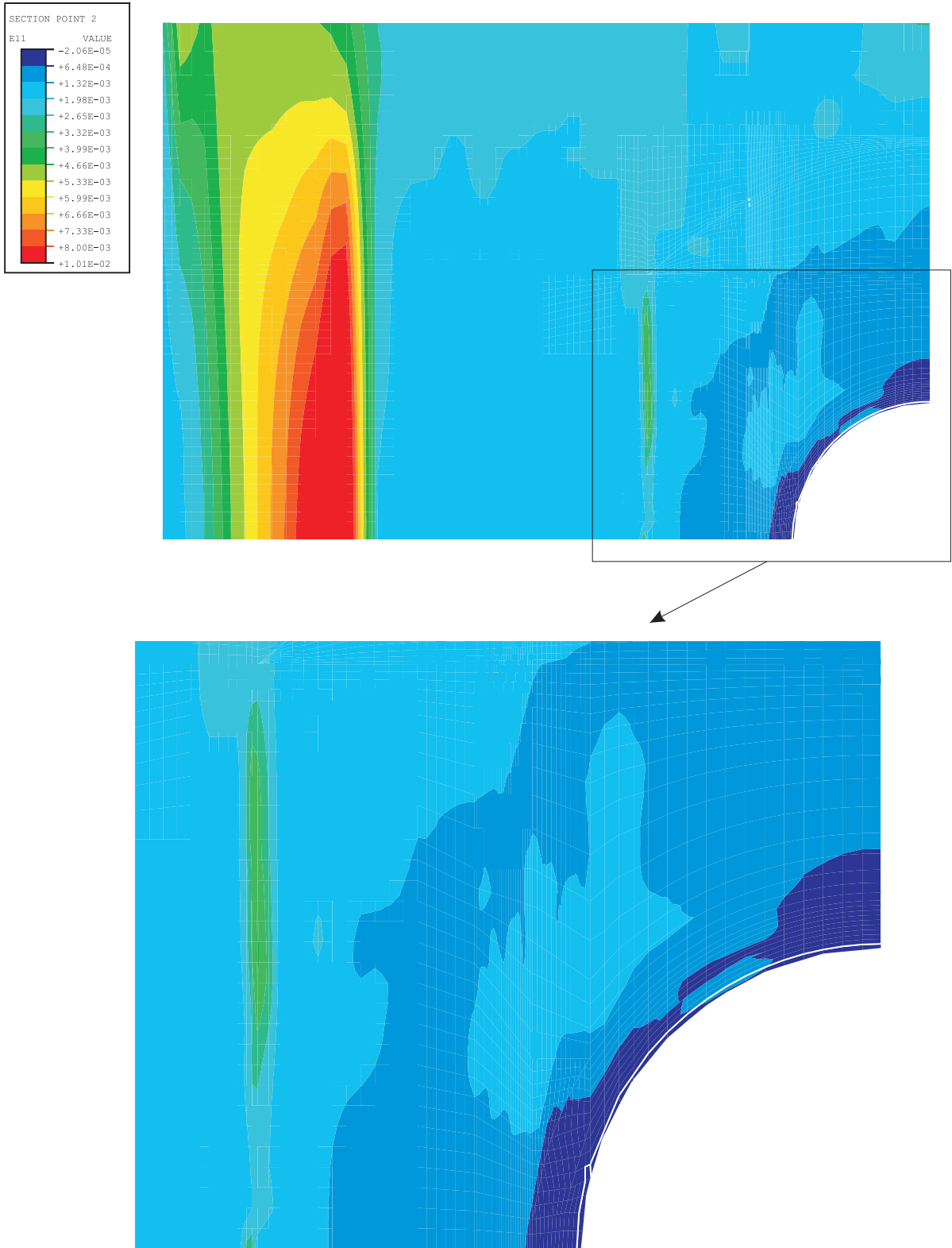Strain, P = 3.0 Pd

Stress, Prestress
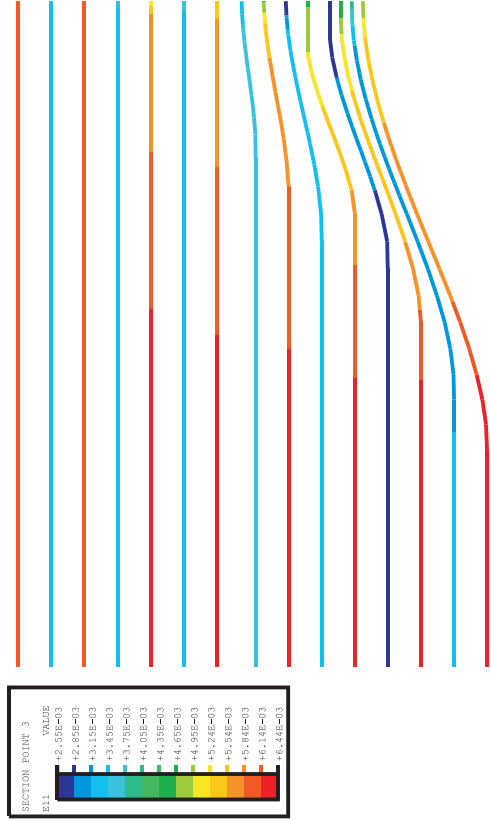
Strain, Prestress

Figure 7-25. Hoop Tendon Stresses and Strains, Posttest Analysis Case C, at Prestress and 3.0 Pd
(Stresses in psi; Multiply by 0.00690 for MPa)

246

Stress, P = 3.6 Pd

Stress, P = 3.5 Pd

Strain, P = 3.6 Pd

Strain, P = 3.5 Pd
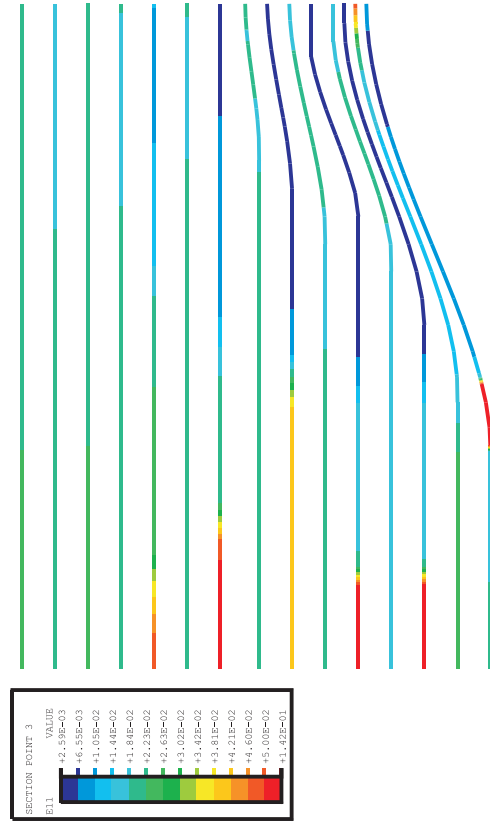
Figure 7-26. Hoop Tendon Stresses and Strains, Posttest Analysis Case C, at 3.5 Pd and 3.6 Pd
(Stresses in psi; Multiply by 0.00690 for MPa)

SECTION POINT 2

E11   VALUE
-9.08E-06
+8.29E-04
+1.67E-03
+2.50E-03
+3.34E-03
+4.18E-03
+5.02E-03
+5.85E-03
+6.69E-03
+7.53E-03
+8.37E-03
+9.20E-03
+1.00E-02
+1.09E-02

Figure 7-27. Liner Hoop Strains, Posttest Analysis Case C, at 3.0 Pd

SECTION POINT 2

E11   VALUE
-1.13E-05
+1.17E-03
+2.34E-03
+3.52E-03
+4.70E-03
+5.87E-03
+7.05E-03
+8.23E-03
+9.40E-03
+1.06E-02
+1.18E-02
+1.29E-02
+1.41E-02
+1.53E-02
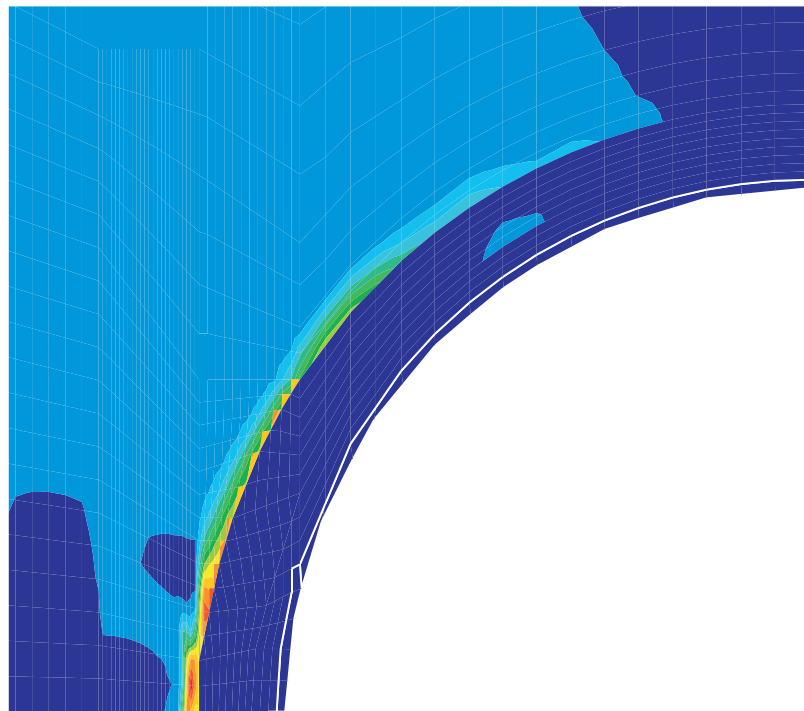
Figure 7-28. Liner Hoop Strains, Posttest Analysis Case C, at 3.2 Pd

P = 3.5 Pd
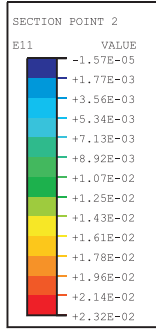
P = 3.6 Pd
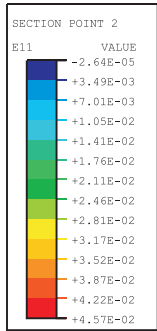
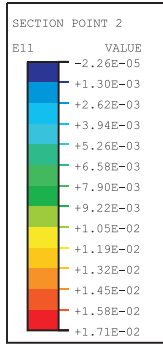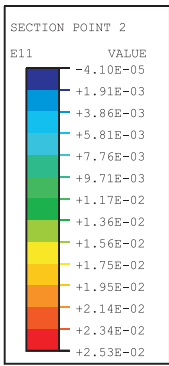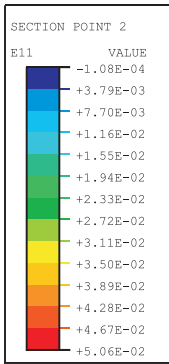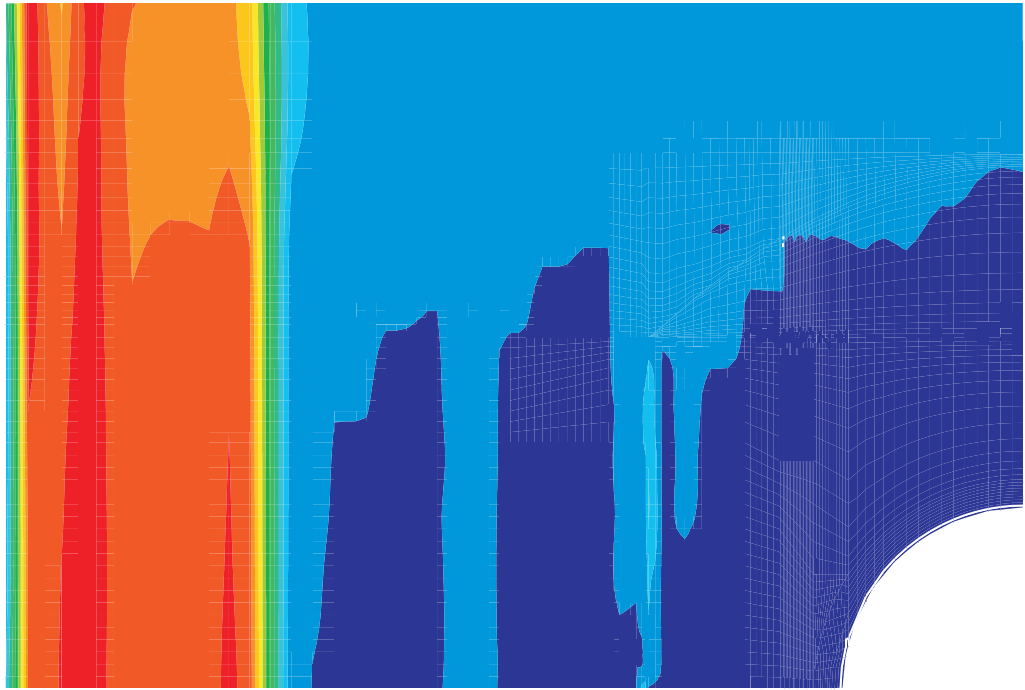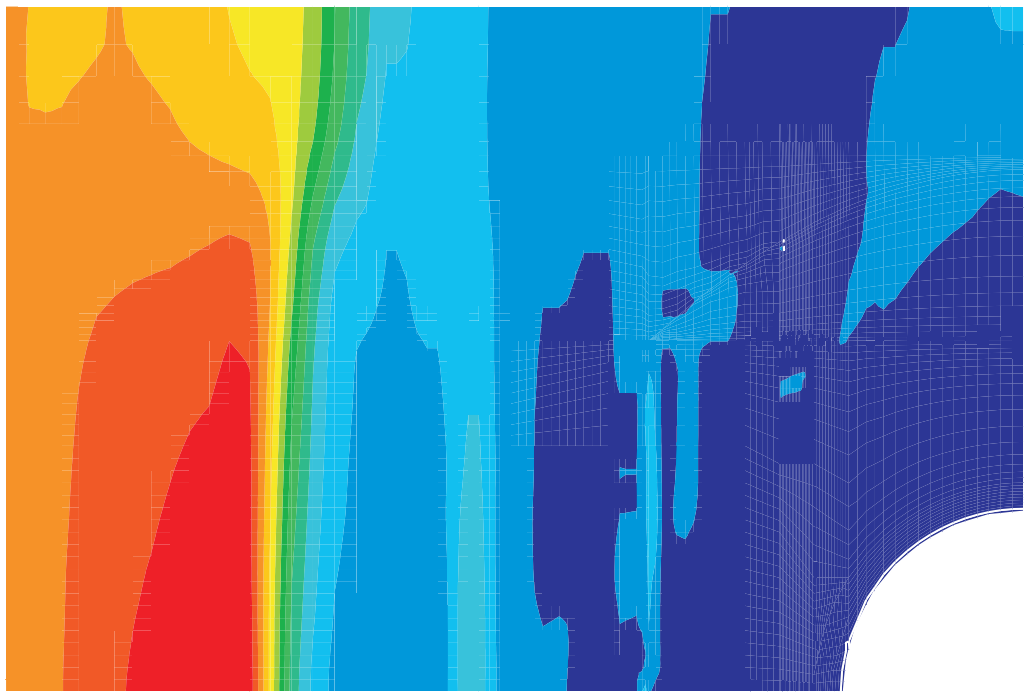Figure 7-29. Liner Hoop Strains, Posttest Analysis Case C, at 3.5 Pd and 3.6 Pd

(5-13A) (-12) (-12A) (5-11B) (5-11A)

(4-10A) 781.2 4-9A 561.9

3153.2 43.0 3153.2

C 56.2

6∅450.45= 793.8 375.4 75.1 6∅450.45=
2702.7 2702.7

.1

324° (4-10B) (4-9B)

(3-11A) 3-10A 188.9

3242.4 3257.3

-11B 1

200∅150.15= 121.1 9∅150.15= 4∅450.45= 375.4
3003 1351.4 1801.8

(3-11C) 29.1 (3-10B) 75.1

(3-11D) ↓D 3-10C

E/H EL.4675

(2-11A) 2-10A 2-9A

(2-11C) 2-10B 2-9B

(2-11D)

(2-11E) 2-10C B↓ ↓B 2-9C

1

C
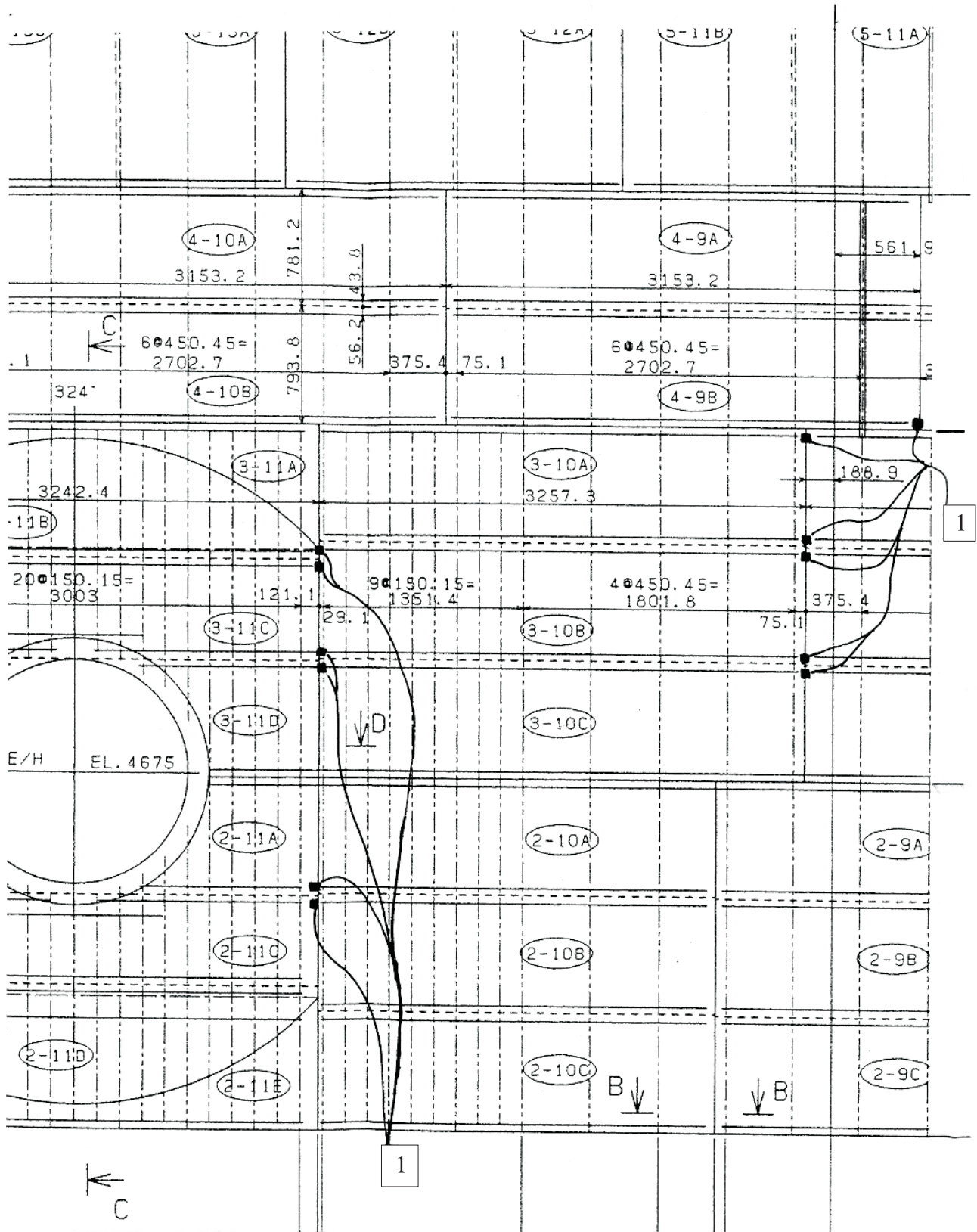
Figure 7-30. Strain Concentration Type 1 Near 270 Degrees Buttress and Near E/H

251
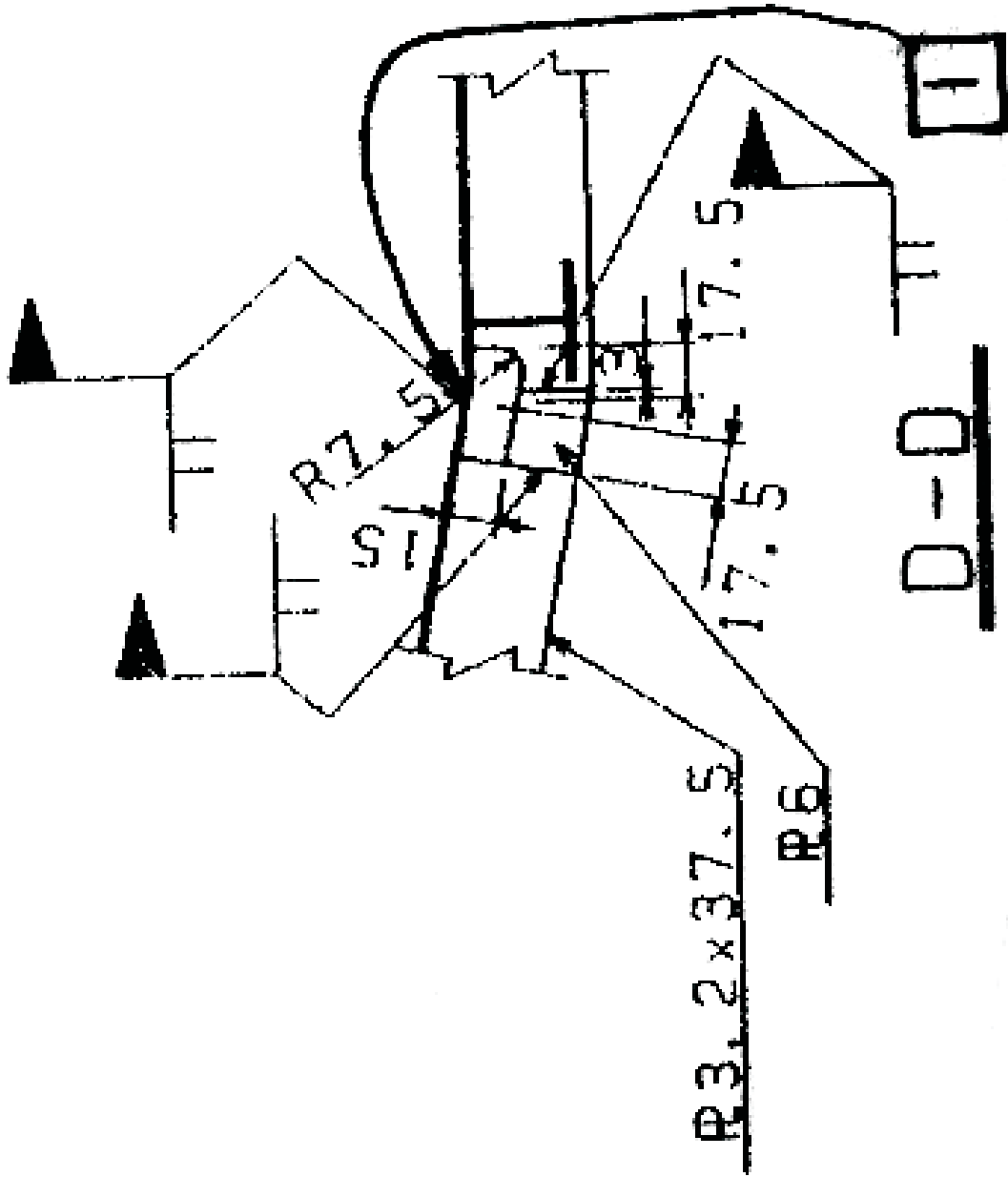
Figure 7-31. Liner Strain Concentration Rat-Hole Detail

252

SECTION POINT 2

E11	VALUE
	-2.39E-05
	+5.71E-04
	+1.17E-03
	+1.76E-03
	+2.35E-03
	+2.95E-03
	+3.54E-03
	+4.14E-03
	+4.73E-03
	+5.33E-03
	+5.92E-03
	+6.52E-03
	+7.11E-03
	+7.71E-03

Figure 7-32. Liner Hoop Strains, Posttest Analysis Case D, at 3.0 Pd

253

Figure 7-33. Liner Hoop Strains, Posttest Analysis Case D, at 3.2 Pd

P = 3.5 Pd

SECTION POINT 2
E11   VALUE
    -4.01E-05
    +1.78E-03
    +3.61E-03
    +5.43E-03
    +7.26E-03
    +9.08E-03
    +1.09E-02
    +1.27E-02
    +1.46E-02
    +1.64E-02
    +1.82E-02
    +2.00E-02
    +2.19E-02
    +2.37E-02

P = 3.6 Pd

SECTION POINT 2
E11   VALUE
    -6.71E-05
    +2.98E-03
    +6.02E-03
    +9.07E-03
    +1.21E-02
    +1.52E-02
    +1.82E-02
    +2.12E-02
    +2.43E-02
    +2.73E-02
    +3.04E-02
    +3.34E-02
    +3.65E-02
    +3.95E-02
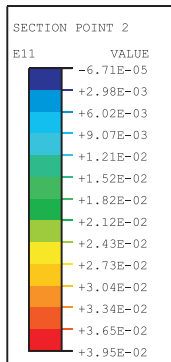
Figure 7-34. Liner Hoop Strains, Posttest Analysis Case D, at 3.5 Pd and 3.6 Pd
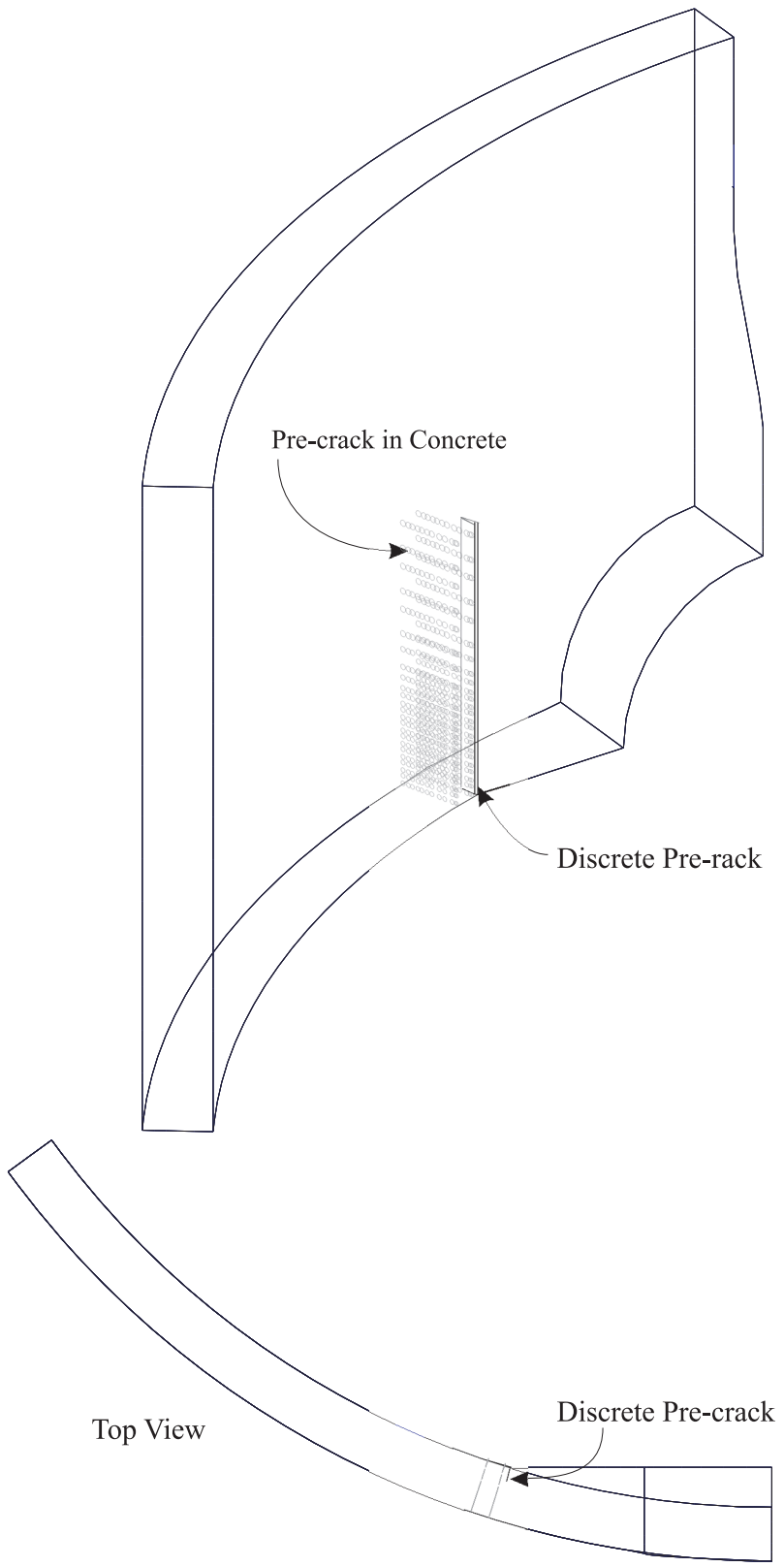
Figure 7-35. Illustration of Case E, Discrete Pre-Crack

256
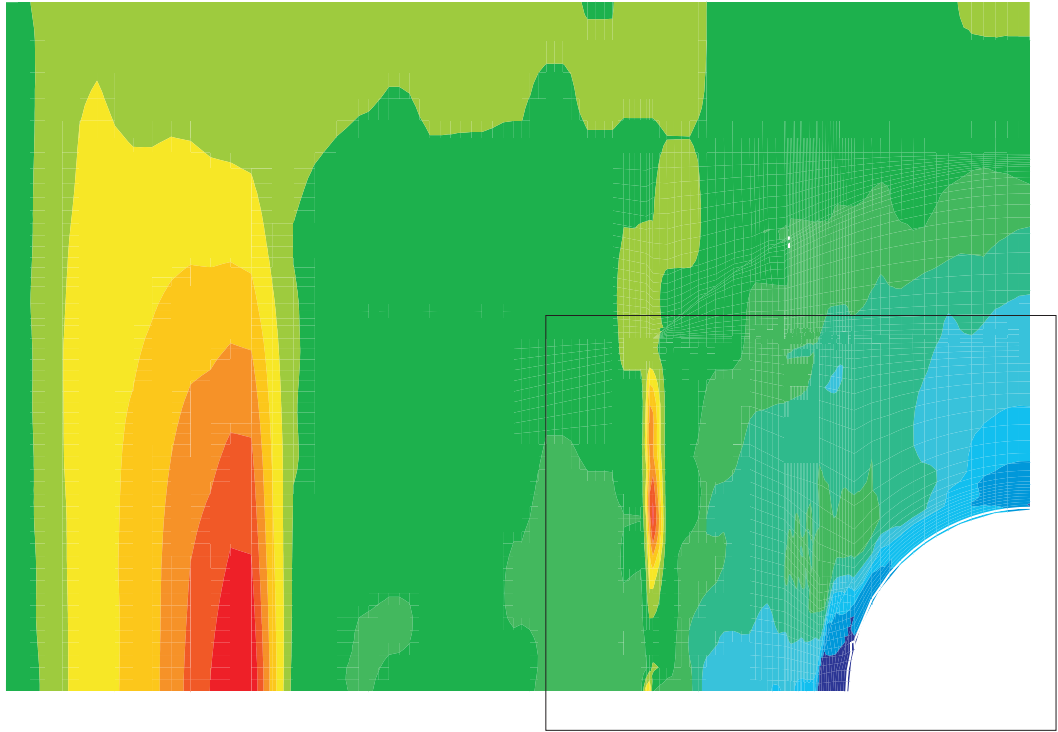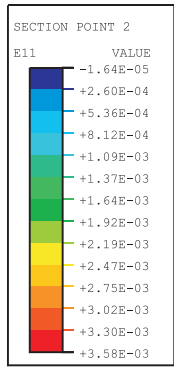
Figure 7-36. Liner Hoop Strains, Posttest Analysis Case E, at 2.8 Pd

SECTION POINT 2

E11   VALUE
-2.06E-05
+6.48E-04
+1.32E-03
+1.98E-03
+2.65E-03
+3.32E-03
+3.99E-03
+4.66E-03
+5.33E-03
+5.99E-03
+6.66E-03
+7.33E-03
+8.00E-03
+1.01E-02

Figure 7-37. Liner Hoop Strains, Posttest Analysis Case E, at 3.0 Pd

SECTION POINT 2

E11   VALUE
        -2.26E-05
        +1.30E-03
        +2.62E-03
        +3.94E-03
        +5.26E-03
        +6.58E-03
        +7.90E-03
        +9.22E-03
        +1.05E-02
        +1.19E-02
        +1.32E-02
        +1.45E-02
        +1.58E-02
        +1.71E-02
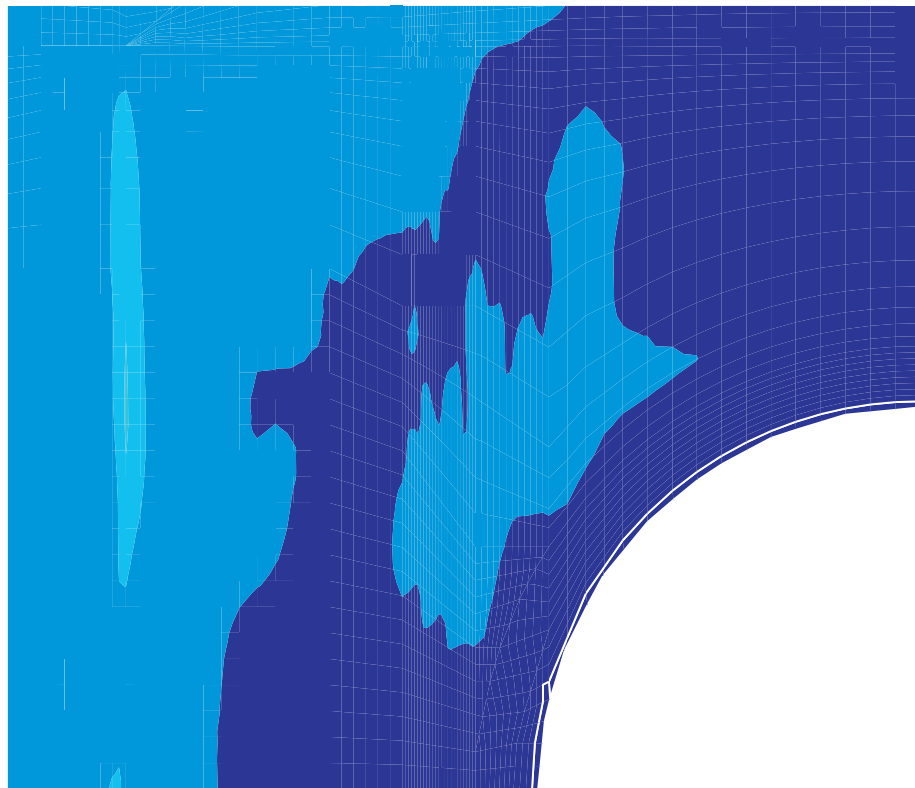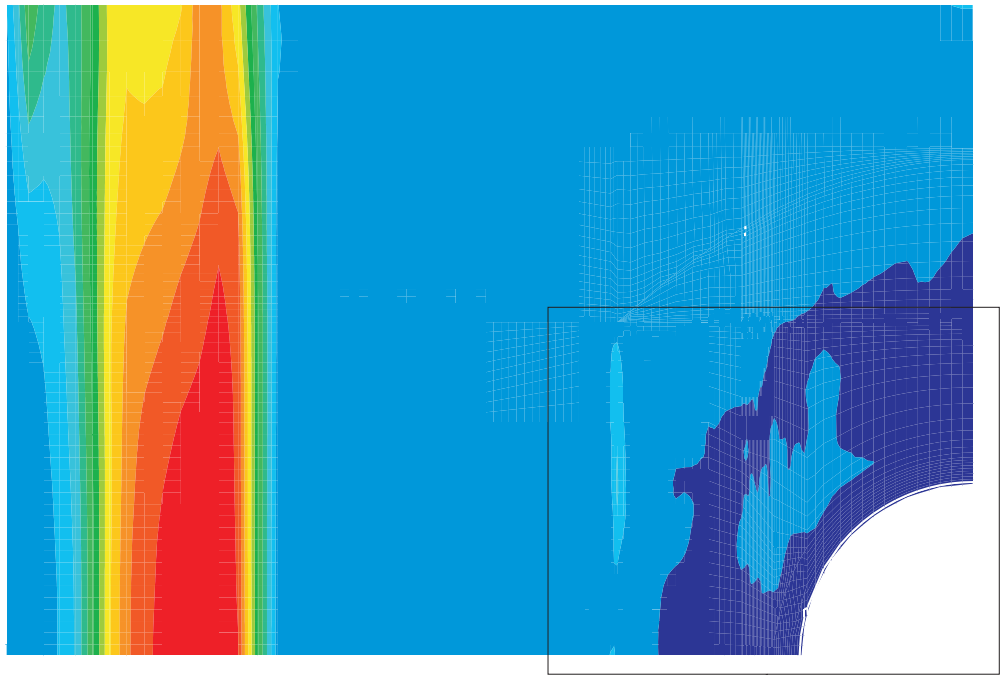
Figure 7-38. Liner Hoop Strains, Posttest Analysis Case E, at 3.2 Pd

259

P = 3.5 Pd

P = 3.6 Pd

Figure 7-39. Liner Hoop Strains, Posttest Analysis Case E, at 3.5 Pd and 3.6 Pd
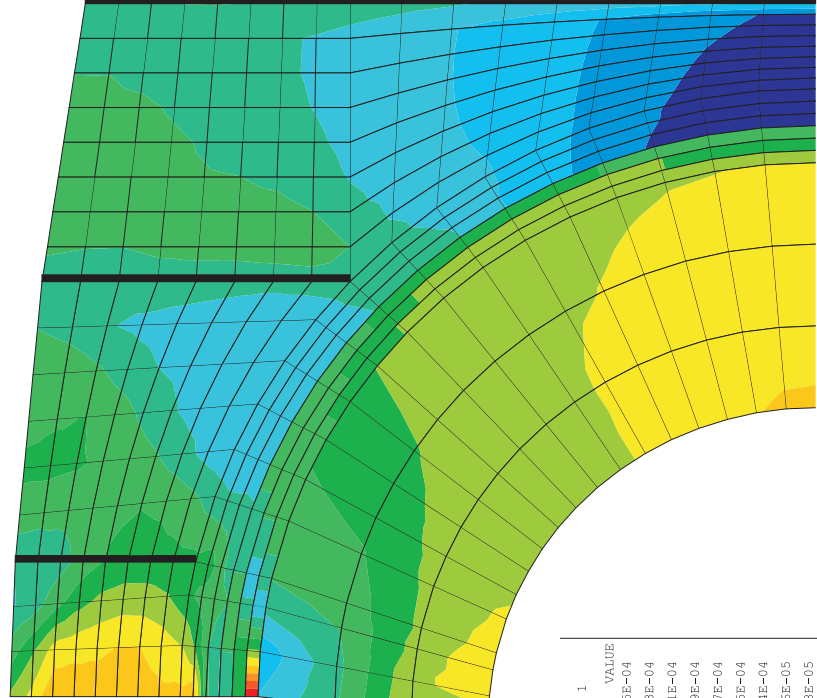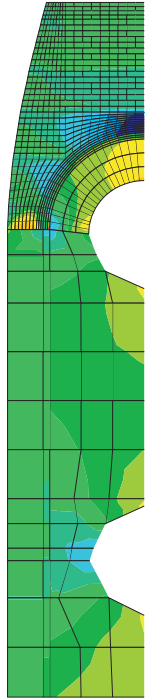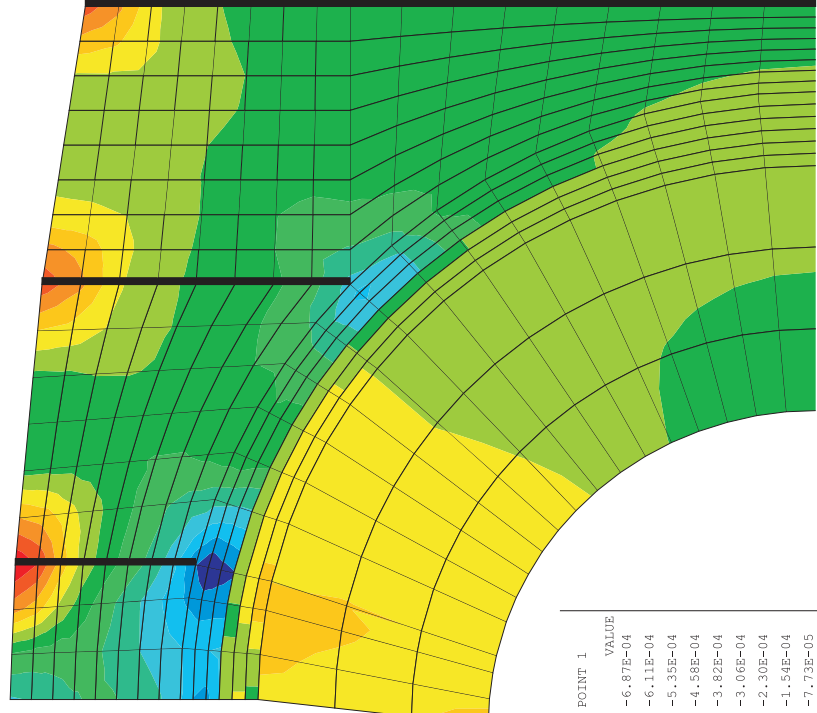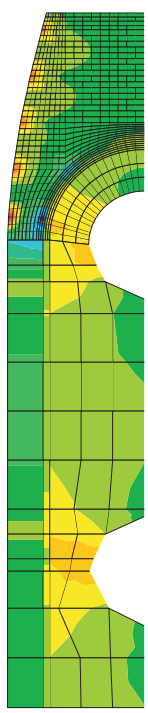
Figure 7-40. Hoop (Left) and Meridional (Right) Strains for Posttest M/S Analysis at Prestress
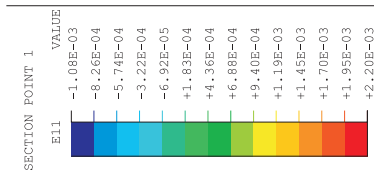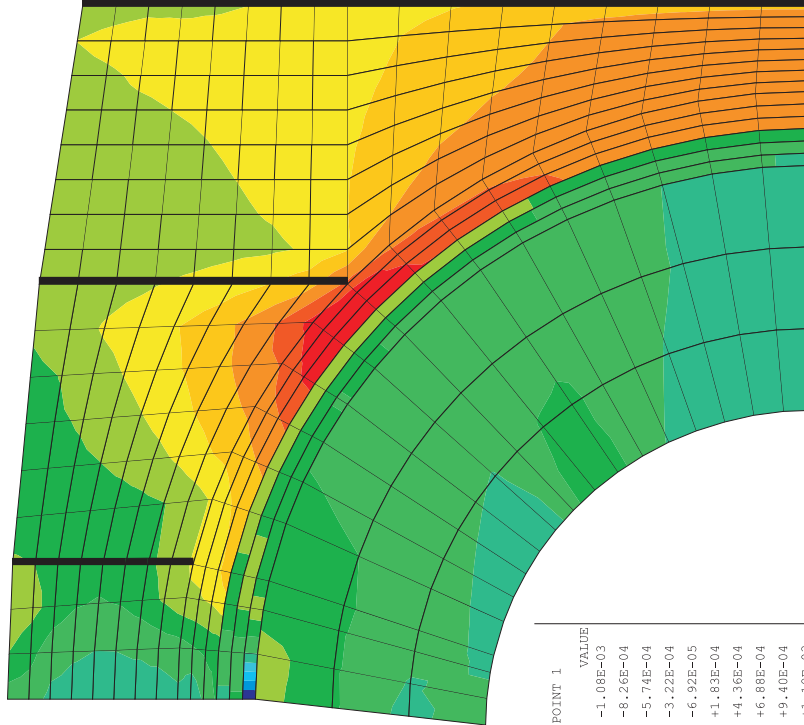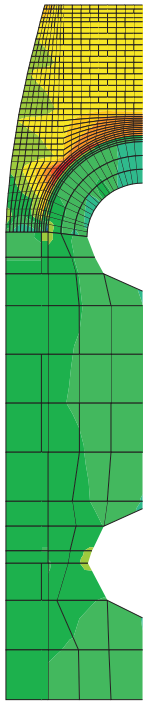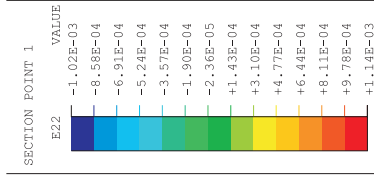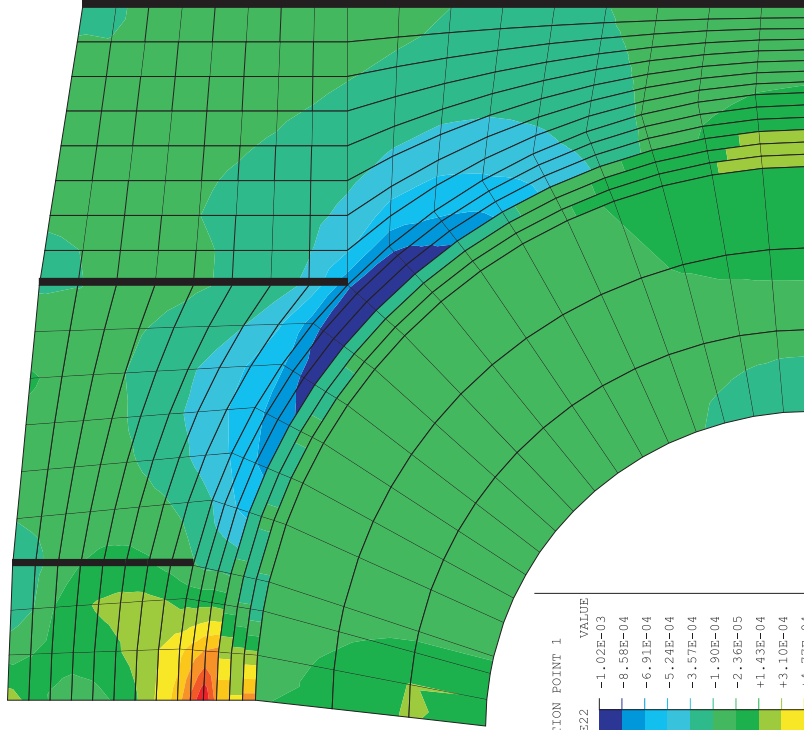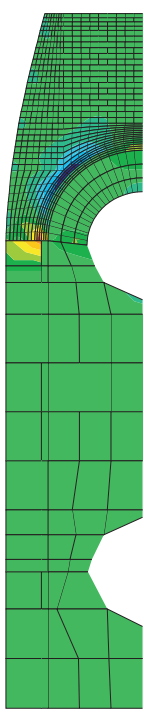
Figure 7-41. Hoop (Left) and Meridional (Right) Strains for Posttest M/S Analysis at P = 2.0 Pd
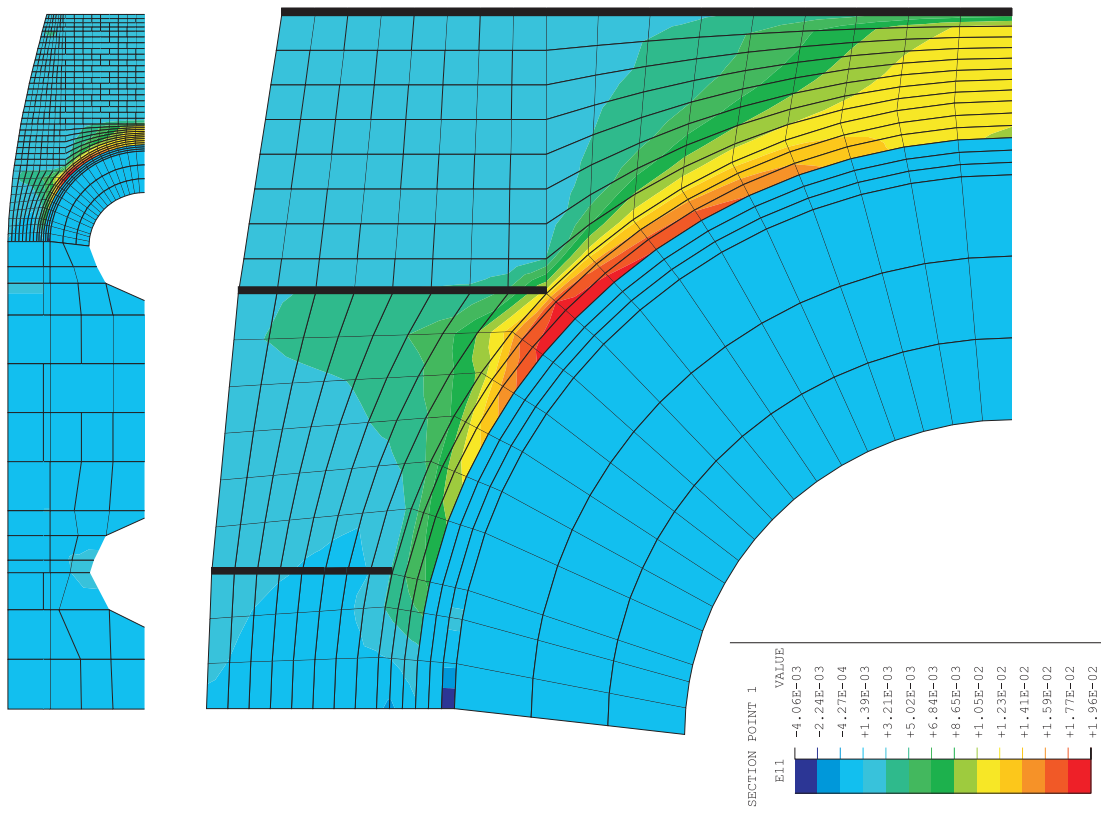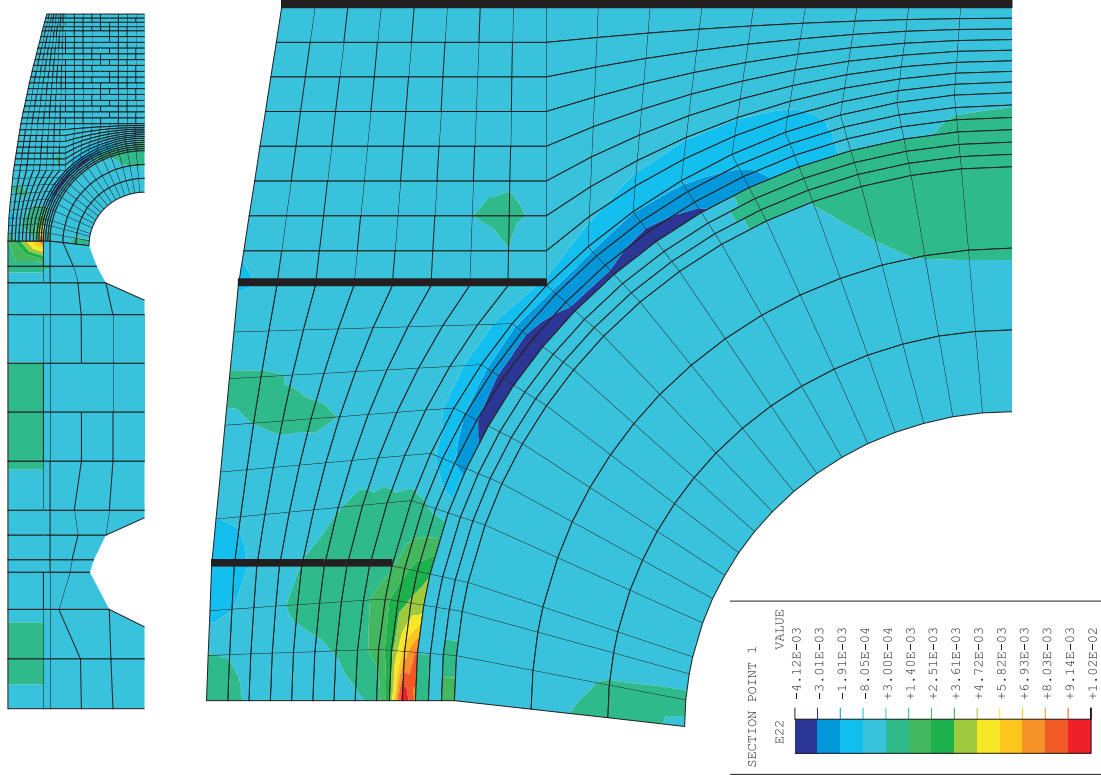
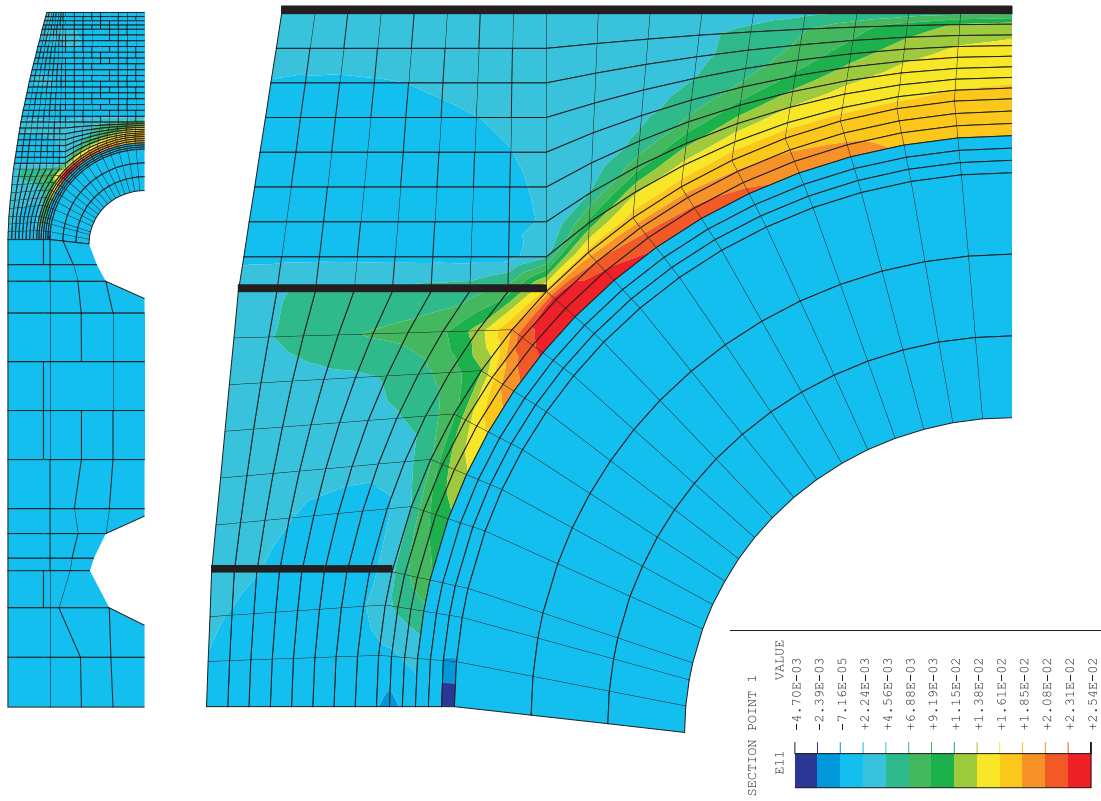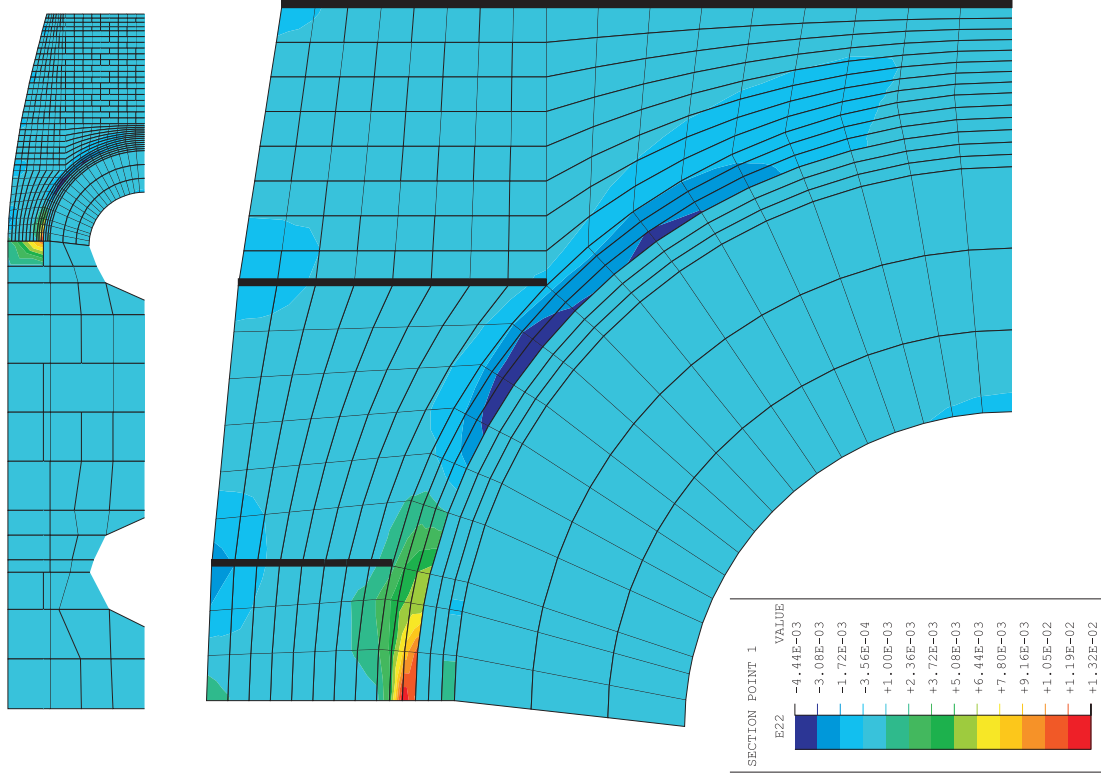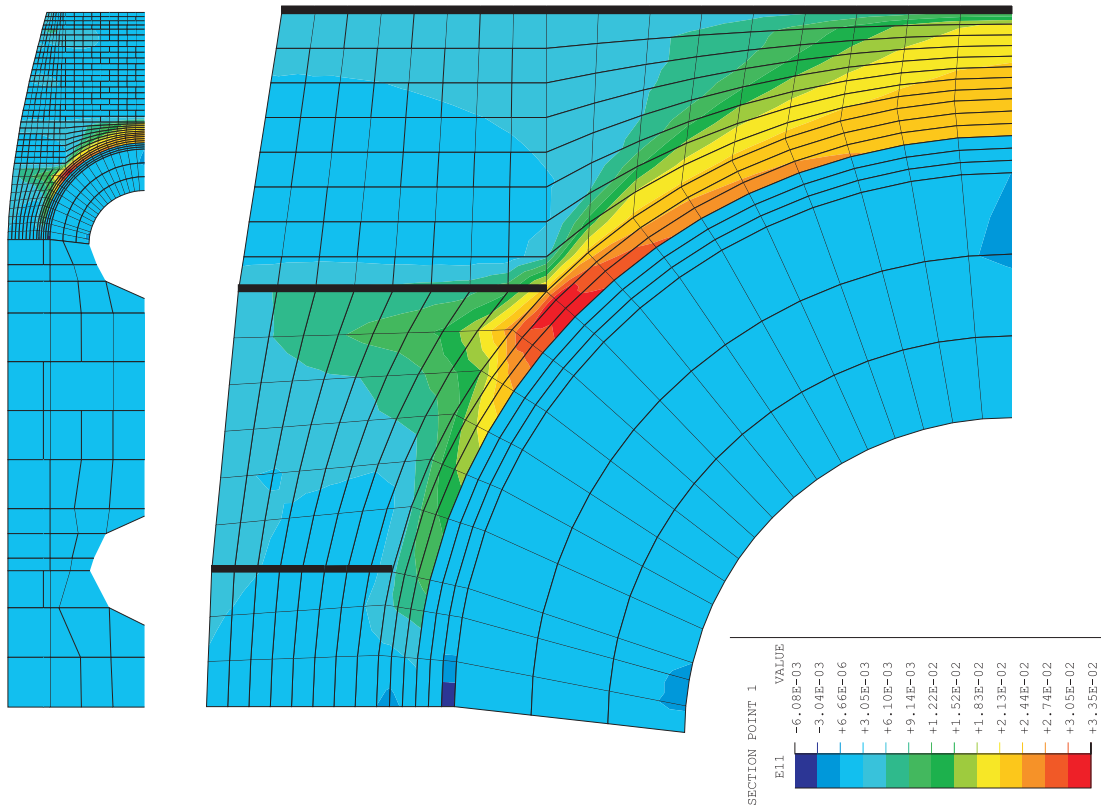Figure 7-42. Hoop (Left) and Meridional (Right) Strains for Posttest M/S Analysis at P = 3.0 Pd

263

Figure 7-43. Hoop (Left) and Meridional (Right) Strains for Posttest M/S Analysis at P = 3.3 Pd
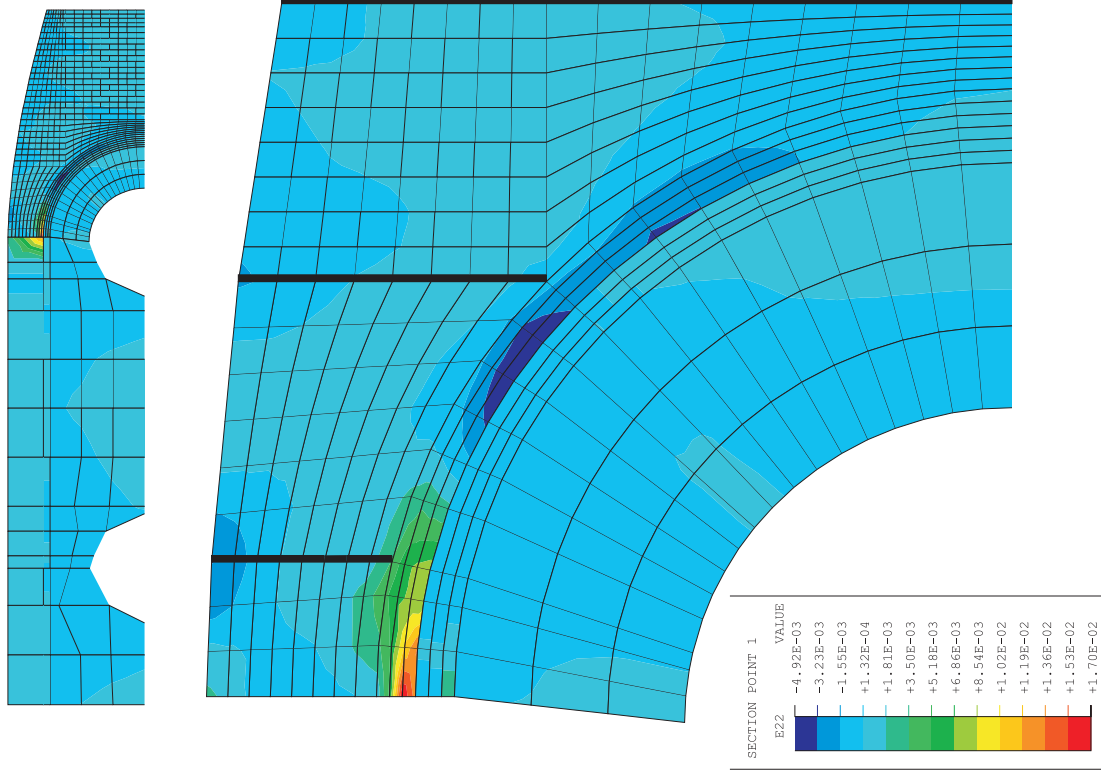
Figure 7-44. Hoop (Left) and Meridional (Right) Strains for Posttest M/S Analysis at P = 3.5 Pd
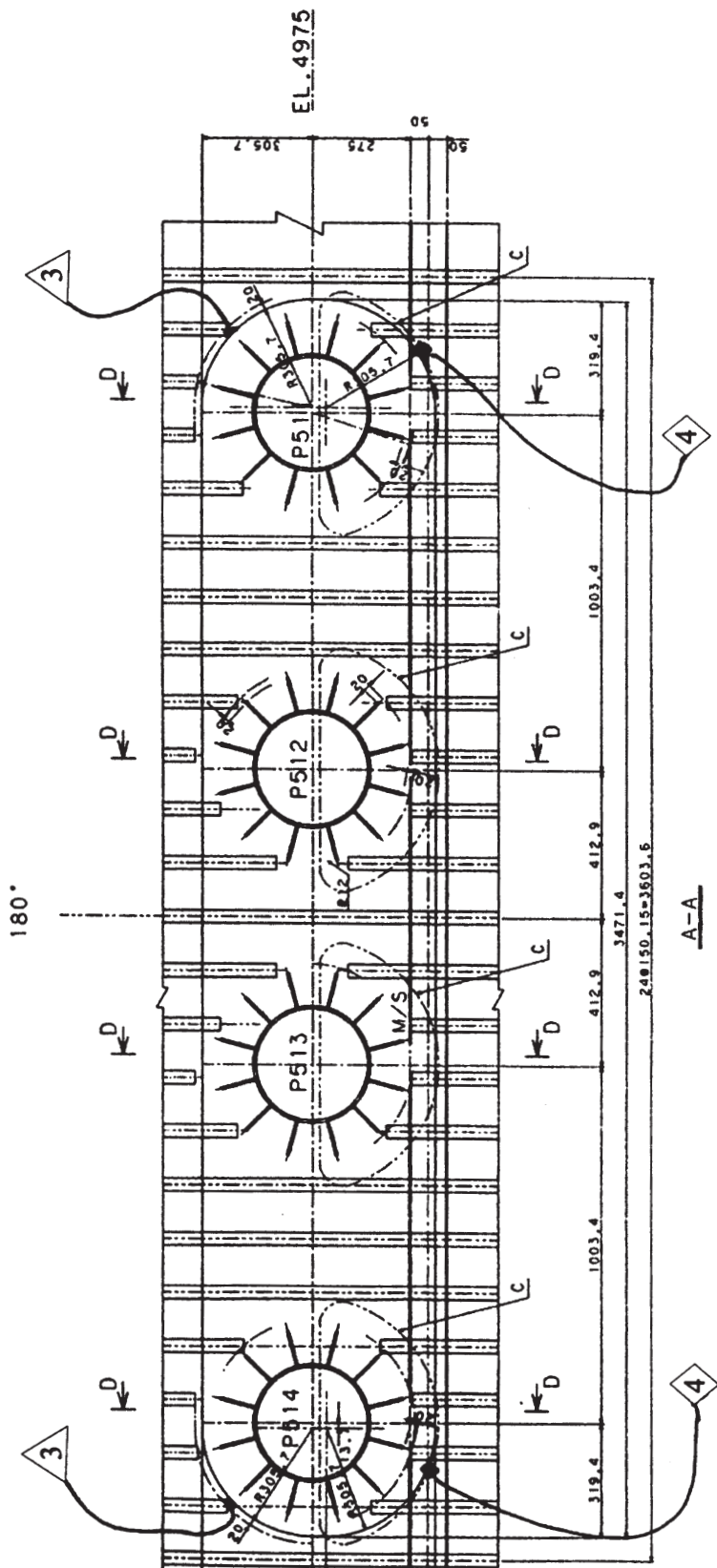
Figure 7-45. Strain Concentration Type 3 and 4 Near M/S Penetrations
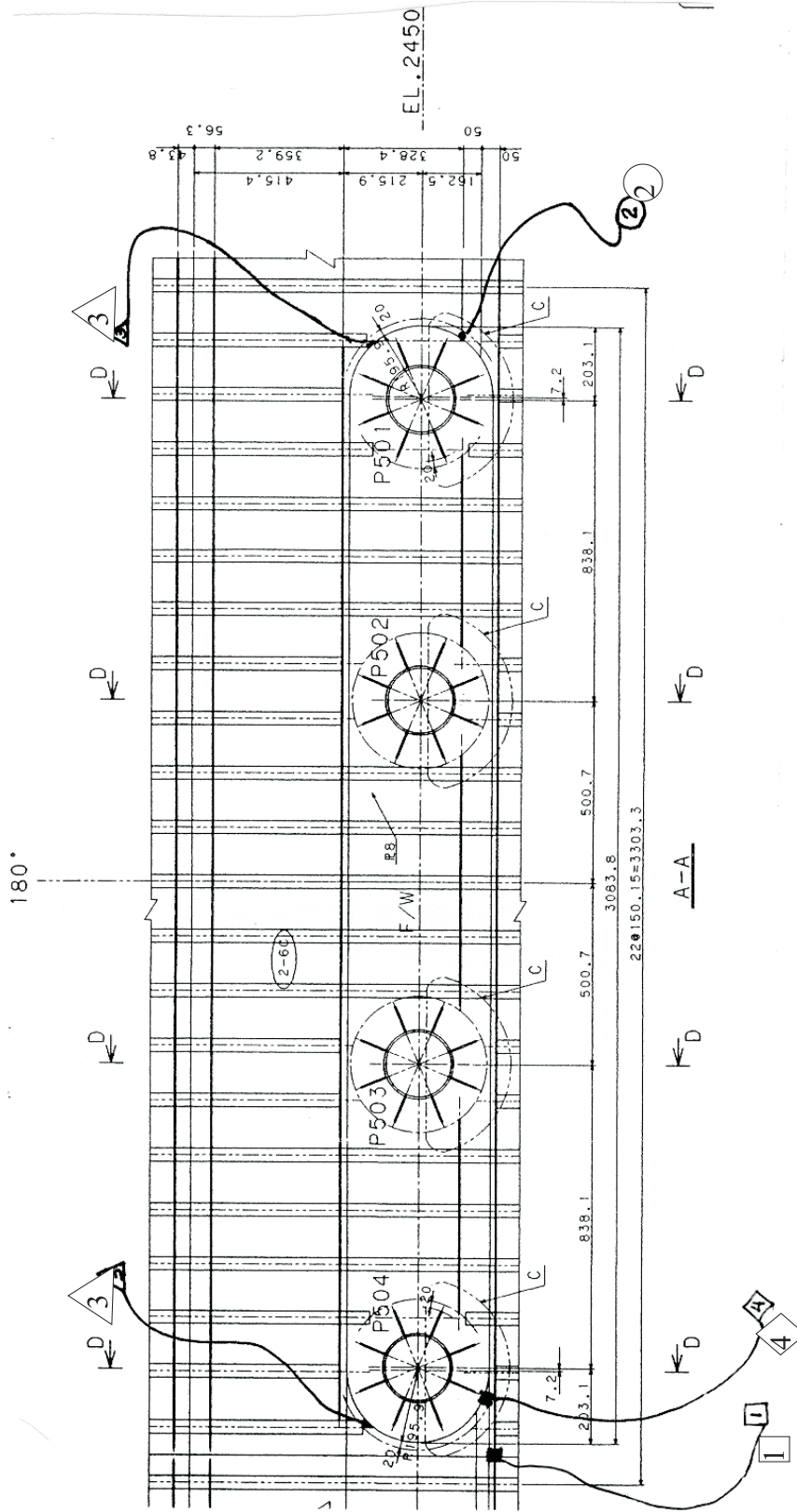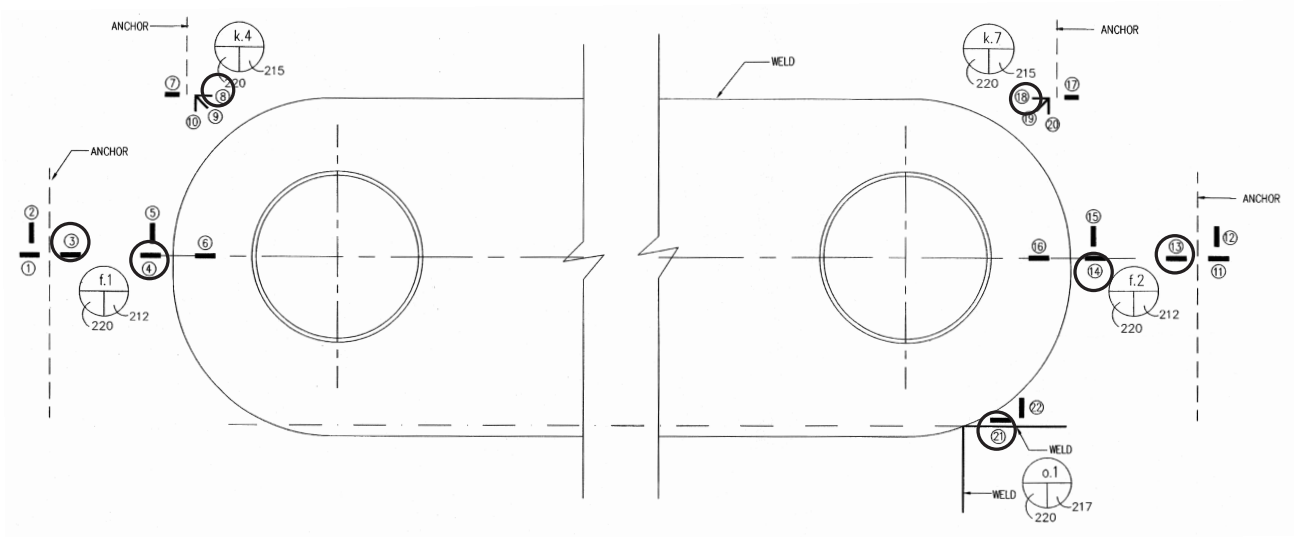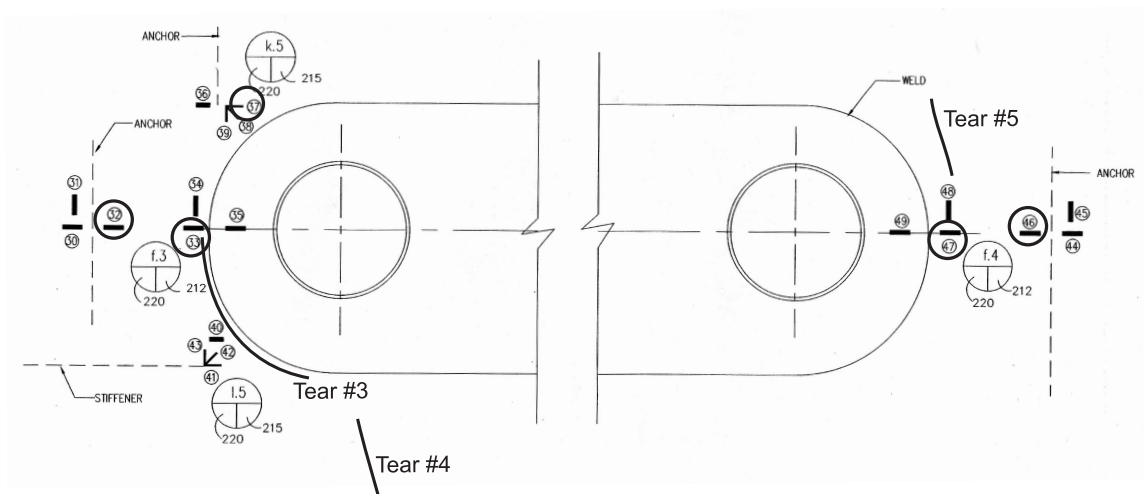
266

Figure 7-46. Strain Concentration Type 1, 2, 3, and 4 Near F/W Penetrations (from [1])

M/S - Inside View

F/W - Inside View

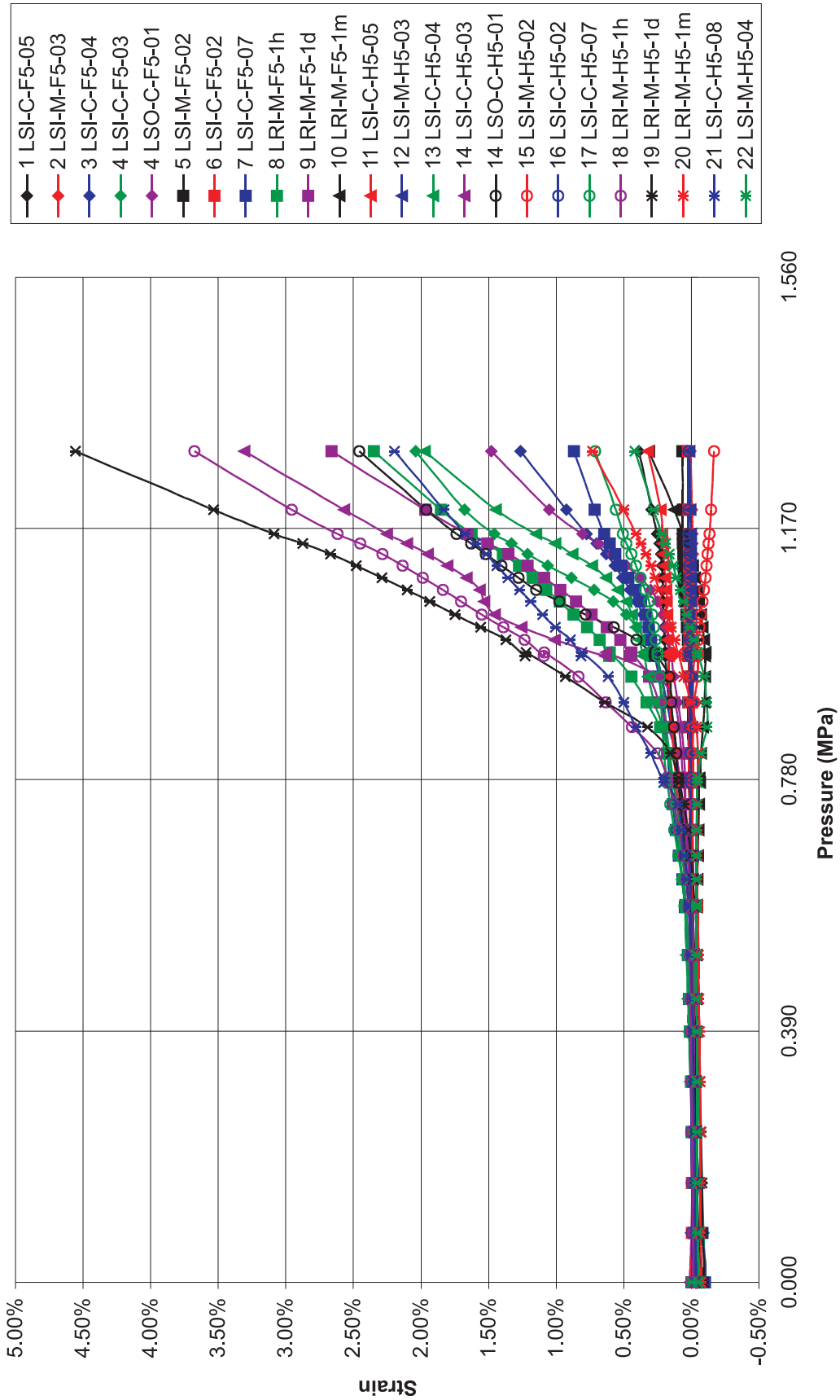Figure 7-47. Strain Gage Locations Near the M/S and F/W Penetrations

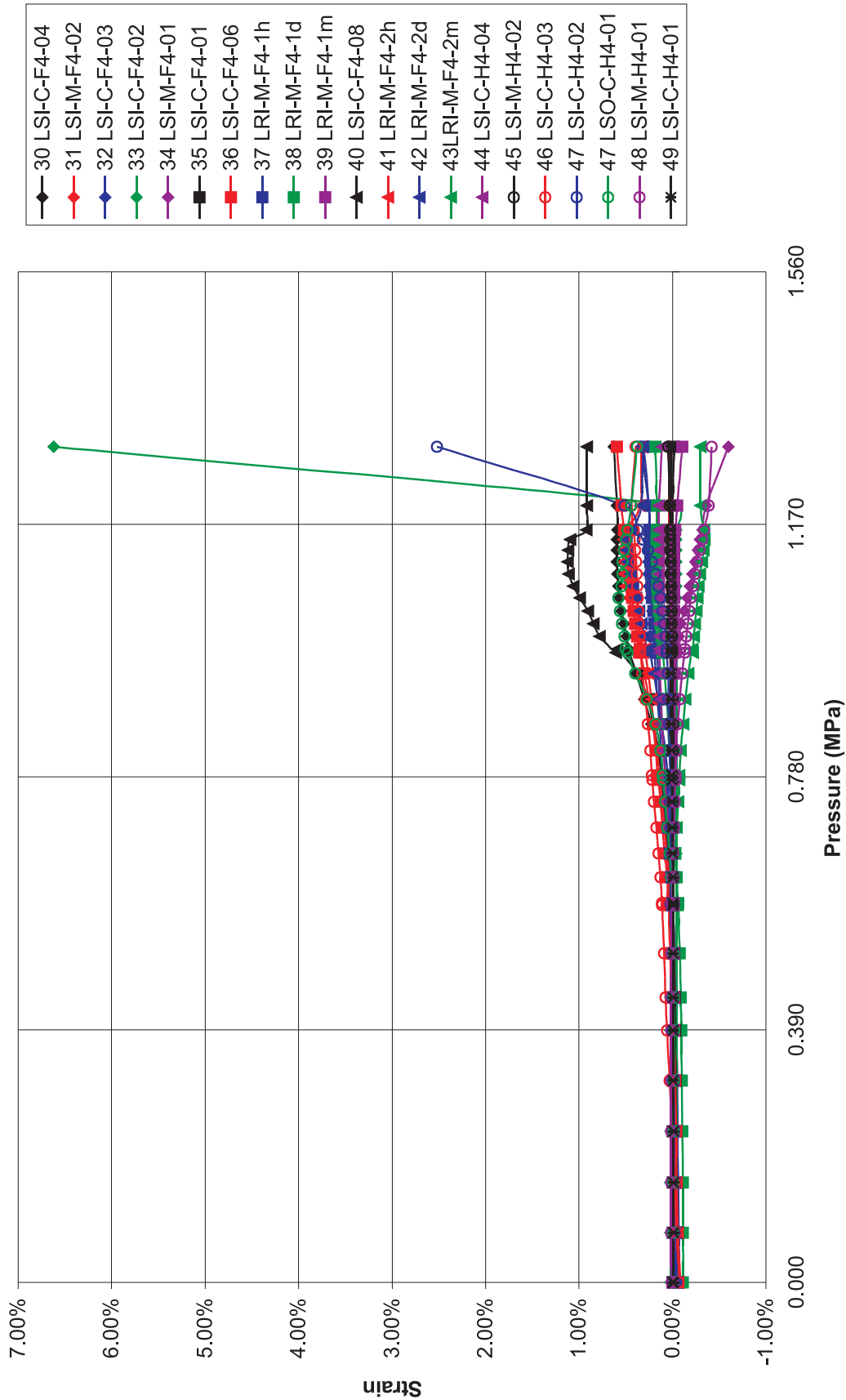Figure 7-48. Liner Strain Histories Measured by the Gages Near the M/S Penetrations

Legend:
1 LSI-C-F5-05
2 LSI-M-F5-03
3 LSI-C-F5-04
4 LSI-C-F5-03
4 LSO-C-F5-01
5 LSI-M-F5-02
6 LSI-C-F5-02
7 LSI-C-F5-07
8 LRI-M-F5-1h
9 LRI-M-F5-1d
10 LRI-M-F5-1m
11 LSI-C-H5-05
12 LSI-M-H5-03
13 LSI-C-H5-04
14 LSI-C-H5-03
14 LSO-C-H5-01
15 LSI-M-H5-02
16 LSI-C-H5-02
17 LSI-C-H5-07
18 LRI-M-H5-1h
19 LRI-M-H5-1d
20 LRI-M-H5-1m
21 LSI-C-H5-08
22 LSI-M-H5-04

Figure 7-49. Linear Strain Histories Measured by the Gages Near the F/W Penetrations

The chart legend includes the following entries:
- 30 LSI-C-F4-04
- 31 LSI-M-F4-02
- 32 LSI-C-F4-03
- 33 LSI-C-F4-02
- 34 LSI-M-F4-01
- 35 LSI-C-F4-01
- 36 LSI-C-F4-06
- 37 LRI-M-F4-1h
- 38 LRI-M-F4-1d
- 39 LRI-M-F4-1m
- 40 LSI-C-F4-08
- 41 LRI-M-F4-2h
- 42 LRI-M-F4-2d
- 43 LRI-M-F4-2m
- 44 LSI-C-H4-04
- 45 LSI-M-H4-02
- 46 LSI-C-H4-03
- 47 LSI-C-H4-02
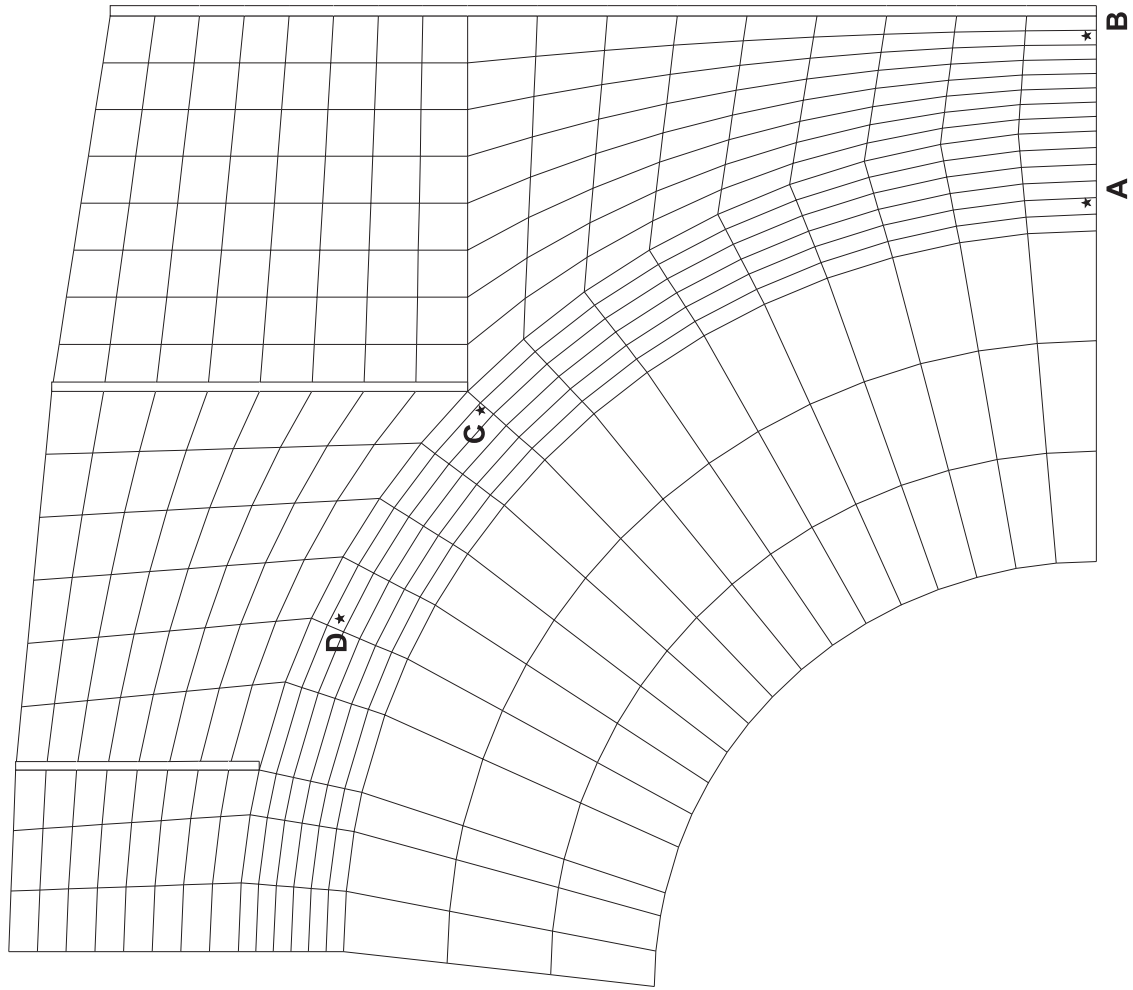- 47 LSO-C-H4-01
- 48 LSI-M-H4-01
- 49 LSI-C-H4-01

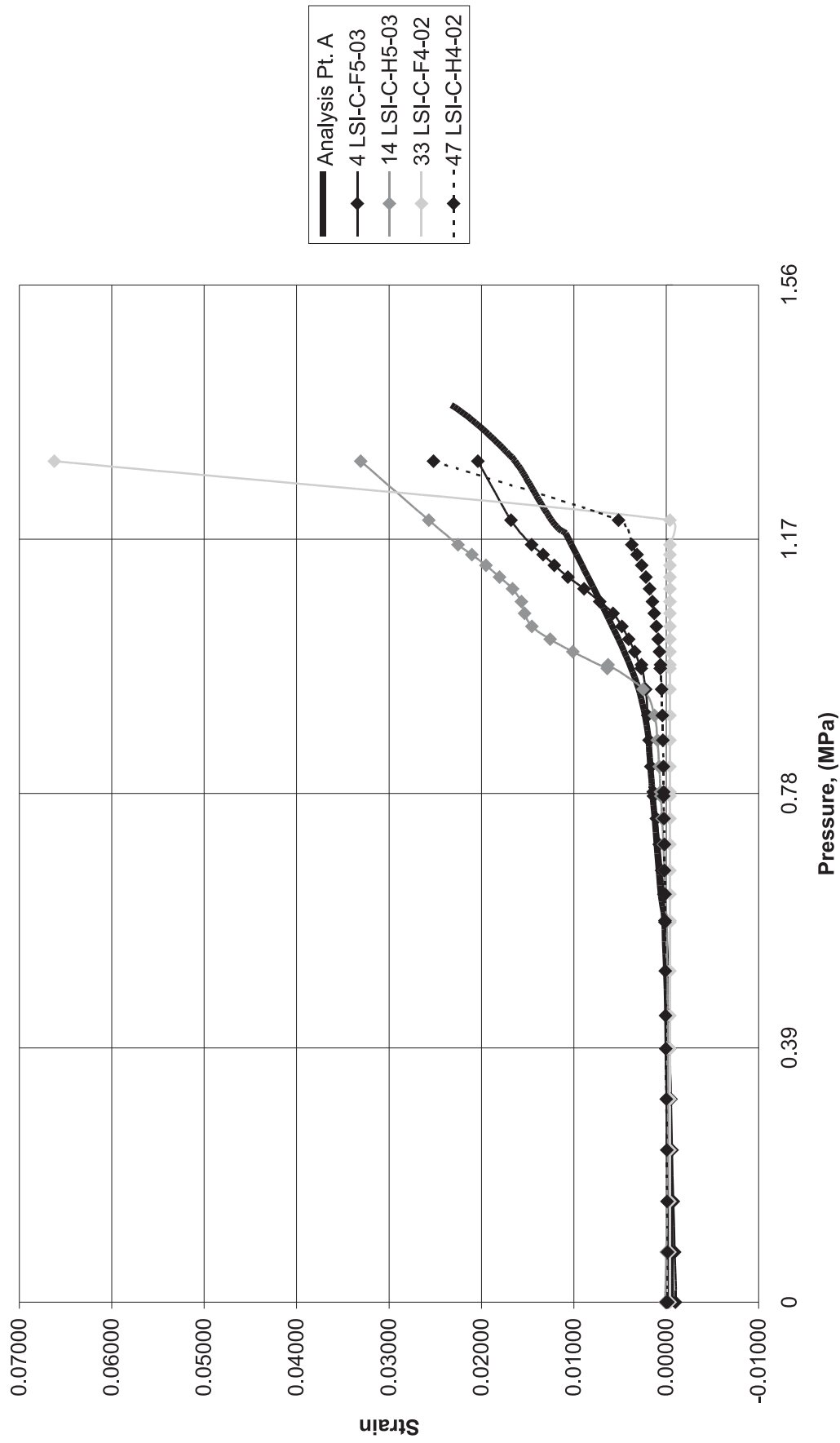Figure 7-50. Liner Strain Locations for Comparing Analysis to M/S and F/W Gage Measurements

Figure 7-51. *M/S and F/W Test vs. Analysis Linear Strain Comparisons at Location "A,"* Near Collar Insert, 3:00, 9:00 Position
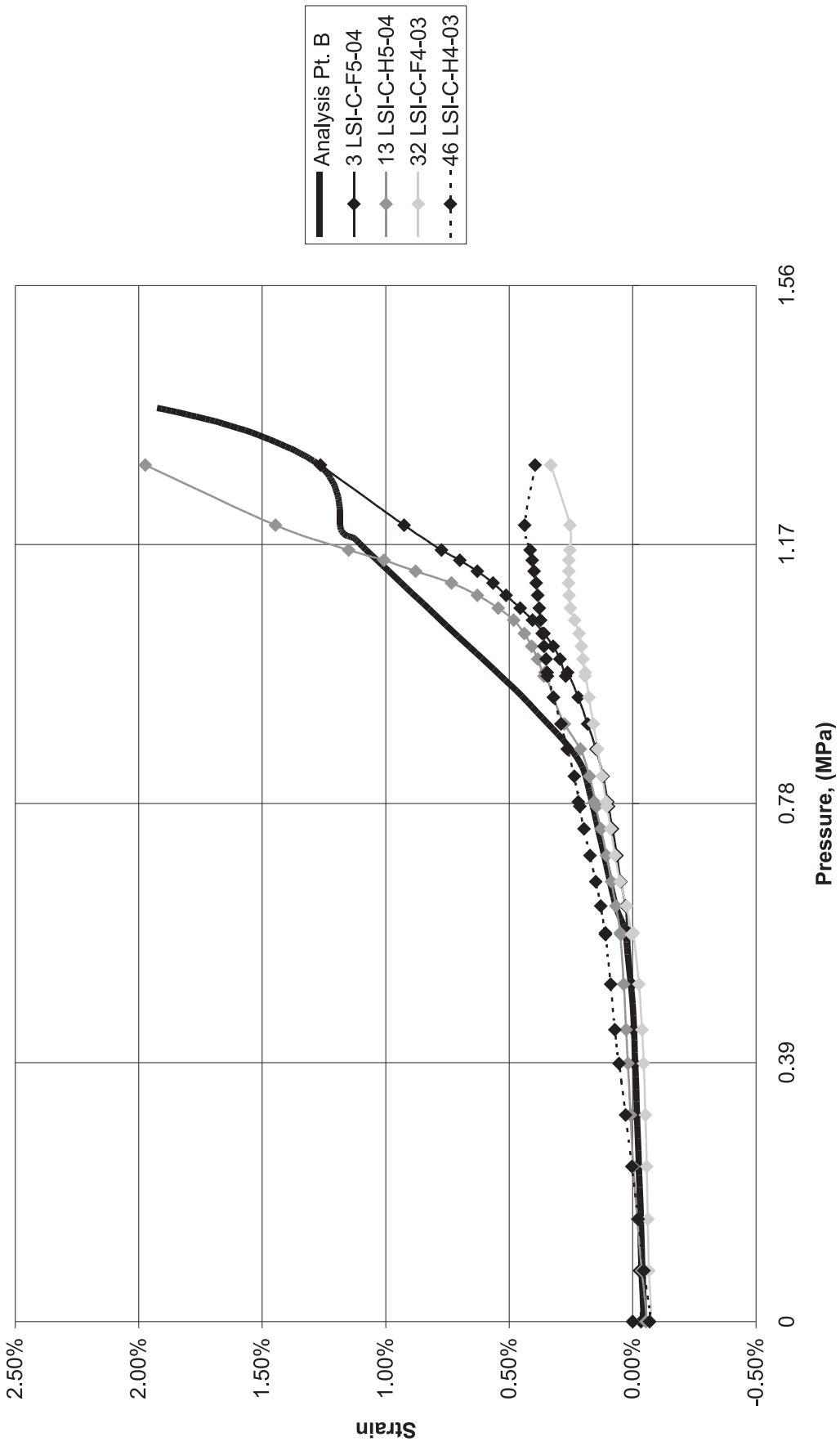
Figure 7-52. M/S and F/W Test *vs.* Analysis Linear Strain Comparisons at Location "B," Near T-Anchor, 3:00, 9:00 Position
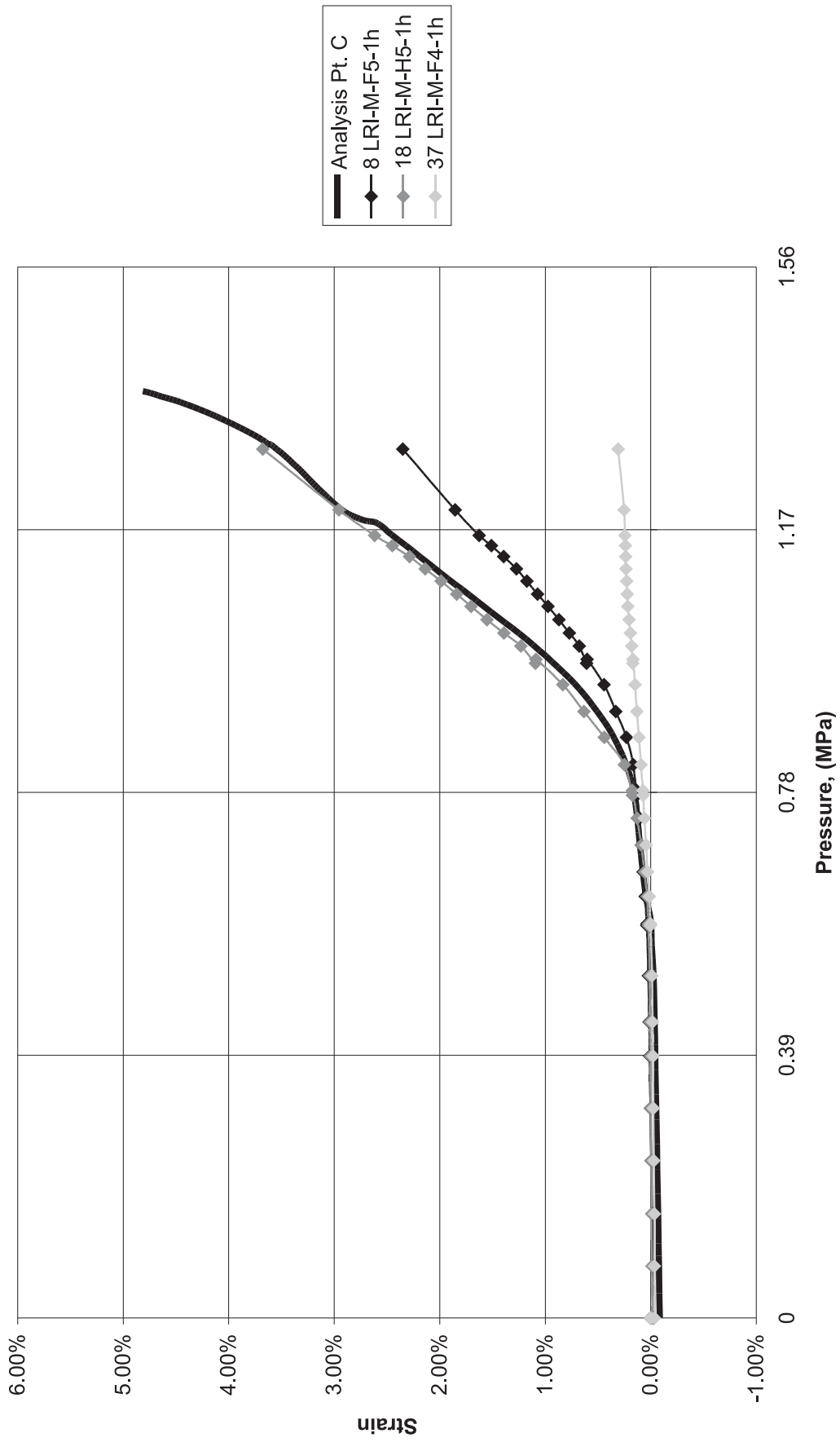
Figure 7-53. M/S and F/W Test *vs.* Analysis Linear Strain Comparisons at Location "C," Near T-Anchor, 3:00, 9:00 Position
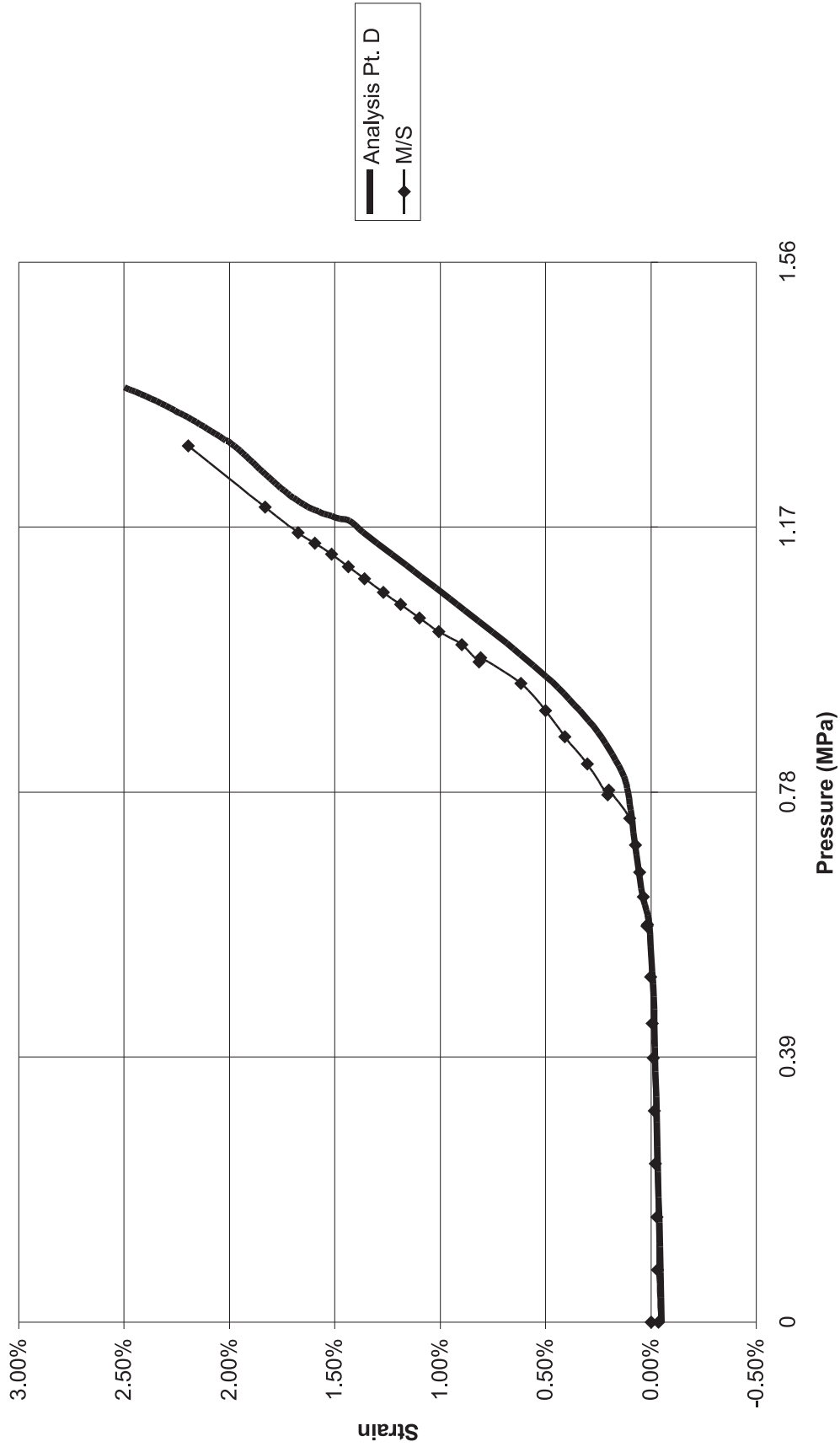
Figure 7-54. M/S Test vs. Analysis Linear Strain Comparisons at Location "D,"
Near Weld-Corner, 3:00, 9:00 Position.